DISSERTATION

STORING CYCLES IN HOPFIELD-TYPE NEURAL NETWORKS

Submitted by

Chuan Zhang

Department of Mathematics

In partial fulfillment of the requirements

For the Degree of Doctor of Philosophy

Colorado State University

Fort Collins, Colorado

Summer 2014

Doctoral Committee:

Advisor: Gerhard Dangelmayr
Co-Advisor: Iuliana Oprea

Patrick Shipman
Chuck Anderson

ABSTRACT

STORING CYCLES IN HOPFIELD-TYPE NEURAL NETWORKS

The storage of pattern sequences is one of the most important tasks in both biological and artificial intelligence systems. Clarifying the underlying mathematical principles for both the storage and retrieval of pattern sequences in neural networks is fundamental for understanding the generation of rhythmic movements in animal nervous systems, as well as for designing electrical circuits to produce and control rhythmic output. In this dissertation, we investigate algebraic structures of *binary cyclic patterns* (or for short *cycles*) and study relations between these structures and the topology and dynamics of Hopfield-type networks with and without delay constructed from cyclic patterns using the pseudoinverse learning rule.

A cycle defined by a binary matrix Σ is called *admissible*, if a connectivity matrix $\mathbf{J}$ satisfying the cycle's transition conditions exists. We show that Σ is admissible, if and only if its discrete Fourier transform contains exactly $r = \mathrm{rank}(\Sigma)$ nonzero columns. Based on the decomposition of the rows of Σ into disjoint subsets corresponding to loops, where a loop is defined by the set of all cyclic permutations of a row, cycles are classified as *simple cycles*, and *separable* or *inseparable composite cycles*. Simple cycles contain rows from one loop only, and the network topology is a feedforward chain with feedback to one neuron if the loop-vectors in Σ are cyclic permutations of each other. For special cases this topology simplifies to a ring with only one feedback. Composite cycles contain rows from at least two disjoint loops, and the neurons corresponding to the loop-vectors in Σ from the same loop are identified with a cluster. Networks constructed from separable composite cycles decompose into completely isolated clusters. For inseparable composite cycles at least two clusters are connected, and the cluster-connectivity is related to the intersections of the spaces spanned by the loop-vectors of the clusters.

The remainder of this thesis deals with the dynamics of Hopfield-type networks with connectivities constructed from admissible cycles. In this approach, the connectivity is composed of two contributions, $C_0\mathbf{J^0}$ and $C_1\mathbf{J}$, where the matrix $\mathbf{J^0}$ serves to store cycle's patterns as fixed points and the matrix $\mathbf{J}$ induces the transitions between the cycle's patterns. Delayed couplings are

associated with the transition matrix **J**. An admissible cycle is called *strongly retrievable* if for appropriate initial data the network dynamics undergoes a persistent oscillation in accordance with cycle's transition conditions. An admissible cycle is called *weakly retrievable* if for any M there exists a sufficiently large delay time τ such that at least M consecutive patterns are retrieved.

When the Hamming distance between successive cycle-patterns is greater than one, the sign-changes in the network dynamics occur asynchronously, leading to the occurrence of intermediate patterns that are not contained in the cycle-matrix. We call the time-intervals with these intermediate patterns *misalignment intervals* and introduce a novel method to analyze the lengths of these intervals, which is referred to as *Misalignment Length Analysis* (MLA). Using this method, intermediate patterns are determined and for a special class of cycles a recurrence relation for successive misalignment intervals is established. In addition, a class of cycles, related to properties of the intermediate patterns, is identified which can be proved to be weakly retrievable in the case $C_0 = 0$ and for sufficiently large values of the gain scaling parameter, λ, of the sigmoid coupling function. More generally, we also prove that for a given **J** constructed from a preselected cycle in that class, all other cycles satisfying the transition conditions associated with **J** are weakly retrievable as well. These results provide an analytic explanation for the long-lasting transient oscillations observed recently in simulations of cooperative Hopfield-type networks with delays.

For general values of C_0, C_1, λ, we perform a linear stability analysis and give a complete description of all possible bifurcations of the trivial solution for networks constructed from admissible cycles. Numerically we illustrate that, depending on the structural features of a cycle, admissible cycles are stored and retrieved either as attracting limit cycles or as long-lasting transient oscillations. Moreover, if the cycle is revealed as attracting limit cycle, this limit cycle is created in a Hopf bifurcation from the trivial solution, and the transition from fixed point attractors to the attracting limit cycle is established through multiple saddle-nodes on limit cycle bifurcations.

Lastly, simulations showing successfully retrieved cycles in continuous-time Hopfield-type networks and in networks of spiking neurons exhibiting up-down states are presented, which strongly suggests that the results of the study presented in this dissertation can be extended to more complicated networks.

ACKNOWLEDGEMENTS

I would like to express my deepest gratitude to my advisers, Dr. Gerhard Dangelmayr and Dr. Iuliana Oprea, for their astute and patient guidance, close collaboration, inspiration, and encouragement throughout my dissertation research at Colorado State University.

My special thanks are extended to my committee members: Dr. Patrick Shipman from the Department of Mathematics and Dr. Chuck Anderson from the Department of Computer Science, for their valuable comments on my qualifying exam part II and preliminary exam presentations and my papers. I would like to pass my sincere appreciation to Dr. Alexander Hulpke for his insightful discussion on the algebraic structures of admissible cycles. I would also like to thank Dr. James Liu and Dr. Yongcheng Zhou for teaching me several analysis and computation courses. My special thanks are also extended to all my friends and colleagues here at Colorado State University, Yang Zou, Roberto Munoz-Alicea, Justin Hughes, Bahaudin Hashmi, Tim Hodges, Rachel Neville, Wenbing Dang, Yiyan Sun, and Ben Zheng, for their support and constructive criticism. I also would like to thank the Department of Mathematics at Colorado State University for the research fellowships which supported my research during the summers 2012 and 2013.

Last but definitely not least, I would like to express my deepest gratitude to my mother Yuzhen Su, my father Deyou Zhang, and my wife Yang Sheng. Without their deepest love and wholeheartedly support, even the completion of this dissertation would not have been possible.

DEDICATION

This dissertation is dedicated to my mother Yuzhen Su,

my father Deyou Zhang, and my wife Yang Sheng.

TABLE OF CONTENTS

CHAPTER 1

INTRODUCTION: NEURAL NETWORKS AND CYCLIC PATTERNS

Storage of pattern sequences is one of the most important tasks in both biological and artificial intelligence systems. A sequence of symbols containing repetitions of the same subsequence is said to be complex [1–3], and cyclic patterns (or cycles of patterns) form one important class of sequences. In animal nervous systems, cyclic patterns of neuronal activity are ubiquitous, and have been suggested to be important in visual processing [4], olfaction [5] and memory formation [6], and partially responsible for generating and controlling rhythmic movements such as locomotion, respiration, swallowing and so on [7–13]. In electronic engineering, analog circuits made with operational amplifiers mimicing neural networks such as cooperative cellular neural network (CNN) rings etc have been extensively used to study the origination and underlying mechanisms of both cyclic patterns [14] and long-lasting transient oscillations [15, 16]. In this chapter, to provide the necessary background and preliminaries for our research on the mathematical principles for both storage and retrieval of cyclic patterns in neural networks, we briefly review relevant recent results on cyclic patterns from neurophysiology, electronic engineering and mathematics, and introduce both the Hopfield-type neural networks and the pseudoinverse learning rule.

1.1 Cyclic Patterns, Delay-Induced Oscillations and Bifurcations

1.1.1 Rhythmic Movements and CPG Networks

Cyclic patterns of neuronal activity are ubiquitous in animal nervous system, and important in different functional tasks from sensory processing, movement production and control to memory formation. Neural networks that can produce cyclic patterned outputs without rhythmic sensory or central input are called *central pattern generators* (CPGs) [9]. Since the first modern experimental evidence of the CPGs networks was demonstrated in the nervous system for controlling flight of locust in 1961 [17], the CPGs networks in different animal species have been extensively

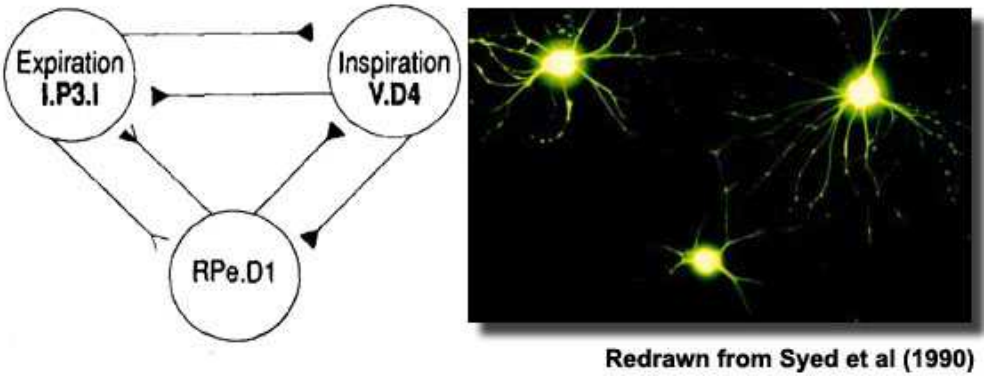

Figure 1.1: Reconstructing snail respiratory CPGs network. **Left:** Schematic diagram of snail (*Mollusk Lymnaea*) respiratory CPGs network (*in vivo*). **Right:** Photomicrograph of the reconstructed snail respiratory CPGs network (*in vitro*). (Redrawn from [18])

investigated both in experiments and theory. While in some lower level invertebrate animals detailed connectivity diagrams among identified CPGs neurons have been experimentally determined (Figure 1.1) [18–20], the anatomic structure of CPGs networks in most higher vertebrate animals including human beings remain largely unknown [10, 11, 21].

According to Yuste [12], the network connectivity problem, i.e. experimentally identifying the connectivity diagram of biological neural networks, is one of the four basic problems that have to be solved to fully understand a biological neural network. However, recent experimental observations [22, 23] suggested that CPGs may be highly flexible, some of them may even be temporarily formed only before the production of motor activity [8]. This makes experimentally identifying the architecture of CPGs very difficult. As indirect approaches to solve the network connectivity problem, observable movement features such as symmetry etc. have been used to infer aspects of CPGs structures [24, 25]. In this dissertation, we directly start from the concept of admissible cycles (cycles that can be stored in a network with the pseudoinverse learning rule), and systematically study the structural features of these cycles and how they determine the topology [26] and the dynamics [27, 28] of networks constructed from them.

1.1.2 Delay-Induced Long-lasting Transient Oscillations

As one of the most popular models of artificial neural networks for content addressable memory, in the past few decades, Hopfield neural network have been widely used in not only associative memory but also pattern recognition, optimization and many other applications [29–36]. Due to its broad applications, ring networks, which are rings of unidirectionally or bidirectionally coupled neurons, have attracted much attention recently [37–42]. In terms of the number of inhibitory connections, unidirectional ring networks can be divided into even and odd networks in accordance to the parity of the number of inhibitory connections [43]. It has been well known that odd networks are capable of generating sustained oscillations, and both numerical and analog circuit simulations showed that although the theoretical results suggested eventual convergence of any solution trajectory in even networks [37,41,44], long lasting oscillations can be very easily observed [15,37]. Figure 1.2 illustrates the analog circuit implementation of an excitatory (even) unidirectional ring network model (upper panel), and a representative experimental recording of the long-lasting transient oscillations (lower panel).

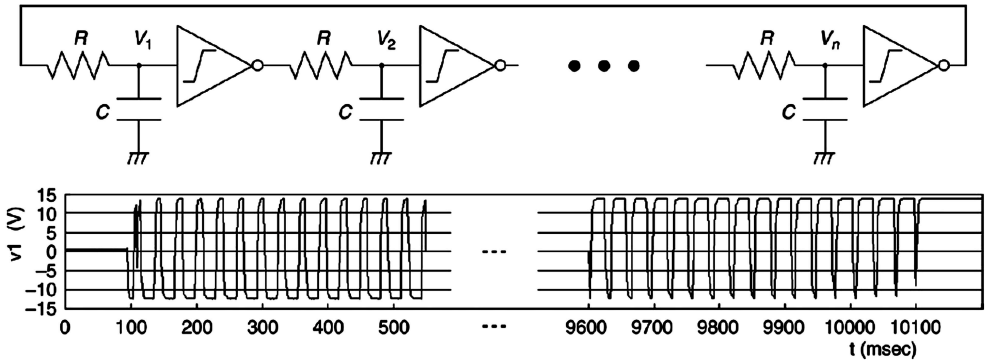

Figure 1.2: Analog circuit made with operational amplifiers implementation of an excitatory ring network (upper panel) and a representative experimental recording of the long-lasting transient oscillations from the analog circuit simulations (lower panel). (Redrawn from [42])

It has been shown that the long lasting transient oscillations can not be explained by the analysis of the asymptotic behavior of the network [37]. More recently, Horikawa and Kitajima [42] studied the waves of transient oscillations traveling along unidirectionally coupled excitatory ring networks. They called the consecutive neurons in a ring network with the neuronal states having the same

sign at the same time instant blocks, and the next block in the direction of boundary propagation forward block. They found that the propagation velocities of the boundaries depend on the length of the blocks (the number of neurons in the blocks). The boundary with shorter forward block propagates faster than that with longer forward block, and the discrepancy in propagating velocities leads to collisions between the boundaries of the shortest blocks, and at each collision between two boundaries, the corresponding block disappears and the adjacent blocks merge into one block. Based on this observation, they proposed a kinematical model to account for the traveling waves of the long-lasting transient oscillations in ring networks with excitatory unidirectional couplings. Recently, the so called long-lasting transition oscillations were reported in other types of ring networks, such as excitatory ring networks with bidirectional couplings [16] etc.

We call the asynchronous sign-changes corresponding to the boundaries between block describe by Horikawa and Kitajima [42] in time domain *misalignments*, and refer to the smallest interval containing all misalignments occuring during the network state transition from one binary pattern to the next as *misalignment interval*. In this dissertation, we propose a novel method for studying transient oscillations in a broader class of networks by analyzing dynamics of misalignments and lengths of misalignment intervals, and refer to the method as *Misalignment Length Analysis* (MLA). The method consists of two parts, one is qualitative, and the other is quantitative. The qualitative method provides a complete qualitative description of the evolution of the network dynamics. For a special type of networks, the quantitative method provides a recurrence equation in misalignment intervals for each one of them, such that the number of binary patterns the network can successfully retrieve can be accurately computed.

1.1.3 Delay-induced Bifurcations in Hopfield-type Neural Networks

Hopfield-type neural networks with delayed couplings are asymmetric generalizations of the symmetric, continuous-time networks introduced by Hopfield [30]. Not only because of its broad applications, but also due to its analytically tractable nature, the dynamics of Hopfield-type networks with discrete/distributed transmission delay(s) has recently attracted considerable research interest from the dynamical systems theory community (see for example [37–42,45–47] etc.). Campbell and collaborators [39, 40, 48] studied the stability and bifurcations of both the trivial solution

and the nontrivial synchronous and asynchronous periodic solutions bifurcating from the trivial solution in ring networks of bidirectionally coupled neurons. Cheng et al [46, 47] studied general continuous-time Hopfield-type neural networks of n neurons with different activation functions with and without delay. Inspired by some geometric consideration, they formulated the parameter conditions for the existence of the 2^n multiple stable stationary solutions, and estimated the basins of attraction of the coexisting multiple stable stationary solutions.

In this dissertation, using a geometric analysis, we show that the transition from fixed points to the attracting limit cycle bifurcating from the trivial solution occurs through multiple saddle-nodes on limit cycle bifurcations. Also, using both the Matlab packages MatCont 3.1 and DDE-BIFTOOL 2.03, we demonstrate that the cyclic patterns prescribed in the corresponding networks are stored and retrieved as different mathematical objects. Depending on their structural features, cyclic patterns are respectively stored and retrieved either as attracting limit cycles, or as unstable periodic solutions bifurcating from the trivial solution, or as long lasting transient oscillations.

1.2 Hopfield-type Neural Networks and Pseudoinverse Learning Rule

Applications of artificial neural networks in studying CPGs networks attracted much interest and efforts [14, 25, 49–55] ever since the first modern evidence of the existence of the CPGs was discovered in 1961 [17]. The dynamics of CPGs networks is determined by phenomena on the intracellular, synaptic, and network levels. As Hopfield-type neural networks neglect specific dynamics of single neurons, and are analytically tractable, in comparison to other network models, Hopfield-type networks are better suitable for studying the role of network structures in generating rhythmic activities. However, most Hopfield-type networks used for studying the generation of cyclic patterns are discrete-time networks [51–53, 56], and in both real biological neural systems and realistic electronic circuits mimicing neural networks, no "neuron" acts like those in discrete-time networks. Moreover, the dynamics of continuous-time Hopfield-type neural networks with delayed couplings has recently motivated and elicited much progress in dynamical system theory [38–40, 45–48, 57–60]. Therefore, clarifying the underlying mathematical principles for both storage and retrieval of cyclic patterns in continuous-time Hopfield-type neural networks is not only

fundamental for understanding the generation of the rhythmic movements in animal nervous systems and better designing analog electronic circuits to produce and control rhythmic output, but also helpful in advancing the study of nonlinear dynamics of functional differential equations, which is in the current interest of research in applied mathematics, and many aspects of the theory are still under development [60–62]. In this section, we introduce both the continuous-time Hopfield-type neural networks and the pseudoinverse learning rule, which was recently shown to be biologically plausible [63]. In this dissertation, we mainly focus on the continuous-time Hopfield-type neural networks constructed from admissible cycles with the pseudoinverse learning rule.

A continuous-time Hopfield-type network [30] is described by a system of ordinary differential equations for $u_i(t)$, $1 \leq i \leq N$, which model the membrane potential of the i-th neuron in the network at time t. Assuming that all neurons are identical, normalizing the neuron amplifier input capacitance and resistance to unity and neglecting external inputs, the governing equations are,

$$\frac{du_i}{dt} = -u_i + \sum_{j=1}^{N} \tilde{J}_{ij} v_j,\ 1 \leq i \leq N, \tag{1.1}$$

where $v_j(t)$ is the firing rate of the j-th neuron and $\tilde{\mathbf{J}} = (\tilde{J}_{ij})_{N\times N}$ is the connectivity matrix. The firing rate v_j is related to the membrane potential u_j through a sigmoid-shaped gain function, $v_j = g(u_j)$, which we choose, following [30], as $g(u_j) = \tanh(\lambda u_j)$, where λ controls the steepness. Using vector notation, $\mathbf{u} = (u_1, \ldots, u_N)^T$, $\mathbf{v} = (v_1, \ldots, v_N)^T$, (1.1) can be more compactly written as (dots denote time derivatives)

$$\dot{\mathbf{u}} = -\mathbf{u} + \tilde{\mathbf{J}} \tanh(\lambda \mathbf{u}), \tag{1.2}$$

where here and subsequently a scalar function applied to a vector or matrix denotes the vector or matrix obtained by applying the function to each component, i.e.

$$\tanh(\lambda \mathbf{u}) = (\tanh(\lambda u_1), \tanh(\lambda u_2), \ldots, \tanh(\lambda u_N))^T.$$

Alternatively, since $u_j = \operatorname{arctanh}(v_j)/\lambda$, (1.2) can be rewritten as a system of differential equations for the firing rates,

$$\dot{\mathbf{v}} = \lambda(\mathbf{I} - \operatorname{diag}(\mathbf{v}^2))(\tilde{\mathbf{J}}\mathbf{v} - \frac{\operatorname{arctanh}(\mathbf{v})}{\lambda}), \tag{1.3}$$

where $\mathbf{I}$ is the $N \times N$ identity matrix.

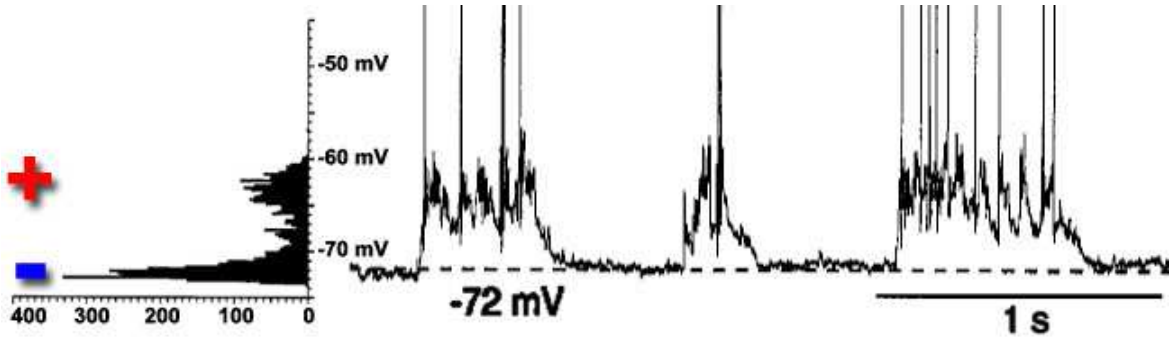

Figure 1.3: Interpretation of the binary states "+1" and "−1" traversed by a single neuron in Hopfield-type networks as the "up" and "down" states observed in typical CPGs and cortical neurons. **Left:** Membrane potential distribution of the spontaneous activity for a striatal medium spiny (MS) neuron whose membrane potential is shown on the right. **Right:** A representative trace of the membrane potential of a striatal MS neuron showing the spontaneous up and down states. The dashed line indicates a voltage at −72mV, and the line segment at the bottom right corner indicates a time lapse of 1 second. (Redrawn from [64])

In order to avoid the unrealistic nature of the two-state McCulloch-Pitts threshold devices [65], Hopfield extended his original discrete neural network model [29] into a continuous-time form [30]. It is necessary to emphasize that this is actually another reason why we choose Hopfield-type neural networks. In neurophysiology it is well known that both CPG neurons and cortical neurons show bistable membrane behaviors, which are commonly referred to as plateau potentials [21, 66, 67] or up-down states [68, 69]. Accordingly, a sequence of the binary states +1 and −1 traversed by a single neuron in a Hopfield-type network can be interpreted as a sequence of up and down states, respectively (Figure 1.3). In this dissertation, we study the structure of binary pattern cycles that can be stored in networks of the above form (1.2). Following [29, 30], any N-dimensional $\{-1, 1\}$-valued column vector is identified with a *binary vector* or *pattern*, and we use + and − to denote 1 and −1.

Personnaz et al. [1, 56] studied the storage of sequences of patterns in discrete-time Hopfield-type networks. A sequence of p patterns $\xi^{(\mu)} = (\xi_1^{(\mu)}, \xi_2^{(\mu)}, \ldots, \xi_N^{(\mu)})^T$, $1 \leq \mu \leq p$, $\xi_i^{(\mu)} = +$ or $-$, is defined by p transition conditions $\xi^{(\mu)} \to f^{(\mu)}$, where $f^{(\mu)}$ is one of the given vectors, i.e., $f^{(\mu)} \in \{\xi^{(1)}, \ldots, \xi^{(p)}\}$ for each μ. Thus a sequence is characterized by two $N \times p$-matrices $\Sigma = (\xi^{(1)}, \ldots, \xi^{(p)})$ and $F = (f^{(1)}, \ldots, f^{(p)})$. The two matrices are related to each other by the transition conditions, which can be conveniently formulated in terms of a $p \times p$ transition matrix as $F = \Sigma \mathbf{P}$,

where $\mathbf{P}_{\nu\mu} = 1$ if $f^{(\mu)} = \xi^{(\nu)}$ and 0 otherwise. For example, for $p = 3$ and the simplest case of a sequence starting at $\xi^{(1)}$ and terminating at $\xi^{(3)}$, $\xi^{(1)} \to \xi^{(2)}$, $\xi^{(2)} \to \xi^{(3)}$, $\xi^{(3)} \to \xi^{(3)}$, we have $F = (\xi^{(2)}, \xi^{(3)}, \xi^{(3)})$ and P is singular, but the general definition in terms of Σ and F allows to consider more complex as well as multiple sequences. Personnaz et al [56] showed that the storage of such a sequence leads to the matrix equation,

$$\mathbf{J}\Sigma = F, \tag{1.4}$$

for the connectivity matrix $\mathbf{J}$ of the discrete network. It was pointed out in [56], that, if $F\Sigma^{+}\Sigma = F$, where Σ^{+} is the Moore-Penrose pseudoinverse of Σ, then (1.4) has the exact solution $\mathbf{J} = F\Sigma^{+}$, which was called *associating learning rule* by these authors.

A *cycle* of p patterns is a sequence with $F = (\xi^{(2)}, \xi^{(3)}, \ldots, \xi^{(p)}, \xi^{(1)})$, i.e., $\xi^{(\mu)} \to \xi^{(\mu+1)}$ for $\mu < p$ and $\xi^{(p)} \to \xi^{(1)}$, and the corresponding transition matrix is

$$\mathbf{P} = \begin{pmatrix} 0 & 0 & 0 & \cdots & 0 & 1 \\ 1 & 0 & 0 & \cdots & 0 & 0 \\ 0 & 1 & 0 & \cdots & 0 & 0 \\ \vdots & \vdots & \vdots & \ddots & \vdots & \vdots \\ 0 & 0 & 0 & \cdots & 0 & 0 \\ 0 & 0 & 0 & \cdots & 1 & 0 \end{pmatrix}. \tag{1.5}$$

We are interested in the storage of cycles in the continuous-time Hopfield networks defined by (1.2). Our approach to compute a connectivity matrix $\tilde{\mathbf{J}}$ for this purpose follows [14]. In this dissertation, the connectivity matrix $\tilde{\mathbf{J}}$ is decomposed as

$$\tilde{\mathbf{J}} = \beta_K(C_0\mathbf{J^0} + C_1\mathbf{J}), \tag{1.6}$$

where $\mathbf{J^0}$ serves to stabilize the network in its current memory state and $\mathbf{J}$ imposes the transitions between the memory states. Here, $C_1 = 1 - C_0$ and C_0, $0 \le C_0 \le 1$, control the relative contributions of the two components of $\tilde{\mathbf{J}}$. The fixed point condition is realized by requiring that $\mathbf{v} = \beta_1\xi^{(\mu)}$, with a parameter $0 < \beta_1 < 1$, is a fixed point if $C_0 = 1$. Noting that $\operatorname{arctanh}(x)$ is an odd function and $|\xi_i^{(\mu)}| = 1$, this leads, according to (1.3), to the condition

$$\tilde{\mathbf{J}}\beta_1\xi^{(\mu)} = \frac{1}{\lambda}\operatorname{arctanh}(\beta_1\xi^{(\mu)}) = \frac{1}{\lambda}\operatorname{arctanh}(\beta_1)\xi^{(\mu)},$$

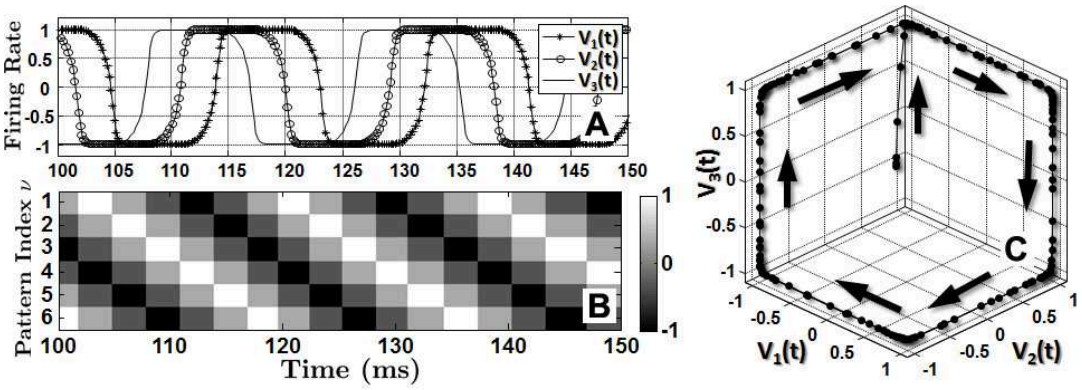

Figure 1.4: A successfully retrieved cycle Σ (see text for details) in a network of three neurons. **A** shows the firing rates $v_i(t)$ of the three neurons and the raster plot **B** shows the overlaps $m^{(\nu)}(t)$, which measure the similarity of the network state $\mathbf{v}(t)$ with each of the six patterns in the cycle (see text). **C** illustrates the retrieval of the cycle in the phase space of the system.

for every μ, hence $\tilde{\mathbf{J}}\Sigma = \beta_K \Sigma$ with $\beta_K = \dfrac{1}{\lambda\beta_1}\text{arctanh}(\beta_1)$, which has the solution $\tilde{\mathbf{J}} = \beta_K \mathbf{J^0}$ with

$$\mathbf{J^0} = \Sigma\Sigma^+. \tag{1.7}$$

Regarding the transition conditions, we stipulate that $\mathbf{v}(t) = \beta_1 \xi^{(\mu)}$ implies $\mathbf{v}(t+\tau) = \beta_1 f^{(\mu)}$ for some τ, and require accordingly for $C_0 = 0$ that $\tilde{\mathbf{J}}\Sigma = \beta_K F$. This leads to equation (1.4), which in terms of the transition matrix $\mathbf{P}$, equation (1.5), becomes

$$\mathbf{J}\Sigma = \Sigma\mathbf{P}. \tag{1.8}$$

According to the associating learning rule of [56], (1.8) has the solution

$$\mathbf{J} = \Sigma\mathbf{P}\Sigma^+, \tag{1.9}$$

provided that $\Sigma\mathbf{P}\Sigma^+\Sigma = \Sigma\mathbf{P}$. If this condition is not satisfied, (1.8) has no solution.

The main objective of the first part of this dissertation is the study of the existence and properties of the solutions of (1.8) along with the structural features of the corresponding cycles, and the network topologies resulting from $\mathbf{J^0}$ and $\mathbf{J}$ defined by (1.7) and (1.9). Although this part of research does not depend on whether there is a time delay in network couplings or not, we consider the extension of (1.2) to a dynamical system with a delay,

$$\dot{\mathbf{u}} = -\mathbf{u} + C_0\beta_K \mathbf{J^0}\tanh(\lambda\mathbf{u}) + C_1\beta_K \mathbf{J}\tanh(\lambda\mathbf{u}_\tau), \tag{1.10}$$

with a delay-time $\tau > 0$ and $\mathbf{u}_\tau(t) = \mathbf{u}(t-\tau)$, and consider the network (1.2) without delay as a special case. As the simulations presented in this dissertation will be all in networks with delayed couplings, we show here one example of a successfully retrieved cycle in (1.2), a network of $N = 3$ neurons. The cycle consists of six states, $\Sigma = (\xi^{(1)}, \ldots, \xi^{(6)})$, with $\xi^{(1)} = (+,+,+)^T$, $\xi^{(2)} = (+,+,-)^T$, $\xi^{(3)} = (+,-,-)^T$ and $\xi^{(3+\mu)} = -\xi^{(\mu)}$ for $\mu = 1,2,3$. The retrieval of the cycle is illustrated in Figure 1.4. The raster plot **B** in this figure shows the overlaps, defined in general as

$$m^{(\nu)}(t) = \frac{1}{N}\sum_{i=1}^{N} v_i(t)\xi_i^{(\nu)},\ 1 \le \nu \le p, \tag{1.11}$$

of the actual network state $\mathbf{v}(t)$ with the patterns of the cycle. The overlap $m^{(\nu)}(t)$ is a normalized measure of the similarity of $\mathbf{v}(t)$ with $\xi^{(\nu)}$. Maximal similarity with $\xi^{(\nu)}$ and $-\xi^{(\nu)}$ occurs for $m^{(\nu)}$ close to 1 and -1, respectively. The raster plot of the overlaps in Figure 1.4**B** as well as the time series in Figure 1.4**A** clearly illustrate that the cycle is retrieved successfully. The parameters C_0 and β used in this simulation were $C_0 = 0.6$ and $\beta = 4$.

CHAPTER 2

ADMISSIBILITY AND NETWORK TOPOLOGY

2.1 Admissible Cycles and Cyclic Permutation Groups

Definition 2.1.1. Let $\mathbf{P}$ be the cyclic $p \times p$-permutation matrix defined in (1.5). A cycle defined by a binary $N \times p$-matrix $\Sigma = (\xi^{(1)}, \xi^{(2)}, \ldots, \xi^{(p)})$ is said to be *admissible*, if there is a real $N \times N$ matrix $\mathbf{J}$ such that equation (1.8) is satisfied.

Note that if Σ is admissible, the solution to (1.8) may be not unique. If there are several solutions, we select (1.9) as distinguished solution because of its close relationship to $\mathbf{J^0}$, see Remark 2.1.1(b) below.

Gencic et al [14] considered a special type of cycles defined by p binary vectors $\Sigma' = (\xi^{(1)}, \xi^{(2)}, \ldots, \xi^{(p)})$, which satisfy the transition condition $\xi^{(1)} \to \xi^{(2)} \to \cdots \xi^{(p)} \to -\xi^{(1)} \to -\xi^{(2)} \to \cdots - \xi^{(p)} \to \xi^{(1)}$. In this dissertation we consider these cycles as special cases of cycles of period $2p$ with $\Sigma = (\Sigma', -\Sigma')$.

For storing sequences, Personnaz et al [56] pointed out that, if the associating learning rule $F\Sigma^{+}\Sigma = F$ is satisfied, the rows of F are linear combinations of the rows of Σ. This follows from the fact that $\Sigma^{+}\Sigma$ is the orthogonal projection matrix onto the subspace of $\mathbb{R}^p$ spanned by the rows of Σ. For storing single cycles, their conclusion can be reformulated geometrically as follows:

Proposition 2.1.1. *A cycle Σ of size $N \times p$ is admissible, if and only if its row space is invariant under $\mathbf{P}$, i.e.*

$$\text{span}\{\text{R}(\Sigma)\} = \text{span}\{\text{R}(\Sigma\mathbf{P})\}, \tag{2.1}$$

where $\text{R}(\Sigma)$ denotes the set of all row vectors of Σ.

Note that $|\text{R}(\Sigma)| \leq N$, and if $|\text{R}(\Sigma)| < N$ then two or more different rows of Σ are identical, that is, the corresponding neurons traverse the same cycle. Although this is a kind of redundancy, we do not exclude this possibility in our general discussion.

We next formulate a useful alternative admissibility criterion involving the eigenspaces of $\mathbf{P}$. Since $\mathbf{P}$ is a circulant matrix, $\mathbf{P}$ has the orthogonal eigenvectors $v^{(k)} = (1, \rho^k, \rho^{2k}, \ldots, \rho^{(p-1)k})^T$ for $0 \leq k < p$, where $\rho = e^{2\pi \mathbf{i}/p}$ ($\mathbf{i} = \sqrt{-1}$) is the basic primitive p-th root of unity [70], and in this special case the eigenvalues are $\bar{\rho}^k$. We set $V = (v^{(0)}, v^{(1)}, \ldots, v^{(p-1)})$, $\lambda_j = \bar{\rho}^{j-1}$ ($1 \leq j \leq p$), $\Lambda = \mathrm{diag}(\lambda_1, \ldots, \lambda_p)$ and note that $\mathbf{P} = V\Lambda V^{-1}$ with $V^{-1} = V^*/p$, where here and subsequently complex conjugation is marked by an overbar and an asterisk denotes the adjoint (complex conjugate transpose) matrix or vector.

Since the transition matrix $\mathbf{P}$ leaves its eigenspaces invariant, it follows that if the row space of Σ coincides with the direct sum of its projections onto the eigenspaces of $\mathbf{P}$, then Σ is admissible. Based on this consideration, we obtain the following admissibility criterion.

Theorem 2.1.2. *Let Σ be a cycle whose matrix form is of size $N \times p$, and let $\hat{\Sigma} = \Sigma V$. Then Σ is admissible, if and only if $\hat{\Sigma}$ has precisely r nonzero columns, where $r = \mathrm{rank}(\Sigma) = \mathrm{rank}(\hat{\Sigma})$.*

Proof: Noting that $\mathbf{J}\Sigma = \Sigma\mathbf{P} = \Sigma V\Lambda V^{-1}$ implies $\mathbf{J}\hat{\Sigma} = \hat{\Sigma}\Lambda$, it follows that Σ is admissible if and only if there exists an $N \times N$-matrix $\mathbf{J}$ such that

$$\mathbf{J}\hat{\Sigma} = \hat{\Sigma}\Lambda, \tag{2.2}$$

which implies

$$\mathbf{J}\mathrm{col}_j(\hat{\Sigma}) = \lambda_j \mathrm{col}_j(\hat{\Sigma}),\ 1 \leq j \leq p, \tag{2.3}$$

where $\mathrm{col}_j(\hat{\Sigma})$ denotes the j-th column of $\hat{\Sigma}$.

Suppose now that Σ is admissible and $\mathrm{rank}(\Sigma) = r$. Since the columns of V consist of eigenvectors associated to distinct eigenvalues of $\mathbf{P}$, it follows that $\hat{\Sigma} = \Sigma V$ has r linearly independent columns. Assume $\mathrm{col}_{\mu_1}(\hat{\Sigma}), \ldots, \mathrm{col}_{\mu_r}(\hat{\Sigma})$ are linearly independent. Then (2.3) implies that λ_{μ_1}, $\ldots$, λ_{μ_r} are eigenvalues of $\mathbf{J}$ and $\mathrm{col}_{\mu_1}(\hat{\Sigma}), \ldots, \mathrm{col}_{\mu_r}(\hat{\Sigma})$ are the corresponding eigenvectors. If $\hat{\Sigma}$ has an additional nonzero column, $\mathrm{col}_j(\hat{\Sigma})$, with $j \notin \{\mu_1, \ldots, \mu_r\}$, then by (2.3) this column is an eigenvector of $\mathbf{J}$ corresponding to the eigenvalue λ_j and $\lambda_j \neq \lambda_{\mu_i}$ for $1 \leq i \leq r$. On the other hand, $\mathrm{col}_j(\hat{\Sigma})$ is a linear combination of $\mathrm{col}_{\mu_1}(\hat{\Sigma}), \ldots, \mathrm{col}_{\mu_r}(\hat{\Sigma})$ which is impossible, since eigenvectors corresponding to different eigenvalues are linearly independent. Thus all columns except $\mathrm{col}_{\mu_1}(\hat{\Sigma}), \ldots, \mathrm{col}_{\mu_r}(\hat{\Sigma})$ must be zero.

Conversely, assume $\hat{\Sigma}$ has r nonzero columns $\mathrm{col}_{\mu_1}(\hat{\Sigma}), \ldots, \mathrm{col}_{\mu_r}(\hat{\Sigma})$ and all other columns of $\hat{\Sigma}$ are zero. Since $\mathrm{rank}(\hat{\Sigma}) = r$, these columns are linearly independent. Let Q be a $p \times p$ permutation matrix that maps the column j to the column μ_j for $1 \leq j \leq r$. Then

$$\begin{aligned} \hat{\Sigma} &= [0, \ldots, 0, \mathrm{col}_{\mu_1}(\hat{\Sigma}), 0, \ldots, 0, \mathrm{col}_{\mu_r}(\hat{\Sigma}), 0, \ldots, 0] \\ &= [\mathrm{col}_{\mu_1}(\hat{\Sigma}), \ldots, \mathrm{col}_{\mu_r}(\hat{\Sigma}), 0, \ldots, 0]Q. \end{aligned}$$

Let $\hat{\Sigma}_0 = [\mathrm{col}_{\mu_1}(\hat{\Sigma}), \ldots, \mathrm{col}_{\mu_r}(\hat{\Sigma})]$ and $\hat{\Sigma}_0^*$ be the adjoint (complex conjugate transpose) matrix of $\hat{\Sigma}_0$ and define

$$\mathbf{J} = \hat{\Sigma}\Lambda Q^T \begin{bmatrix} (\hat{\Sigma}_0^* \hat{\Sigma}_0)^{-1} \hat{\Sigma}_0^* \\ O_{(p-r)\times N} \end{bmatrix}.$$

Then

$$\begin{aligned} \mathbf{J}\hat{\Sigma} &= \hat{\Sigma}\Lambda Q^T \begin{bmatrix} (\hat{\Sigma}_0^* \hat{\Sigma}_0)^{-1} \hat{\Sigma}_0^* \\ O_{(p-r)\times N} \end{bmatrix} [\hat{\Sigma}_0, O_{N\times(p-r)}]Q \\ &= \hat{\Sigma}\Lambda Q^T \begin{bmatrix} \mathbf{I}_{r\times r} & O_{r\times(p-r)} \\ O_{(p-r)\times r} & O_{(p-r)\times(p-r)} \end{bmatrix} Q \\ &= \hat{\Sigma}\Lambda \mathrm{diag}(s_1, \ldots, s_p) \\ &= \hat{\Sigma}\Lambda. \end{aligned}$$

where $\mathbf{I}_{r\times r}$ is the identity matrix of size $r \times r$, $O_{m\times n}$ is zero matrix of size $m \times n$, and

$$s_j = \begin{cases} 1, \text{if} j \in \{\mu_1, \ldots, \mu_r\} \\ 0, \text{if} j \notin \{\mu_1, \ldots, \mu_r\} \end{cases}.$$

Remark 2.1.1. A group theoretical interpretation of admissible cycles Σ and the associated matrices $\mathbf{J^0}$ and $\mathbf{J}$ can be given as follows:

(a) We denote by $\mathbb{Z}_p$ the cyclic group of order p defined by addition of integers modulo p. Viewed as permutation group, the generator of $\mathbb{Z}_p$, addition by 1 mod p, corresponds to the cyclic permutation $\{0, 1, \ldots, p-1\} \to \{1, 2, \ldots, p-1, 0\}$, and the matrix $\mathbf{P}$ is an orthogonal representation of this generator in $\mathbb{R}^p$ or $\mathbb{C}^p$ that cyclically permutes row vectors to the left. Accordingly, the matrices $\mathbf{P}^k$, $0 \leq k < p$, form a p-dimensional representation of $\mathbb{Z}_p$ with $\mathbf{P}^p = \mathbf{I}$, the $p \times p$ identity matrix.

(b) The admissibility condition $\mathrm{span}\{\mathrm{R}(\Sigma)\} = \mathrm{span}\{\mathrm{R}(\Sigma\mathbf{P})\}$ means that the rows of Σ span a subspace of $\mathbb{R}^p$ or $\mathbb{C}^p$ that is invariant under $\mathbf{P}$, and hence under the full representation of $\mathbb{Z}_p$, that is,

$$\mathrm{span}\{\mathrm{R}(\Sigma)\} = \mathrm{span}\{\mathrm{R}(\Sigma\mathbf{P}^k)\},\ 0 \le k < p.$$

Moreover, with $\mathbf{J} = \Sigma\mathbf{P}\Sigma^+$ and $\Sigma\mathbf{P}\Sigma^+\Sigma = \Sigma\mathbf{P}$, we find that $\mathbf{J}^2 = \Sigma\mathbf{P}^2\Sigma^+$ and inductively

$$\mathbf{J}^k = \Sigma\mathbf{P}^k\Sigma^+,\ 0 \le k < p, \tag{2.4}$$

which shows that $\mathbf{J}^p = \Sigma\Sigma^+ = \mathbf{J^0}$ and $\mathbf{J}^k\Sigma = \Sigma\mathbf{P}^k$ for $0 \le k < p$. This means that $\mathbf{J}$ restricted to the column space $\mathrm{span}\{\mathrm{C}(\Sigma)\}$, where $\mathrm{C}(\Sigma)$ denotes the set of column vectors of Σ, generates a representation of $\mathbb{Z}_p$ in this subspace of $\mathbb{R}^N$. We also note that $\mathbf{J}^0$ is the orthogonal projection onto $\mathrm{span}\{\mathrm{C}(\Sigma)\}$, and

$$\mathbf{J^0}\mathbf{J}^k = \mathbf{J}^k\mathbf{J^0} = \mathbf{J}^k, \tag{2.5}$$

for all $0 \le k < p$, which is a straightforward consequence of the basic properties $\Sigma\Sigma^+\Sigma = \Sigma$ and $\Sigma^+\Sigma\Sigma^+ = \Sigma^+$ of the pseudoinverse and (2.4). Clearly, the ranks of $\mathbf{J}$, $\mathbf{J^0}$ and Σ coincide and are equal to the dimensions of the vector spaces $\mathrm{span}\{\mathrm{C}(\Sigma)\}$ and $\mathrm{span}\{\mathrm{R}(\Sigma)\}$ in which $\mathbb{Z}_p$ acts with matrix generators $\mathbf{J}$ and $\mathbf{P}$, respectively.

(c) The group $\mathbb{Z}_p$ has exactly p irreducible complex representations which are all one-dimensional and are generated by multiplication of a complex number by $\bar{\rho}^k$, $0 \le k < p$ [71]. When restricted to real spaces and $\rho^k \notin \mathbb{R}$, the multiplications by $\bar{\rho}^k$ and $\rho^k = \bar{\rho}^{p-k}$ can be combined to form a two-dimensional real irreducible representation space, in which the generator of $\mathbb{Z}_p$ acts by rotation of vectors by the angle $2\pi k/p$. For the representation of $\mathbb{Z}_p$ in the full space of p-dimensional row vectors generated by $\mathbf{P}$, the rows in V^* are (complex) basis vectors for these irreducible subspaces, and those basis vectors with eigenvalues $\bar{\rho}^k$ for which $\hat{\Sigma}$ has a nonzero column span the irreducible subspaces in $\mathrm{span}\{\mathrm{R}(\Sigma)\}$. (Real bases in case of $\bar{\rho}^k \notin \mathbb{R}$ are obtained by taking real and imaginary parts of these vectors, but we prefer to use the complex basis vectors.) Likewise, the non-zero columns of $\hat{\Sigma}$ form complex bases of the irreducible subspaces of the $\mathbb{Z}_p$-representation generated by $\mathbf{J}$ in $\mathrm{span}\{\mathrm{C}(\Sigma)\}$. We note that, given a row-vector $x \in \mathbb{C}^p$, xV is the discrete Fourier transform of x, and the components of xV are the expansion coefficients of x represented by the basis vectors in V^*/p.

Closely related to the group $\mathbb{Z}_p$ are the p-th roots of unity, which in turn are intimately related to the cyclotomic polynomials. In sections 2.1 to 2.3 we will make some use of these polynomials and therefore summarize their basic properties in the appendix.

(d) Given a row-vector $x \in \mathbb{R}^p$, the orbit of x under $\mathbf{P}$ is defined as the the set $\{x, x\mathbf{P}, \ldots, x\mathbf{P}^{p-1}\}$. For generic $x \in \mathbb{R}^p$, this set is a basis of $\mathbb{R}^p$, however the set of binary row vectors, $x = \eta$, is finite and the orbit of η, which we call a loop, may span only a proper subspace of $\mathbb{R}^p$. In the next section we classify (admissible) cycles according to the decomposition of $\mathrm{R}(\Sigma)$ into sets of rows belonging to different loops. To pursue this, we will introduce a concept of irreducibility that differs from the standard group-theoretical version above.

2.2 Classification of Cycles

2.2.1 Simple Cycles

Definition 2.2.1. Let $\eta = (\eta^1, \eta^2, \ldots, \eta^p)$ be a p-dimensional binary row vector. The set

$$\{\eta_\nu : \eta_\nu = \eta\mathbf{P}^\nu, \nu = 0, 1, 2, \ldots, p-1\},$$

is called a *loop* and is denoted by $\mathcal{L}_\eta$.

Remark 2.2.1. For any loop $\mathcal{L}_\eta$, $|\mathcal{L}_\eta| \leq p$. More precisely, $|\mathcal{L}_\eta| = m$, where m is a factor of p. In particular, if $\eta = (+, +, \ldots, +)$, then $|\mathcal{L}_\eta| = 1$, as $\eta\mathbf{P} = \eta$.

Definition 2.2.2. A cycle Σ is called *simple*, if its row vectors are from a loop generated by some row vector η, i.e.,

$$\mathrm{R}(\Sigma) \subseteq \mathcal{L}_\eta. \tag{2.6}$$

A cycle Σ is *composite*, if it is not simple.

Definition 2.2.3. Let Σ be a cycle. The set $G_\Sigma = \{\eta_1, \eta_2, \ldots, \eta_q\}$ is said to be a *generator* of Σ, if

$$\mathcal{L}_{\eta_i} \cap \mathcal{L}_{\eta_j} = \emptyset, \forall i \neq j, \tag{2.7}$$

and

$$G_\Sigma = \{\eta_1, \eta_2, \ldots, \eta_q\} \subseteq \mathrm{R}(\Sigma) \subseteq \bigcup_{i=1}^{q} \mathcal{L}_{\eta_i}. \tag{2.8}$$

Note that any vector in $\mathcal{L}_{\eta_i} \cap \mathrm{R}(\Sigma)$ can be chosen as generator instead of η_i in G_Σ, that is, the generators are unique up to cyclic permutations and the condition to be vectors in $\mathrm{R}(\Sigma)$. In particular, for simple cycles there is only one generator, $|G_\Sigma| = 1$, and every row in $\mathrm{R}(\Sigma)$ can be chosen for this generator. A simple criterion for admissibility is the following.

Proposition 2.2.1. *A cycle Σ is admissible if $\mathcal{L}_\eta \subset \mathrm{span}\{\mathrm{R}(\Sigma) \cap \mathcal{L}_\eta\}$ for every $\eta \in G_\Sigma$.*

Proof: This follows immediately from the fact that, under the given hypothesis, every row in $\mathrm{R}(\Sigma\mathbf{P})$ can be represented as linear combination of a subset of rows in $\mathrm{R}(\Sigma)$.

Definition 2.2.4. Let η be any row vector. The *rank* of η is defined as the dimension of the vector space spanned by the row vectors in the loop generated by η, i.e.,

$$\mathrm{rank}(\eta) = \dim \mathrm{span}\{\mathcal{L}_\eta\}. \tag{2.9}$$

Theorem 2.2.2. *Let Σ be a simple cycle generated by η, i.e., $\eta \in \mathrm{R}(\Sigma) \subseteq \mathcal{L}_\eta$. Then Σ is admissible, if and only if*

$$\mathrm{rank}(\Sigma) = \mathrm{rank}(\eta). \tag{2.10}$$

Proof: Suppose $\mathrm{rank}(\Sigma) = \mathrm{rank}(\eta)$. Then $\mathrm{span}\{\mathrm{R}(\Sigma)\} = \mathrm{span}\{\mathcal{L}_\eta\}$ as $\mathrm{R}(\Sigma) \subseteq \mathcal{L}_\eta$. Since $\mathbf{P}$ is nonsingular and $\mathcal{L}_\eta\mathbf{P} = \mathcal{L}_\eta$, it follows that $\mathrm{span}\{\mathrm{R}(\Sigma\mathbf{P})\} = \mathrm{span}\{\mathcal{L}_\eta\}$, hence Σ is admissible. Conversely, suppose that Σ is admissible, i.e. $\mathrm{span}\{\mathrm{R}(\Sigma)\} = \mathrm{span}\{\mathrm{R}(\Sigma\mathbf{P}^m)\}$ for all $m \in \mathbb{N}$. Assume $\mathrm{rank}(\Sigma) < \mathrm{rank}(\eta)$. Then there exists $\hat{\eta} \in \mathcal{L}_\eta$ with $\hat{\eta} \notin \mathrm{span}\{\mathrm{R}(\Sigma)\}$. Let $\hat{\eta} = \eta\mathbf{P}^\mu$ for some $0 < \mu < p$. Since $\eta \in \mathrm{R}(\Sigma)$, it follows that

$$\hat{\eta} \in \mathrm{R}(\Sigma\mathbf{P}^\mu) \subset \mathrm{span}\{\mathrm{R}(\Sigma\mathbf{P}^\mu)\} = \mathrm{span}\{\mathrm{R}(\Sigma)\},$$

which contradicts $\hat{\eta} \notin \mathrm{span}\{\mathrm{R}(\Sigma)\}$.

Remark 2.2.2. In general, although $\mathbf{P}$ preserves the rank of any cycle Σ, the vector space spanned by the row vectors of Σ may not be invariant under $\mathbf{P}$. For simple cycles, the condition (2.10) guarantees that the vector space spanned by the rows of Σ is invariant under $\mathbf{P}$, and hence guarantees the admissibility of Σ. The condition (2.10) will be referred to as *admissibility condition* for simple cycles.

2.2.2 Separable Composite Cycles

In order to generalize the class of simple admissible cycles to the class of separable composite cycles, we first introduce the concept of decomposability of the row space of a cycle into irreducible subspaces.

Definition 2.2.5. Let Σ be an admissible cycle of period p, and let $\mathcal{U} = \text{span}\{\text{R}(\Sigma)\}$. Note that admissibility implies $\mathcal{U}\mathbf{P} = \mathcal{U}$, i.e. $\mathcal{U}$ is invariant under $\mathbf{P}$. Let $\mathcal{V} \subseteq \mathcal{U}$ be a subspace of $\mathcal{U}$ and assume $\mathcal{V}\mathbf{P} = \mathcal{V}$ and $\text{R}(\Sigma) \cap \mathcal{V} \neq \emptyset$. Then

(a) The subspace $\mathcal{V}$ is called *reducible* if there exists a proper subspace $\mathcal{W}$ of $\mathcal{V}$ such that $\mathcal{W}\mathbf{P} = \mathcal{W}$ and $\text{R}(\Sigma) \cap \mathcal{W} \neq \emptyset$.

(b) The subspace $\mathcal{V}$ is said to be *decomposable*, if $\mathcal{V}$ has the direct sum decomposition

$$\mathcal{V} = \mathcal{V}_1 \oplus \mathcal{V}_2 \oplus \cdots \oplus \mathcal{V}_n, \tag{2.11}$$

where $n \geq 2$, $\mathcal{V}_i$ is invariant under $\mathbf{P}$ and $\mathcal{V}_i \cap \text{R}(\Sigma) \neq \emptyset$ for every $1 \leq i \leq n$. The subspace $\mathcal{V}$ is said to be *indecomposable*, if it is not decomposable. If $\mathcal{V}_i$ in (2.11) is indecomposable for every i, then (2.11) is called a *complete decomposition* of $\mathcal{V}$.

(c) The vector space $\mathcal{U}$ is called *semisimple*, if $\mathcal{U}$ is the direct sum of irreducible subspaces in the sense of (a). Note that semisimplicity of $\mathcal{U}$ includes the case where $\mathcal{U}$ is irreducible, in which case we call $\mathcal{U}$ simple.

Remark 2.2.3. We emphasize that, because our purpose is to study the structure of the invariant subspaces spanned by the row vectors of Σ, the concepts of *reducibility* and *decomposability* introduced in Definition 2.2.5 are slightly different from the standard definitions used in the representation theory of finite groups (we require that each subspace contains a row vector of Σ). An irreducible/indecomposable invariant subspace in the sense of Definition 2.2.5 may be reducible/decomposable in terms of the standard definitions of representation theory applied to the cyclic group $\mathbb{Z}_p$ generated by $\mathbf{P}$.

It is clear that if Σ is simple and admissible, then $\mathcal{U}$ is simple and consequently indecomposable, as $\eta \in \mathcal{U}_i$ implies that $\eta\mathbf{P}^k \in \mathcal{U}_i$ for every $k \in \mathbb{N}$. However, the converse is not necessarily true. In the next example, we show that the vector space spanned by the row vectors of a composite cycle may be reducible but not decomposable.

Example 2.2.1. Consider

$$\Sigma = \begin{pmatrix} + & + & + & - & - & - \\ + & + & - & - & - & + \\ + & - & - & - & + & + \\ + & - & + & - & + & - \end{pmatrix},$$

and let $\eta_j = \mathrm{row}_j(\Sigma)$. Clearly, Σ is a composite cycle, as it is generated by $\{\eta_1, \eta_4\}$. Let $\mathcal{U} = \mathrm{span}\{\mathrm{R}(\Sigma)\}$, $\mathcal{U}_1 = \mathrm{span}\{\mathcal{L}_{\eta_1}\}$ and $\mathcal{U}_2 = \mathrm{span}\{\mathcal{L}_{\eta_4}\}$. Since $\eta_4 = \eta_1 - \eta_2 + \eta_3$, i.e. $\eta_4 \in \mathcal{U}_1$, we have that $\mathcal{U}_2 \subset \mathcal{U}_1 = \mathcal{U}$. Moreover, $\mathrm{R}(\Sigma\mathbf{P}) = \{\eta_2, \eta_3, -\eta_1, -\eta_4\}$ implies $\mathcal{U}\mathbf{P} = \mathcal{U}$, hence Σ is admissible. Since both $\mathcal{U}_1$ and $\mathcal{U}_2$ are invariant under $\mathbf{P}$ it follows that $\mathcal{U}$ is reducible, however, $\mathcal{U}$ is not decomposable.

Proposition 2.2.3. *Let Σ be an admissible cycle with generator $G_\Sigma = \{\eta_1, \ldots, \eta_q\}$. Assume $\mathcal{U} = \mathrm{span}\{\mathrm{R}(\Sigma)\}$ is semisimple and let $\mathcal{U} = \mathcal{U}_1 \oplus \mathcal{U}_2 \oplus \cdots \oplus \mathcal{U}_n$ be a decomposition of $\mathcal{U}$ into irreducible subspaces. Then $n \leq q$ and there exists a subset $\{i_1, \ldots, i_n\} \subseteq \{1, \ldots, q\}$ such that $\mathcal{U}_j = \mathrm{span}\{\mathcal{L}_{\eta_{i_j}}\}$ for $1 \leq j \leq n$. Moreover, if $\mathrm{span}\{\mathcal{L}_{\eta_i}\} \neq \mathrm{span}\{\mathcal{L}_{\eta_j}\}$ for every $i, j \in \{1, \ldots, q\}$ with $i \neq j$, then $n = q$.*

Proof: Let $\eta \in G_\Sigma$ and let $\mathcal{V} \in \{\mathcal{U}_j | 1 \leq j \leq n\}$ be the subspace in the decomposition of $\mathcal{U}$ that contains η. Invariance of $\mathcal{V}$ implies $\eta\mathbf{P} \in \mathcal{V}$, hence $\eta\mathbf{P}^2 \in \mathcal{V}$ and by induction $\mathcal{L}_\eta \subset \mathcal{V}$, thus $\mathrm{span}\{\mathcal{L}_\eta\} \subset \mathcal{V}$. Since $\mathrm{span}\{\mathcal{L}_\eta\}$ is invariant, $\mathrm{span}\{\mathcal{L}_\eta\} \cap \mathrm{R}(\Sigma) \neq \emptyset$ and $\mathcal{V}$ is irreducible, it follows that $\mathcal{V} = \mathrm{span}\{\mathcal{L}_\eta\}$, and there exists no $\eta' \in G_\Sigma$, $\eta' \neq \eta$, such that $\mathrm{span}\{\mathcal{L}_{\eta'}\}$ is a proper subspace of $\mathrm{span}\{\mathcal{L}_\eta\}$ and vice versa. Thus, for $i \neq j$, either $\mathrm{span}\{\mathcal{L}_{\eta_i}\} \cap \mathrm{span}\{\mathcal{L}_{\eta_j}\} = \{\mathbf{0}\}$ or $\mathrm{span}\{\mathcal{L}_{\eta_i}\} = \mathrm{span}\{\mathcal{L}_{\eta_j}\}$. It follows that there exists $i_1, \ldots, i_n \in \{1, \ldots, q\}$, $i_j \neq i_k$ if $j \neq k$, such that

$$\mathrm{span}\{\mathrm{R}(\Sigma)\} = \mathrm{span}\{\bigcup_{i=1}^{q} \mathcal{L}_{\eta_i}\} = \bigoplus_{j=1}^{n} \mathrm{span}\{\mathcal{L}_{\eta_{i_j}}\}.$$

Example 2.2.2. Let $\eta_1 = (+, +, -, +, +, -)$, $\eta_2 = -\eta_1$ and $\eta_3 = (+, +, +, -, -, -)$. Let Σ be the 9×6-cycle defined by

$$\Sigma = (\Sigma_1^T, \Sigma_2^T, \Sigma_3^T)^T,$$

where $\Sigma_j = (\eta_j^T, (\eta_j \mathbf{P})^T, (\eta_j \mathbf{P}^2)^T)^T$ for $j = 1, 2, 3$. Then $G_\Sigma = \{\eta_1, \eta_2, \eta_3\}$, $\text{span}\{\text{R}(\Sigma)\} = \text{span}\{\mathcal{L}_{\eta_1}\} \oplus \text{span}\{\mathcal{L}_{\eta_3}\}$, and $\text{span}\{\mathcal{L}_{\eta_2}\} = \text{span}\{\mathcal{L}_{\eta_1}\}$. Clearly, $\text{span}\{\mathcal{L}_{\eta_1}\}$ and $\text{span}\{\mathcal{L}_{\eta_3}\}$ are irreducible, thus $\text{span}\{\text{R}(\Sigma)\}$ is semisimple. Likewise, for the cycle $\Sigma = (\Sigma_1^T, \Sigma_2^T)$, $\text{span}\{\text{R}(\Sigma)\} = \text{span}\{\mathcal{L}_{\eta_i}\}$, $i = 1, 2$, hence $\text{span}\{\text{R}(\Sigma)\}$ is simple.

In general, the vector space $\mathcal{U} = \text{span}\{\text{R}(\Sigma)\}$ of an arbitrary composite cycle Σ may have subspaces which are not invariant or do not contain any binary row vector of Σ, or both. By contrast, if $\mathcal{U}$ is semisimple, $\mathcal{U}$ can be decomposed into irreducible subspaces corresponding to the loops of their generators, but some of these subspaces may coincide. This coincidence is still considered as a degeneracy (see Section 4.3), which we exclude in the class of separable cycles introduced next.

Definition 2.2.6. Let Σ be a composite cycle with generator G_Σ, i.e. $|G_\Sigma| \geq 2$. We call Σ *separable*, if $\text{span}\{\text{R}(\Sigma)\}$ is semisimple and $\text{span}\{\mathcal{L}_\eta\} \neq \text{span}\{\mathcal{L}_{\eta'}\}$ for any $\eta, \eta' \in G_\eta$ with $\eta \neq \eta'$. If Σ is not separable, Σ is said to be *inseparable*.

Note that the hypotheses for a cycle Σ to be separable require that $\mathcal{U} = \text{span}\{\text{R}(\Sigma)\}$ is invariant under $\mathbf{P}$, i.e. separable cycles are a priori admissible.

Theorem 2.2.4. *(**Separability Condition for Composite Cycles**) Let Σ be a composite cycle with generator $G_\Sigma = \{\eta_1, \eta_2, \ldots, \eta_q\}$. Then Σ is separable, if and only if*

$$\text{rank}(\Sigma) = \sum_{i=1}^{q} \text{rank}(\eta_i). \tag{2.12}$$

Proof: If Σ is separable, (2.12) follows directly from Proposition 2.2.3 and Definition 2.2.6.

Conversely, suppose (2.12) holds. Since

$$\text{span}\{\text{R}(\Sigma)\} = \text{span}\{(\bigcup_{i=1}^{q} \mathcal{L}_{\eta_i}) \cap \text{R}(\Sigma)\} \subseteq \text{span}\{\bigcup_{i=1}^{q} \mathcal{L}_{\eta_i}\},$$

(2.12) implies that $\text{span}\{\mathcal{L}_{\eta_i} \cap \text{R}(\Sigma)\} = \text{span}\{\mathcal{L}_{\eta_i}\}$ for each $1 \leq i \leq q$, $\text{span}\{\mathcal{L}_{\eta_i}\} \cap \text{span}\{\mathcal{L}_{\eta_j}\} = \{\mathbf{0}\}$, if $i \neq j$, and hence

$$\text{span}\{\text{R}(\Sigma)\} = \bigoplus_{i=1}^{q} \text{span}\{\mathcal{L}_{\eta_i}\}.$$

It follows that each span$\{\mathcal{L}_{\eta_i}\}$ is irreducible, thus Σ is separable according to Definitions 2.2.5 and 2.2.6.

Example 2.2.3. Consider

$$\Sigma = \begin{pmatrix} + & + & + & + & - & - & - & - \\ + & + & + & - & - & - & - & + \\ + & + & - & - & - & - & + & + \\ + & - & - & - & - & + & + & + \\ + & + & - & - & + & + & - & - \\ + & - & - & + & + & - & - & + \\ + & - & + & - & + & - & + & - \end{pmatrix}.$$

We have that $G_\Sigma = \{\eta_1, \eta_5, \eta_7\}$, where $\eta_j = \text{row}_j(\Sigma)$, $1 \leq j \leq 7$. It is easy to see that $\mathcal{U}_1 = \text{span}\{\mathcal{L}_{\eta_1}\}$, $\mathcal{U}_2 = \text{span}\{\mathcal{L}_{\eta_5}\}$, and $\mathcal{U}_3 = \text{span}\{\mathcal{L}_{\eta_7}\}$ intersect trivially, hence

$$\mathcal{U} = \text{span}(\text{R}(\Sigma)) = \mathcal{U}_1 \oplus \mathcal{U}_2 \oplus \mathcal{U}_3,$$

which implies that Σ is separable, and hence admissible.

2.2.3 Inseparable Composite Cycles

By Definition 2.2.6, inseparability of a composite cycle Σ happens in two different cases. In the first case, the vector space $\mathcal{U} = \text{span}\{\text{R}(\Sigma)\}$ has a reducible but indecomposable invariant subspace, which entirely contains another invariant subspace as a subspace (see Example 2.2.1). This includes the case where $\mathcal{U}$ is semisimple and $\text{span}\{\mathcal{L}_\eta\} = \text{span}\{\mathcal{L}_{\eta'}\}$ for two different generators η and η' (see Example 2.2.2). In the second case, the vector space $\mathcal{U}$ has two or more indecomposable (reducible or not) invariant subspaces sharing a nontrivial intersection as common proper subspaces. We now discuss the admissibility of these two types of inseparable composite cycles.

Definition 2.2.7. Let $G_\Sigma = \{\eta_1, \eta_2, \ldots, \eta_q\}$ be a generator of a cycle Σ. A subset $EG_\Sigma = \{\epsilon_1, \epsilon_2, \ldots, \epsilon_r\}$, $r \leq q$, of G_Σ is called an *essential generator* of Σ, if EG_Σ is minimal in the sense that

(a) $\text{span}\{\text{R}(\Sigma)\} \subseteq \text{span}\{\bigcup_{i=1}^{r} \mathcal{L}_{\epsilon_i}\}$;

(b) for any ϵ_i, $\epsilon_j \in EG_\Sigma$ with $i \neq j$, $\text{span}(\mathcal{L}_{\epsilon_i}) \cap \text{span}(\mathcal{L}_{\epsilon_j})$ is a proper subspace of both $\text{span}(\mathcal{L}_{\epsilon_i})$ and $\text{span}(\mathcal{L}_{\epsilon_j})$;

(c) for every $\eta_i \in G_\Sigma$, if $\eta_i \notin \text{span}\{\bigcup_{j=1,j\neq i}^{q} \mathcal{L}_{\eta_j}\}$, then $\eta_i \in EG_\Sigma$.

Note that an admissible cycle may have different sets of essential generators, i.e. EG_Σ is in general not unique. Proposition 2.2.1 can be directly rephrased in terms of essential generators.

Proposition 2.2.5. *A cycle Σ is admissible, if for any essential generator EG_Σ, $\mathcal{L}_\epsilon \subset \text{span}\{\text{R}(\Sigma) \cap \mathcal{L}_\epsilon\}$ for every $\epsilon \in EG_\Sigma$. Conversely, if Σ is admissible and $EG_\Sigma = \{\epsilon_1, \ldots, \epsilon_r\}$ is an essential generator of Σ, then*

$$\text{rank}(\Sigma) \leq \sum_{i=1}^{r} \text{rank}(\epsilon_i) \leq |\text{R}(\Sigma)| \leq N. \tag{2.13}$$

Remark 2.2.4. The condition (b) in Definition 2.2.7 includes three cases.

(a) For every $i \neq j$, $\text{span}\{\mathcal{L}_{\epsilon_i}\} \cap \text{span}\{\mathcal{L}_{\epsilon_j}\} = \{\mathbf{0}\}$, and $q = r$. Composite cycles in this case are separable.

(b) For every $i \neq j$, $\text{span}\{\mathcal{L}_{\epsilon_i}\} \cap \text{span}\{\mathcal{L}_{\epsilon_j}\} = \{\mathbf{0}\}$, but $q < r$. Composite cycles in this case are inseparable and degenerate. In this case $\mathcal{U}$ may be semisimple or not, and has the complete decomposition $\mathcal{U} = \bigoplus_{i=1}^{q} \text{span}\{\mathcal{L}_{\epsilon_i}\}$ (see Proposition 2.2.3). Accordingly, we have that a degenerately inseparable composite cycle Σ is admissible, if and only if $\text{rank}(\Sigma) = \sum_{i=1}^{q} \text{rank}(\epsilon_i)$. This generalizes separable cycles and includes, for example, the case where for some $\eta \in \text{R}(\Sigma)$ also $-\eta \in \text{R}(\Sigma)$, but $\mathcal{L}_\eta \cap \mathcal{L}_{-\eta} = \emptyset$ (see Example 2.2.2).

(c) For some $i \neq j$, $\text{span}\{\mathcal{L}_{\epsilon_i}\} \cap \text{span}\{\mathcal{L}_{\epsilon_j}\}$ is a nontrivial proper subspace of both invariant subspaces $\text{span}\{\mathcal{L}_{\epsilon_i}\}$ and $\text{span}\{\mathcal{L}_{\epsilon_j}\}$. Composite cycles in this case are genuinely inseparable. This type of cycles is more complicated than the other two. We next study the structure of this type of cycles, and establish an admissibility condition.

Proposition 2.2.6. *Let η and $\tilde{\eta}$ be two p-dimensional row vectors. If $\eta \in \text{span}\{\mathcal{L}_{\tilde{\eta}}\}$, then $\text{span}\{\mathcal{L}_\eta\} \subseteq \text{span}\{\mathcal{L}_{\tilde{\eta}}\}$.*

Proof: If $\eta \in \mathcal{L}_{\tilde{\eta}}$, we are done. Suppose $\eta \in \mathrm{span}\{\mathcal{L}_{\tilde{\eta}}\}$, i.e., $\eta = \sum_{\nu=1}^{p} \alpha_\nu \tilde{\eta}\mathbf{P}^\nu$, $\alpha_\nu \in \mathbb{R}$, but $\eta \notin \mathcal{L}_{\tilde{\eta}}$, then for every $t \in \{1, 2, \ldots, p\}$, $\eta\mathbf{P}^t = \left(\sum_{\nu=1}^{p} \alpha_\nu \tilde{\eta}\mathbf{P}^\nu\right)\mathbf{P}^t = \sum_{\nu=1}^{p} \left(\alpha_\nu \tilde{\eta}\mathbf{P}^{\nu+t}\right)$, i.e., $\mathcal{L}_\eta \subseteq \mathrm{span}\{\mathcal{L}_{\tilde{\eta}}\}$, hence $\mathrm{span}\{\mathcal{L}_\eta\} \subseteq \mathrm{span}\{\mathcal{L}_{\tilde{\eta}}\}$.

Remark 2.2.5. Proposition 2.2.6 tells that if a row vector is in the vector space spanned by the loop generated by another row vector of the same dimension, then the vector space spanned by the loop generated by this row vector is a subspace of the vector space spanned by the other one. Since for any genuinely inseparable composite cycle, at least two indecomposable invariant subspaces intersect nontrivially, it is natural to ask:

(a) Does there exist a row vector such that this nontrivial intersection is spanned by the loop generated by it?

(b) If this row vector exists, can it be $\{-1, 1\}$-valued?

As we will see below in Proposition 2.2.9, the answer to the first question is affirmative, however, it remains unclear whether there always exists a binary row vector such that the loop generated by it spans the nontrivial intersection of two indecomposable invariant subspaces. The approach we will use in the proof of Proposition 2.2.9 only guarantees the existence of a genuine row vector, which may or may not be binary.

Let V be defined as in Theorem 2.1.2, i.e. $V = (v^{(0)}, v^{(1)}, \ldots, v^{(p-1)})$, where $v^{(k)} = (1, \rho^k, \rho^{2k}, \ldots, \rho^{(p-1)k})^T$ and $\rho = e^{2\pi\mathbf{i}/p}$.

Definition 2.2.8. A row vector η (not necessarily binary) is said to *annihilate* the column $v^{(k)}$ of V, if $\eta v^{(k)} = 0$, i.e. the two vectors are orthogonal.

Note that, since $v^{(k)}$ is an eigenvector of $\mathbf{P}$ and all eigenvalues of $\mathbf{P}$ are nonzero, η annihilates $v^{(k)}$ if and only if $\eta\mathbf{P}^\nu$ annihilates $v^{(k)}$ for every $\nu \in \mathbb{Z}$. We need the following fact about the eigenvectors and eigenvalues of circulant matrices, see, e.g., [70].

Lemma 2.2.7. *Let $\eta = (\eta^1, \ldots, \eta^p)$ be an arbitrary real and nonzero row vector, and let Σ_η be the $p \times p$-matrix defined by $\mathrm{row}_j(\Sigma_\eta) = \eta(\mathbf{P}^T)^{(j-1)}$ for $1 \leq j \leq p$. Then $V^*\Sigma_\eta = \Lambda_\eta V^*$, where $\Lambda_\eta = \mathrm{diag}(\lambda_{\eta,1}, \ldots, \lambda_{\eta,p})$ with $\lambda_{\eta,k} = \sum_{j=1}^{p} \eta^j \rho^{(j-1)(k-1)}$.*

Extending Definition 2.2.1 to non-binary real row vectors and noting that $\mathrm{R}(\Sigma_\eta) = \mathcal{L}_\eta$, an immediate consequence of Lemma 2.2.7 is the following:

Corollary 2.2.8. *Assume that $\eta v^{(j)} \neq 0$ if and only if $j \in \{k_1, \ldots, k_s\} \subset \mathbb{Z}_p$, where $\mathbb{Z}_p = \{0, 1, 2, \ldots, p-1\}$. Then $\{v^{(k_1)*}, \ldots, v^{(k_s)*}\}$ is a (complex) basis for* $\mathrm{span}\{\mathcal{L}_\eta\}$.

Proposition 2.2.9. *Let Σ be a cycle with essential generator $EG_\Sigma = \{\epsilon_1, \ldots, \epsilon_r\}$. Assume that for some $i \neq j$ the indecomposable subspaces $\mathcal{U}_i = \mathrm{span}(\mathcal{L}_{\epsilon_i})$ and $\mathcal{U}_j = \mathrm{span}(\mathcal{L}_{\epsilon_j})$ intersect nontrivially, and $\mathcal{U}_i \cap \mathcal{U}_j$ is a proper subspace of both $\mathcal{U}_i$ and $\mathcal{U}_j$. Then there exists a row vector η such that* $\mathcal{U}_i \cap \mathcal{U}_j = \mathrm{span}\{\mathcal{L}_\eta\}$.

Proof: Assume that $\epsilon_i v^{(k)} \neq 0$ and $\epsilon_j v^{(k)} \neq 0$ if and only if $k \in K_i \subset \mathbb{Z}_p$ and $k \in K_j \subset \mathbb{Z}_p$, respectively. Assume further that $K \equiv K_i \cap K_j = \{k_1, \ldots, k_s\}$. According to Corollary 1, $\{v^{(k_1)*}, \ldots, v^{(k_s)*}\}$ is a basis for $\mathcal{U}_i \cap \mathcal{U}_j$. Let $p_i(x)$ and $p_j(x)$, $x \in \mathbb{C}$, be the polynomials $p_i(x) = \epsilon_i \mathbf{x}$, $p_j(x) = \epsilon_j \mathbf{x}$, where $\mathbf{x} = (1, x, x^2, \ldots, x^{p-1})^T$. Since the row vectors defined by the coefficients of $p_i(x)$ and $p_j(x)$ annihilate exactly the $v^{(k)}$ with $k \in \mathbb{Z}_p \backslash K_i$ and $k \in \mathbb{Z}_p \backslash K_j$, respectively, $p_i(x)$ and $p_j(x)$ contain the minimal polynomials of ρ^k for every $k \in \mathbb{Z}_p \backslash K_i$ and $k \in \mathbb{Z}_p \backslash K_j$, respectively, as factors. Multiplying these factors yields a polynomial $p_{ij}(x)$ of degree $\leq p-1$ with $p_{ij}(\rho^k) = 0$ for every $k \in \mathbb{Z}_p \backslash K$ and $p_{ij}(\rho^k) \neq 0$ for every $k \in K$. Set $p_0(x) = p_{ij}(x)$ if the degree of $p_{ij}(x)$ is $p-1$. If the degree of $p_{ij}(x)$ is $< p-1$, set $p_0(x) = p_{ij}(x)\tilde{p}_{ij}(x)$, where $\tilde{p}_{ij}(x)$ is any polynomial such that $\tilde{p}_{ij}(\rho^k) \neq 0$ for every $k \in K$ and the degree of $p_0(x)$ is $p-1$. Let η be the row vector of coefficients of $p_0(x)$. Then η and $\eta \mathbf{P}^\nu$ for any $\nu \in \mathbb{Z}$ annihilate every $v^{(k)}$ for $k \in \mathbb{Z}_p \backslash K$, and $\eta v^{(k)} \neq 0$ for every $k \in K$, hence $\mathrm{span}\{\mathcal{L}_\eta\} = \mathrm{span}\{v^{(k_1)*}, \ldots, v^{(k_s)*}\} = \mathcal{U}_i \cap \mathcal{U}_j$.

Example 2.2.4. In this example, we demonstrate how to find a row vector as claimed in Proposition 2.2.9 with the method described in the proof. Consider the composite cycle with $N = 10$ and $p = 18$ defined by $\Sigma = (\Sigma_1^T, \Sigma_2^T)^T$, where

$$\Sigma_1 = (\epsilon_1^T, (\epsilon_1 \mathbf{P})^T, \ldots, (\epsilon_1 \mathbf{P}^6)^T)^T, \Sigma_2 = (\epsilon_2^T, (\epsilon_2 \mathbf{P})^T, (\epsilon_1 \mathbf{P}^2)^T)^T,$$

and

$$\epsilon_1 = (\ +\ +\ +\ +\ +\ +\ +\ -\ +\ -\ -\ -\ -\ -\ -\ -\ +\ -\ ),$$
$$\epsilon_2 = (\ +\ +\ +\ -\ -\ -\ +\ +\ +\ -\ -\ -\ +\ +\ +\ -\ -\ -\ ).$$

This is a genuinely inseparable composite cycle with $G_\Sigma = EG_\Sigma = \{\epsilon_1, \epsilon_2\}$. The polynomials $p_1(x)$ and $p_2(x)$ can be factorized as follows,

$$p_1(x) = (1-x)(1+x+x^2)(1-x+x^2)(1+x^3+x^6)(1+2x+2x^2+x^3+x^6),$$
$$p_2(x) = (1-x)(1+x+x^2)(1-x^3+x^6)(1+x^3+x^6)(1+x-x^2).$$

The factors $1-x$, $1+x+x^2$, $1+x^3+x^6$, $1-x+x^2$ and $1-x^3+x^6$ are cyclotomic factors (see e.g. [72]), and the sum of their degrees happens to be 17. Multiplying them out gives

$$p_0(x) = \sum_{j=0}^{17} (-1)^j x^j,$$

thus the row vector η constructed in the proof of Proposition 2.2.9 is obtained as the binary vector with alternating signs, $\eta = (+,-,+,-,\ldots,+,-)$, and $\mathrm{span}\{\mathcal{L}_\eta\} = \mathrm{span}\{\eta\}$. One can easily verify that $\mathrm{span}\{\eta\} = \mathrm{span}\{\mathcal{L}_{\epsilon_1}\} \cap \mathrm{span}\{\mathcal{L}_{\epsilon_2}\}$.

Based on their structural features and using a simple inclusion-exclusion argument, an admissibility condition for inseparable composite cycles can be formulated as follows.

Theorem 2.2.10. *(**Admissibility Condition for Inseparable Composite Cycles**) Let Σ be a cycle with essential generator $EG_\Sigma = \{\epsilon_1, \ldots, \epsilon_r\}$. Then Σ is admissible if and only if*

$$\begin{aligned} \mathrm{rank}(\Sigma) &= \sum_{i=1}^{r} \mathrm{rank}(\epsilon_i) - \sum_{i,j;i\neq j}^{r} \dim(\mathrm{span}\{\mathcal{L}_{\epsilon_i}\} \cap \mathrm{span}\{\mathcal{L}_{\epsilon_j}\}) \\ &+ \sum_{i,j,k;i\neq j\neq k}^{r} \dim(\mathrm{span}\{\mathcal{L}_{\epsilon_i}\} \cap \mathrm{span}\{\mathcal{L}_{\epsilon_j}\} \cap \mathrm{span}\{\mathcal{L}_{\epsilon_k}\}) \\ &- \cdots \pm \dim(\bigcap_{i=1}^{r} \mathrm{span}\{\mathcal{L}_{\epsilon_i}\}). \end{aligned} \tag{2.14}$$

Remark 2.2.6. The admissibility condition (2.14) is valid for any cycle, and the conditions (2.12) and (2.10) for separability and admissibility of simple cycles, respectively, can be thought of as special cases thereof.

Example 2.2.5. Let Σ be the cycle from Example 2.2.4. One can easily verify that $\mathrm{rank}(\epsilon_1) = 7$ and $\mathrm{rank}(\epsilon_2) = 3$. Since $\dim(\mathrm{span}\{\mathcal{L}_{\epsilon_1}\} \cap \mathrm{span}\{\mathcal{L}_{\epsilon_2}\}) = 1$, this cycle is admissible.

2.3 Network Topology

To simplify the discussion, we exclude in this section multiple appearances of a binary row vector in a cycle, that is, we consider only cycles Σ with $|\mathrm{R}(\Sigma)| = N$.

The classification of cycles Σ in Section 2.2 was based on the decomposition of $\mathrm{R}(\Sigma)$ into subsets of rows associated with disjoint loops. It is, therefore, natural to identify the neurons corresponding to the same loop with a cluster. However, if a cycle has fewer essential generators than generators, the row vectors of a non-essential generator must be combined with one or more essential generators and, moreover, there may be several choices for essential generators. We therefore make the simplifying assumption that all generators are essential generators. For admissible cycles Σ this means that for any two distinct generators η_1, η_2, the intersection of their spaces $\mathrm{span}\{\mathcal{L}_{\eta_j} \cap \mathrm{R}(\Sigma)\}$, $j = 1, 2$, is a proper subspace of both of them ($\{\mathbf{0}\}$ if the cycle is separable). An immediate consequence of this assumption is that

$$\mathrm{rank}(\Sigma) \leq \sum_{j=1}^{q} \mathrm{rank}(\eta_j) \leq N, \tag{2.15}$$

if Σ is admissible and $G_\Sigma = \{\eta_1, \ldots, \eta_q\}$. The clusters are isolated if and only if Σ is separable. If Σ is inseparable, some of the clusters are connected.

Regarding the connectivity within a cluster, linear dependences among its row vectors will prevent any special structure. We call cycles for which such dependences do not occur minimal.

Definition 2.3.1. An admissible cycle Σ with generator $G_\Sigma = \{\eta_1, \eta_2, \ldots, \eta_q\}$ is *minimal*, if $EG_\Sigma = G_\Sigma$ and for every $1 \leq i \leq q$,

$$|\mathcal{L}_{\eta_i} \cap \mathrm{R}(\Sigma)| = \mathrm{rank}(\eta_i). \tag{2.16}$$

Remark 2.3.1. If Σ is a minimal simple or separable composite cycle, then Σ is of full row rank. If Σ is a minimal inseparable cycle, then the row vectors in $\mathrm{R}(\Sigma) \cap \mathcal{L}_{\eta_i}$ form a basis of $\mathrm{span}\{\mathcal{L}_{\eta_i}\}$ for every $\eta_i \in G_\Sigma$. Thus for any minimal cycle Σ, (2.15) holds and the inequalities become equalities if and only if Σ is simple or separable. In this case, Σ has full row rank and $\Sigma^+ = \Sigma^T(\Sigma\Sigma^T)^{-1}$, which implies that $\mathbf{J^0} = \Sigma\Sigma^+ = \mathbf{I}$, the $N \times N$ identity matrix.

For any two $(N \times p)$-cycles Σ and Σ' with $\mathrm{R}(\Sigma) = \mathrm{R}(\Sigma')$, the cycle matrices are related to each other by $\Sigma' = \mathbf{Q}\Sigma$, where $\mathbf{Q}$ is an $N \times N$ permutation matrix. If in addition Σ is admissible with connectivity matrix $\tilde{\mathbf{J}}$, then Σ' is also admissible and has connectivity matrix $\tilde{\mathbf{J}}' = \mathbf{Q}\tilde{\mathbf{J}}\mathbf{Q}^{-1}$. Accordingly, if $\mathbf{u}$ is the state of the network with connectivity matrix $\tilde{\mathbf{J}}$, then $\mathbf{u}' = \mathbf{Q}\mathbf{u}$ is the network state corresponding to $\tilde{\mathbf{J}}'$, and solutions $\mathbf{u}(t)$ and $\mathbf{u}'(t)$ of the corresponding differential equations are just permutations of each other as $\tanh(\mathbf{u}') = \tanh(\mathbf{Q}^{-1}\mathbf{u}) = \mathbf{Q}^{-1}\tanh(\mathbf{u})$.

Without loss of generality, we therefore may assume that a minimal cycle with generators $\eta_1, \ldots, \eta_q$ has the form

$$\Sigma = (\Sigma_1^T, \Sigma_2^T, \ldots, \Sigma_q^T)^T, \tag{2.17}$$

where $\mathrm{R}(\Sigma_j) \subseteq \mathcal{L}_{\eta_j}$, $1 \leq j \leq q$, and the vectors in Σ_j are sorted from top to bottom as $\eta_j, \eta_{j_1}, \eta_{j_2}, \ldots$, with $\eta_{j_i} = s_{j_i}\eta_j\mathbf{P}^{\nu_{j_i}}$, $s_{j_i} = 1$ if $-\eta_j \notin \mathcal{L}_{\eta_j}$ and $s_{j_i} \in \{-1, 1\}$ if $-\eta_j \in \mathcal{L}_{\eta_j}$, and $0 < \nu_{j_i} < \nu_{j_k}$ if $i < k$. We call this form the *standard form* of a minimal cycle.

The minimality requirement does not suffice in general to induce a special network topology within the clusters. We have to require in addition that the powers in the Σ_j are consecutive.

Definition 2.3.2. A minimal cycle Σ in standard form is said to be a *minimal consecutive cycle*, or briefly MC-cycle, if the powers of $\mathbf{P}$ in Σ_j above are consecutive, that is, $\nu_{j_i} = i$ for all $1 \leq i < \mathrm{rank}(\eta_j)$.

In order that Definition 2.3.2 is consistent with the minimality requirement, the rows in Σ_j must be linearly independent. The next proposition shows that this is indeed the case, where for simplicity we consider only the case $s_{j_i} = 1$.

Proposition 2.3.1. *Let $\eta \neq 0$ be any p-dimensional row vector with $\mathrm{rank}(\eta) = k$. Then the vectors $\{\eta, \eta\mathbf{P}, \eta\mathbf{P}^2, \ldots, \eta\mathbf{P}^{k-1}\}$ are linearly independent.*

Proof: Let s be the largest positive integer such that $\{\eta, \eta\mathbf{P}, \ldots, \eta\mathbf{P}^{s-1}\}$ are linearly independent. Then $\eta\mathbf{P}^s$ is a linear combination of $\{\eta, \eta\mathbf{P}, \ldots, \eta\mathbf{P}^{s-1}\}$,

$$\eta\mathbf{P}^s = \sum_{\nu=0}^{s-1} \alpha_\nu \eta\mathbf{P}^\nu. \tag{2.18}$$

Right-multiplying this equation by $\mathbf{P}$ yields a representation of $\eta\mathbf{P}^{s+1}$ as linear combination of $\{\eta\mathbf{P}, \eta\mathbf{P}^2, \ldots, \eta\mathbf{P}^s\}$, and replacing $\eta\mathbf{P}^s$ in this representation by (2.18) shows that $\eta\mathbf{P}^{s+1}$ is also a

linear combination of $\{\eta, \eta\mathbf{P}, \ldots, \eta\mathbf{P}^{s-1}\}$. By induction we find that, for any $0 \leq \nu < s - p$, $\eta\mathbf{P}^{s+\nu}$ is a linear combination of $\{\eta, \eta\mathbf{P}, \ldots, \eta\mathbf{P}^{s-1}\}$, hence this set is a basis for $\mathcal{L}_\eta$.

For simple MC-cycles there is only one cluster. In Subsection 2.3.1 we discuss the possible connectivity structures in such networks in some detail, including the possible values of N for a given p, and we also comment on the network topology of simple minimal but non-consecutive cycles. Semisimple MC-cycles consist of isolated clusters corresponding to the different loops in the cycle. Each of these loops forms a simple MC-cycle, and we just give an example in Subsection 2.3.2. Inseparable minimal (consecutive or non-consecutive) cycles are more complicated and will be discussed in Subsection 2.3.3. In Subsection 2.3.4 we demonstrate the effects of fewer essential generators than generators by two examples.

2.3.1 Simple MC-Cycles

2.3.1.1 Network Topology

According to Definition 2.3.2, a simple MC-cycle has the form

$$\Sigma = (\eta^T, s_1(\eta\mathbf{P})^T, s_2(\eta\mathbf{P}^2)^T, \ldots, s_{N-1}(\eta\mathbf{P}^{N-1})^T)^T, \tag{2.19}$$

with $\text{rank}(\eta) = N \leq p$ and $s_i \in \{-1, 1\}$. Since the image of the last row vector of Σ under $\mathbf{P}$ is a linear combination of the row vectors of Σ, $\Sigma\mathbf{P}$ has the form $\Sigma\mathbf{P} = \mathbf{A}\Sigma$, where

$$\mathbf{A} = \begin{pmatrix} 0 & s_1 & 0 & \ldots & 0 & 0 \\ 0 & 0 & s_1 s_2 & \ldots & 0 & 0 \\ \vdots & \vdots & \vdots & \ddots & \vdots & \vdots \\ 0 & 0 & 0 & \ldots & s_{N-3}s_{N-2} & 0 \\ 0 & 0 & 0 & \ldots & 0 & s_{N-2}s_{N-1} \\ a_1 & a_2 & a_3 & \ldots & a_{N-1} & a_N \end{pmatrix}, \tag{2.20}$$

with $a_1, \ldots, a_N \in \mathbb{R}$ and $a_1 \neq 0$. Moreover, since Σ has full row rank, $\Sigma^+ = \Sigma^T(\Sigma\Sigma^T)^{-1}$, which implies

$$\mathbf{J} = \Sigma\mathbf{P}\Sigma^+ = \mathbf{A}. \tag{2.21}$$

Equations (2.20) and (2.21) show that the network constructed from a simple MC-cycle consists of a feed-forward chain from the Nth neuron to the first neuron, and feedback to the Nth neuron

from the subset of the neurons for which $a_i \neq 0$, which in any case includes the first neuron. If $a_j = 0$ for $j > 1$, then $a_1 = \pm 1$, and the network topology is that of a ring, with either excitatory ($a_1 = 1$, $\mathbf{J} = \mathbf{P}^T$ if all $s_j = 1$) or inhibitory connection ($a_1 = -1$) from neuron 1 to neuron N. Vectors of the form $\eta = (\sigma, \sigma)$ or $(\sigma, -\sigma)$ have $\text{rank}(\eta) \leq p/2$, and if $\text{rank}(\eta) = p/2 = N$ we have either of these two types of ring structures (see Subsection 2.3.1.3).

Example 2.3.1. In Figure 2.1**A** and **B**, we illustrate the topology of the networks constructed from the following two simple MC-cycles,

$$\Sigma = \begin{pmatrix} + & + & + & + & + & + & + & - & - & - & - & - & - & - \\ + & + & + & + & + & + & - & - & - & - & - & - & - & + \\ + & + & + & + & + & - & - & - & - & - & - & - & + & + \\ + & + & + & + & - & - & - & - & - & - & - & + & + & + \\ + & + & + & - & - & - & - & - & - & - & + & + & + & + \\ + & + & - & - & - & - & - & - & - & + & + & + & + & + \\ + & - & - & - & - & - & - & - & + & + & + & + & + & + \end{pmatrix},$$

and

$$\tilde{\Sigma} = \begin{pmatrix} + & + & - & + & - & - \\ + & - & + & - & - & + \\ - & + & - & - & + & + \\ + & - & - & + & + & - \\ - & - & + & + & - & + \end{pmatrix},$$

respectively. The cycle Σ has a "repeating block structure", $\Sigma = [B, -B]$, where B is the block consisting of the first 7 columns of Σ ($N = p/2 = 7$). This causes the image of the last row to be the negative copy of the first row, i.e. $\eta_7 \mathbf{P} = -\eta_1$, where $\eta_i = \text{row}_i(\Sigma)$. It follows that $a_1 = -1$ and $a_i = 0$ for $i > 1$, thus the first neuron only sends an inhibitory feedback to the seventh neuron (Figure 2.1**A**). Similarly, for the cycle $\tilde{\Sigma}$, $N = p - 1 = 5$, and in this case the image of the last row is a linear combination of all other row vectors, $\tilde{\eta}_5 \mathbf{P} = -\tilde{\eta}_1 - \tilde{\eta}_2 - \tilde{\eta}_3 - \tilde{\eta}_4 - \tilde{\eta}_5$, where $\tilde{\eta}_i = \text{row}_i(\tilde{\Sigma})$. Accordingly for this cycle $a_i = -1$ for every i, i.e. every neuron sends inhibitory feedback to the fifth neuron in the network (Figure 2.1**B**).

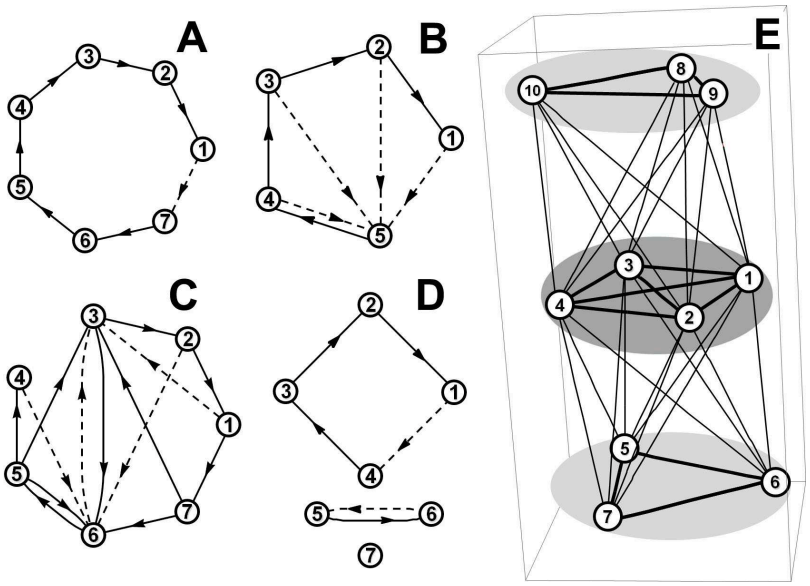

Figure 2.1: Topology of networks constructed, respectively, by a simple MC-cycle with $N = p/2 = 7$ (**A**, Example 2.3.1), a simple MC-cycle with $N = p - 1 = 5$ (**B**, Example 2.3.1), a minimal simple but non-consecutive cycle with $N = p - 2 = 7$ (**C**, Example 2.3.2), a separable MC-cycle (**D**, Example 2.3.5) and a minimal genuinely inseparable composite cycle (**E**, Example 2.3.6). In panels **A-D**, excitatory (inhibitory) synaptic connections are labeled with red (blue) lines with arrowhead indicating the direction of the connections. In panel **E**, in order to highlight the clusters in the network, connections within the same clusters are labeled with black lines, and connections between neurons in different clusters are labeled with dark red lines. Directions and polarities of the connections are not shown in **E**. For all of the 5 networks illustrated in this figure, self-connectivities are not included.

The two examples above demonstrate that the value of $N = \text{rank}(\eta)$ plays an important role for the network topology of simple MC-cycles. We discuss possible values of N for given cycle-lengths p in the next paragraph.

For minimal but non-consecutive cycles with $N < p - 1$ we can have "gaps" in the standard form which lead to feedforward chains interrupted by neurons with higher connectivities. The next example demonstrates this possibility.

Example 2.3.2. Consider $\eta = (+, +, +, +, +, +, -, -, -)$ $(p = 9)$, and

$$\Sigma = (\eta^T, (\eta\mathbf{P})^T, (\eta\mathbf{P}^2)^T, (\eta\mathbf{P}^4)^T, (\eta\mathbf{P}^5)^T, (\eta\mathbf{P}^6)^T, (\eta\mathbf{P}^8)^T)^T.$$

This cycle is minimal as $\text{rank}(\eta) = \text{rank}(\Sigma) = 7$, but not consecutive. The gaps are between the third and fourth rows, and the sixth and seventh rows. Since the seventh and first rows are consecutive, there are no other gaps. The connectivity matrix is

$$\mathbf{J} = \begin{pmatrix} 0 & 1 & 0 & 0 & 0 & 0 & 0 \\ 0 & 0 & 1 & 0 & 0 & 0 & 0 \\ -1 & 0 & 1 & 0 & 1 & -1 & 1 \\ 0 & 0 & 0 & 0 & 1 & 0 & 0 \\ 0 & 0 & 0 & 0 & 0 & 1 & 0 \\ 0 & -1 & 1 & -1 & 1 & 0 & 1 \\ 1 & 0 & 0 & 0 & 0 & 0 & 0 \end{pmatrix},$$

and shows that we still have the forward chain $3 \to 2 \to 1 \to 7 \to 6 \to 5 \to 4$, but neurons 3 and 6 receive multiple inputs. The network topology is shown in Figure 2.1**C**.

2.3.1.2 N-p relations

Definition 2.3.3. Let $N_p : \mathbb{X}^p \to \Omega$ be the function defined by $N_p(\eta) = n$ if η annihilates $(p - n)$ columns of V, where V is defined as in Theorem 2.1.2, $\mathbb{X}^p$ is the set of binary row vectors of length p, and $\Omega = \{1, 2, \ldots, p - 1\}$.

Remark 2.3.2. It is a direct consequence of Theorem 2.1.2 that $N_p(\eta) = \text{rank}(\eta)$. Therefore, for a given value of p, the image-set $N_p(\mathbb{X}^p)$ contains all possible values of N for which there exists $\eta \in \mathbb{X}^p$ such that (2.19) defines a simple MC-cycle. Furthermore, in Section 2.2.3 we have

associated with $\eta \in \mathbb{X}^p$ the polynomial $p_\eta(x) = \eta(1, x, \ldots, x^{p-1})^T$, where x is a complex variable. Since $p_\eta(\rho^k) = \eta v^{(k)}$, $\eta v^{(k)} = 0$ (i.e. η annihilates $v^{(k)}$) if and only if $p_\eta(x)$ has a factor which is a multiple of the minimal polynomial of ρ^k. Thus $N_p(\eta) = \mathrm{rank}(\eta)$ is intimately related to the factorization of $p_\eta(x)$.

There appears to be no general characterization of or formula for $N_p(\eta)$. Even for row vectors with repeating block structure such as $\eta = (\sigma, -\sigma)$ or $(\sigma, -\sigma, \sigma)$ ($\sigma \in \mathbb{X}^{p/2}$ or $\mathbb{X}^{p/3}$), the factorization of $p_\eta(x)$ does not reveal a formalizable pattern. We therefore just list the sets $N_p(\mathbb{X}^p)$ in Table 2.1 for $1 \le p \le 20$. Note that $N_q(\mathbb{X}^q) \subset N_p(\mathbb{X}^p)$ if q divides p, since $\mathrm{rank}(\eta) = \mathrm{rank}(\sigma)$ if $\eta = (\sigma, \sigma, \ldots, \sigma)$ (p/q repetitions) and $\sigma \in \mathbb{X}^q$. We therefore include in Table 2.1 only those values $N \in N_p(\mathbb{X}^p)$, for which there exists a row vector $\eta \in \mathbb{X}^p$ with $N = \mathrm{rank}(\eta)$, and η is NOT a repetition of some shorter vector σ. To illustrate how Table 2.1 was obtained, we compute $N_p(\eta)$ for a row vector with $p = 6$ in Example 2.3.3.

Vectors η of the form $\eta = (\sigma, \sigma, \ldots) \in \mathbb{X}^p$ with $\sigma \in \mathbb{X}^q$ have minimal period $\le q$ under cyclic permutations. The number of binary vectors of minimal period p is found by subtracting the number of all vectors with smaller minimal period from 2^p. An inclusion/exclusion argument shows that this number is given by

$$M_p = 2^p - \sum_{k=1}^{s} (-1)^{k-1} \sum_{1 \le i_1 < \cdots < i_k \le s} 2^{p/(p_{i_1} p_{i_2} \cdots p_{i_k})},$$

if $p_1, p_2, \ldots, p_s$ are the distinct prime numbers occurring in the prime factorization of p ($M_p = 2^p - 2$ if p is prime). Accordingly, the number of maximal loops, i.e. loops with $|\mathcal{L}_\eta| = p$, is M_p/p.

Example 2.3.3. Let $\eta = (+, +, -, -, -, +)$. This vector has a repeating block structure, $\eta = (\sigma, -\sigma)$, where $\sigma = (+, +, -)$. For $p = 6$ the matrix V is given by

$$V = (v^{(0)}, v^{(1)}, \ldots, v^{(5)}) = \begin{pmatrix} 1 & 1 & 1 & 1 & 1 & 1 \\ 1 & \rho & \rho^2 & -1 & \rho^4 & \rho^5 \\ 1 & \rho^2 & \rho^4 & 1 & \rho^2 & \rho^4 \\ 1 & -1 & 1 & -1 & 1 & -1 \\ 1 & \rho^4 & \rho^2 & 1 & \rho^4 & \rho^2 \\ 1 & \rho^5 & \rho^4 & -1 & \rho^2 & \rho \end{pmatrix},$$

Table 2.1: Values of $N \in N_p(\mathbb{X}^p)$ attained by some $\eta \in \mathbb{X}^p$ that is NOT of the form $(\sigma, \sigma, \ldots, \sigma)$ with $\sigma \in \mathbb{X}^q$, $q < p$, for $p \leq 20$.

p	N	p	N
1	1	11	11
2	1	12	6,7,8,9,10,11,12
3	3	13	13
4	2,4	14	7,13,14
5	5	15	11,13,15
6	3,5,6	16	8,10,11,12,13,14,15,16
7	7	17	17
8	4,6,7,8	18	7,9,11,12,13,14,15,16,17,18
9	7,9	19	19
10	5,9,10	20	10,12,13,14,15,16,17,18,19,20

where $\rho = e^{2\pi \mathbf{i}/6}$. The polynomial $p_\eta(x)$ has the following factorization,

$$\begin{aligned} p_\eta(x) &= 1 + x - x^2 - x^3 - x^4 + x^5 \\ &= (1 - x^3)(1 + x - x^2) \\ &= (1 - x)(1 + x + x^2)(1 + x - x^2). \end{aligned}$$

Since $\Phi_1(x) = x - 1$ and $\Phi_3(x) = x^2 + x + 1$ are the first and the third cyclotomic polynomials, and $\rho^0 = 1$ is the primitive first root of unity and ρ^2 and ρ^4 are the primitive third roots of unity, it follows that η annihilates $v^{(0)}$, $v^{(2)}$ and $v^{(4)}$. Therefore, $N_6(\eta) = 6 - 3 = 3$.

Some of the N-values in $N_p(\mathbb{X}^p)$ in Table 2.1 can be explained directly, without factorizing $p_\eta(x)$. We summarize three simple but important facts.

Proposition 2.3.2. *(a)* $\{1, p\} \subset N_p(\mathbb{X}^p)$ *for any* $p > 2$.
(b) If $p > 2$ *is prime, then* $N_p(\mathbb{X}^p) = \{1, p\}$.
(c) $p - 1 \in N_p(\mathbb{X}^p)$ *if* p *is even and* $p > 4$.

Proof: Since $\text{rank}(+, +, \ldots, +) = 1$, it follows that $1 \in N_p(\mathbb{X}^p)$ for any p. To show that $p \in N_p(\mathbb{X}^p)$ for $p > 2$, consider $\eta = (-, +, +, \ldots, +)$ and let Σ_η be the $p \times p$-matrix defined by $\text{row}_j(\Sigma_\eta) = \eta(\mathbf{P}^T)^{j-1}$, $1 \leq j \leq p$. By induction, one shows that $\det(\Sigma_\eta) = (-2)^{p-1}(p - 2)$ which completes the proof of (a).

Statement (b) is an immediate consequence of the fact that $\Phi_p(x) = \sum_{j=1}^{p} x^{j-1}$ is the minimal polynomial of ρ^k, $0 < k < p$, if p is prime and is irreducible over $\mathbb{Q}$, hence if $\eta \neq \pm(+, +, \ldots, +)$, $\Phi_p(x)$ and $p_\eta(x)$ cannot contain a common factor.

To show (c), let $\sigma = (+,-,+,-,\ldots,+,-) \in \mathbb{X}^{p-2}$ and set $\eta = (\sigma,-,+)$. By performing elementary row operations on the matrix Σ_η with rows $\mathrm{row}_i(\Sigma_\eta) = \eta\mathbf{P}^{i-1}$, $1 \le i \le p-1$, it can be shown that Σ_η has full rank. The details are straightforward but tedious to write down explicitly and will be omitted.

Remark 2.3.3. (a) If p is prime, then $\mathrm{rank}(\eta) = p$ for any $\eta \neq \pm(+,+,\ldots,+)$. For non-prime values of p one also can construct several different vectors with $\mathrm{rank}(\eta) = p$. For example, if p is odd, then $\mathrm{rank}(\eta) = p$ if $\eta = (+,-,+,-,\ldots,+,-,+)$, which is easily shown using elementary row operations. A generalization is provided by vectors η with $\sum_i \eta^i = 1$. All our case studies indicate that these vectors have $\mathrm{rank}(\eta) = p$ as well.

(b) For even $p > 4$, the vector constructed in the proof of Proposition 2.3.2(c) is just one example of a vector with $\mathrm{rank}(\eta) = p-1$. In general, if $\eta = (\eta^1,\ldots,\eta^p)$ and $\sum_i \eta^i = 0$, then η is orthogonal to $(+,+,\ldots,+)$, and $\mathrm{rank}(\eta) \le p-1$. Case studies indicate that such a vector has maximal rank $p-1$ if it does not have a "repeating block structure".

2.3.1.3 Simple anti-symmetric cycles

The characteristics of the cycles considered by [14] are that the cycle length p is even and the second $p/2$ columns of the cycle matrix are the negatives of the first $p/2$ columns in the same order. We call such cycles *anti-symmetric*. Here we discuss the possible values of the rank of the cycle matrix if these cycles are simple and admissible.

Proposition 2.3.3. *Assume p is even, $p = 2n$, and $\eta = (\sigma,-\sigma)$ with $\sigma = (\sigma^1,\ldots,\sigma^n) \in \mathbb{X}^n$. Then we have the following possibilities for* $\mathrm{rank}(\eta)$.

(a) $1 \le \mathrm{rank}(\eta) \le n$. *Moreover, $d \equiv n - \mathrm{rank}(\eta)$ is even, and if $d \ge 2$ the σ^j satisfy d linearly independent homogeneous linear equations with integer coefficients.*

(b) If $p = 2^k$, $k \ge 2$, then $\mathrm{rank}(\eta) = n$.

(c) If $p = 2n$ with $n > 2$ prime and $\sigma \neq \pm(+,-,+,\ldots,+,-,+)$, then $\mathrm{rank}(\eta) = n$.

Proof: (a) Let $\eta = (\sigma, -\sigma)$, $\sigma \in \mathbb{X}^n$, and define the $p \times p$-matrix Σ by $\mathrm{row}_j(\Sigma) = \eta(\mathbf{P}^T)^{j-1}$, $1 \le j \le p$. This matrix is a circulant matrix and contains all rows of $\mathcal{L}_\eta$, hence $\mathrm{rank}(\eta) = \mathrm{rank}(\Sigma)$. According to the properties of circulant matrices, the eigenvalues of Σ are of the form

$$\lambda = \sum_{i=1}^{p} \eta^i \rho^{i-1} = \sum_{i=1}^{n} (\sigma^i - \sigma^i \rho^n)\rho^{i-1}, \tag{2.22}$$

where ρ is any pth root of unity. Thus $\mathrm{rank}(\eta)$ coincides with the number of distinct pth roots of unity for which the right-hand side of (2.22) is nonzero. Since $\eta\mathbf{P}^n = -\eta$, it follows that $\mathrm{rank}(\eta) \le n$, and clearly $\mathrm{rank}(\eta) \ge 1$, which proves the first statement of (a). To complete the proof of (a), we note that the $2n$ distinct roots of $x^{2n} = 1$ ($x \in \mathbb{C}$) comprise n roots with $x^n = 1$ and n roots with $x^n = -1$. Thus $d = n - \mathrm{rank}(\eta)$ coincides with the number of distinct roots of $x^n = -1$ for which

$$p_\sigma(x) = \sum_{i=1}^{n} \sigma^i x^{i-1} = 0. \tag{2.23}$$

If n is odd, $p_\sigma(-1) \neq 0$, and if n is even, $(-1)^n = 1$, thus all roots in question have nonzero imaginary parts, which implies that d is even. If $d \ge 2$, $p_\sigma(x)$ is divisible by a cyclotomic polynomials $\Phi_m(x)$, where m divides n but not $2n$. The degree of $\Phi_m(x)$ is given by Euler's totient function, $\varphi(m)$, and is even. The condition that $p_\sigma(x)$ factors through $\Phi_m(x)$ then leads to $\varphi(m)$ linearly independent homogeneous equations that must be satisfied by the σ^i, and since $\Phi_m(x)$ has integer coefficients, the coefficients of these equations can be chosen as integers as well. If $p_\sigma(x)$ contains several cyclotomic polynomials $\Phi_{m_j}(x)$, $1 \le j \le r$, as factors, the number of linear equations satisfied by σ is $\varphi(m_1) + \cdots + \varphi(m_r)$, and all these relations are linearly independent as the cyclotomic polynomials are distinct and irreducible over the rationals.

(b) If $p = 2^k$, $k \ge 2$, the only factor that divides p but not $n = 2^{k-1}$ is p. The cyclotomic polynomial of p is $\Phi_p(x) = 1 + x^n$ and has degree n, that is, $\Phi_p(x)$ cannot be a factor of $p_\sigma(x)$ which has degree $n - 1$.

(c) Assume now that $n > 2$ is prime. In this case, $\Phi_{2n}(x) = \Phi_n(-x)$ is the only cyclotomic polynomial in question and is given by $\Phi_n(-x) = 1 - x + x^2 - x^3 + \cdots + x^n$. Thus, if σ is not of the form $\sigma = \pm(+,-,+,-,\ldots,+,-,+)$, $\Phi_n(-x)$ does not factor through $p_\sigma(x)$.

Since for $\eta = (\sigma, -\sigma)$ a "rank deficiency" ($\mathrm{rank}(\eta) < n$) occurs only if σ satisfies a system of linear equations, the number of σ's for which $\mathrm{rank}(\eta) = n$ is considerably larger than the number

of σ's for which η has a rank-deficiency. Thus "generically" we expect that vectors of the form $(\sigma, -\sigma)$ have full rank n. The vector $\sigma = (+, -, +, -, \ldots, +, -, +)$ is, of course, a very special case as $(\sigma, -\sigma)$ has the repeating block structure $(+, -, +, -, \ldots, +, -)$ which has minimal rank 1. We illustrate the occurrence of rank deficiencies by an example.

Example 2.3.4. Let $p = 18 = 2 \cdot 3^2$, i.e. $n = 9$. The cyclotomic polynomials that can give rise to a rank deficiency are here $\Phi_6(x) = 1 - x + x^2$ and $\Phi_{18}(x) = 1 - x^3 + x^6$. The condition that $p_\sigma(x) = \sigma^1 + \sigma^2 x + \cdots + \sigma^9 x^8$ factors through $\Phi_6(x)$ leads to the equations

$$\begin{aligned} \sigma^1 - \sigma^3 - \sigma^4 + \sigma^6 + \sigma^7 - \sigma^9 &= 0, \\ \sigma^2 + \sigma^3 - \sigma^5 - \sigma^6 + \sigma^8 + \sigma^9 &= 0. \end{aligned}$$

The only binary vector satisfying these conditions (up to cyclic permutations) are $\pm\sigma^{(1)}$, $\pm\sigma^{(2)}$ and $\pm\sigma^{(3)}$, where

$$\begin{aligned} \sigma^{(1)} &= (+, +, +, +, +, +, +, -, +), \\ \sigma^{(2)} &= (+, +, +, -, +, +, -, -, +), \\ \sigma^{(3)} &= (+, +, -, +, +, -, +, -, +). \end{aligned}$$

Since $\Phi_6(x)$ has a single pair of complex conjugate roots, $\mathrm{rank}(\sigma^{(\nu)}, -\sigma^{(\nu)}) = 9 - 2 = 7$, $\nu = 1, 2, 3$. Similarly, in order that $\Phi_{18}(x)$ factors through $p_\sigma(x)$, the conditions $\sigma^j + \sigma^{j+3} = 0$ for $1 \le j \le 6$ must be satisfied, leading to $\mathrm{rank}(\sigma, -\sigma) = 3$. All vectors with block structure $\sigma = (\tilde{\sigma}, -\tilde{\sigma}, \tilde{\sigma})$ with $\tilde{\sigma} \in \mathbb{X}^3$ have this property, and lead to $\eta = (\hat{\sigma}, \hat{\sigma}, \hat{\sigma})$ with $\hat{\sigma} = (\tilde{\sigma}, -\tilde{\sigma})$, i.e. $\mathrm{rank}(\eta) = \mathrm{rank}(\hat{\sigma})$. This includes $\tilde{\sigma} = (+, +, +)$ with $\mathrm{rank}(\hat{\sigma}) = 3$, and $\tilde{\sigma} = (+, -, +)$ with $\mathrm{rank}(\hat{\sigma}) = 1$. In the latter case, both $\Phi_6(x)$ and $\Phi_{18}(x)$ are factors of $p_\sigma(x)$.

The rank of generic vectors (without rank deficiency) of the form (σ, σ) or $(\sigma, -\sigma)$ is equal to the length of σ. The converse question is under which circumstances a vector $\eta \in \mathbb{X}^p$ with p even and $\mathrm{rank}(\eta) = p/2$ has this form. We state two simple sufficient conditions for this property.

Proposition 2.3.4. *Assume $p = 2n$, $\eta \in \mathbb{X}^p$, and $\mathrm{rank}(\eta) = n$. If $p = 2^k$, $k \ge 2$, or $n > 2$ is prime, then η is either of the form (σ, σ) or $(\sigma, -\sigma)$ for some $\sigma \in \mathbb{X}^n$.*

Proof: Let $\eta = (\sigma, \hat{\sigma})$ with σ, $\hat{\sigma} \in \mathbb{X}^n$. We consider again the matrix Σ defined in the proof of Proposition 2.3.3 with eigenvalues

$$\lambda = \sum_{i=1}^{n} (\sigma^i + \rho^n \hat{\sigma}^i) \rho^{i-1},$$

where ρ is a pth root of unity, $p = 2n$. Assuming that $\mathrm{rank}(\eta) = n$, there exist precisely n distinct roots ρ of $x^{2n} = 1$ for which $\lambda = 0$. We decompose these roots again into roots satisfying $x^n = 1$ and $x^n = -1$, respectively, and set accordingly

$$\lambda_\pm(x) = \sum_{i=1}^{n} (\sigma^i \pm \hat{\sigma}^i) x^{i-1}.$$

(a) Assume that $p = 2^k$ ($n = 2^{k-1}$) for $k \geq 2$. If there exists a root ρ of $x^n = -1$ for which $\lambda = 0$, $\lambda(x)$ must contain the cyclotomic polynomial $\Phi_{2n}(x) = 1 + x^n$ as a factor, which is only possible if $\sigma^i - \hat{\sigma}^i = 0$ for all i, because $\lambda(x)$ has at most degree $n - 1$. Thus $\eta = (\sigma, \sigma)$ in this case. Conversely, assume that all roots ρ for which $\lambda = 0$ are roots of $x^n = 1$. Then $\lambda_+(x)$ must contain all cyclotomic polynomials $\Phi_\nu(x)$ for $\nu = 1, 2, \ldots, 2^{k-1}$ as factors. Since the product of these polynomials is $1 - x^n$, this cannot hold unless $\sigma^i + \hat{\sigma}^i = 0$ for all i, thus $\eta = (\sigma, -\sigma)$ in this case.

(b) The case $p = 2n$ with $n > 1$ prime is treated similarly. Here the cyclotomic polynomials which factor through $x^n - 1$ are $1 - x$ and $\Phi_n(x) = 1 + x + \cdots + x^{n-1}$, and the cyclotomic polynomials which factor through $1 + x^n$ are $1 + x$ and $\Phi_n(-x)$. Since $n > 1$, either $\Phi_n(x)$ is a factor of $\lambda_+(x)$ or $\Phi_n(-x)$ is a factor of $\lambda_-(x)$, which implies that either $\hat{\sigma} = \sigma$ or $\hat{\sigma} = -\sigma$.

An extension of Proposition 2.3.4 to more general values of p appears highly nontrivial, because a multitude of cyclotomic polynomials have to be considered if the prime factorization of n is more complicated. We have examined all vectors η with $\mathrm{rank}(\eta) = p/2$ for $p \leq 20$ and found that all these vectors have the form (σ, σ) or $(\sigma, -\sigma)$. Other vectors with $\mathrm{rank}(\eta) = p/2$ may exist for larger values of p, but if so we expect the number of these vectors to be much smaller than the number of (σ, σ)- or $(\sigma, -\sigma)$-vectors of full rank.

2.3.2 Separable MC-Cycles

For separable MC-cycles with generators $G_\Sigma = \{\eta_1, \eta_2, \ldots, \eta_q\}$, the spaces $\mathrm{span}\{\mathcal{L}_{\eta_j}\}$ and $\mathrm{span}\{\mathcal{L}_{\eta_k}\}$ intersect trivially if $j \neq k$. If Σ is in standard form, this implies immediately that $\mathbf{J}$ has a block structure, $\mathbf{J} = \mathrm{diag}(\mathbf{J}_1, \ldots, \mathbf{J}_r)$, where $\mathbf{J}_k$ is an $N_k \times N_k$-matrix of the form (2.20) with $N_k = \mathrm{rank}(\eta_k)$. Accordingly, a network constructed from a separable MC-cycle is decomposed into r disconnected clusters and for each cluster the connectivity matrix has the form corresponding to a simple MC-cycle.

Example 2.3.5. Consider the 7×8-cycle

$$\Sigma = \begin{pmatrix} + & + & + & + & - & - & - & - \\ + & + & + & - & - & - & - & + \\ + & + & - & - & - & - & + & + \\ + & - & - & - & - & + & + & + \\ + & + & - & - & + & + & - & - \\ + & - & - & + & + & - & - & + \\ + & - & + & - & + & - & + & - \end{pmatrix}.$$

This cycle has the generators η_1, η_5, η_7 ($\eta_j = \mathrm{row}_j(\Sigma)$) and is separable and in standard form. Moreover, $\eta_4\mathbf{P} = -\eta_1$, $\eta_6\mathbf{P} = -\eta_5$, and $\eta_7\mathbf{P} = -\eta_7$. Thus the network is decomposed into three clusters consisting of neurons 1, 2, 3, 4, neurons 5, 6, and neuron 7, with cycle-connectivity matrices

$$\begin{pmatrix} 0 & 1 & 0 & 0 \\ 0 & 0 & 1 & 0 \\ 0 & 0 & 0 & 1 \\ -1 & 0 & 0 & 0 \end{pmatrix}, \begin{pmatrix} 0 & 1 \\ -1 & 0 \end{pmatrix},$$

and -1, respectively. The topology of this network is illustrated in Figure 2.1**D**. We note, however, that the cluster consisting of neuron 7 cannot show oscillations without delay, since a $1D$ dynamical system does not have limit cycles. By contrast, with delay included, we can find oscillations already for $N = 1$ for appropriate parameter values.

General separable cycles still can be decomposed into isolated clusters as $\mathrm{span}\{\mathrm{R}(\Sigma)\}$ is semisimple, however, the network topology in each cluster maybe more complicated (see Subsection 2.3.4). The issue with separable cycles is that, even if the subcycles corresponding to the different clusters are retrieved, these oscillations are in general not synchronized. We comment on this issue further in Chapter 6.

2.3.3 Minimal Inseparable Cycles

For minimal inseparable cycles Σ with generators $G_\Sigma = \{\eta_1, \eta_2, \ldots, \eta_q\}$, at least two subspaces $\mathrm{span}\{\mathcal{L}_{\eta_j} \cap \mathrm{R}(\Sigma)\}$ and $\mathrm{span}\{\mathcal{L}_{\eta_k} \cap \mathrm{R}(\Sigma)\}$ ($j \neq k$) have a nontrivial intersection. Accordingly, Σ does

not have full row-rank, $\operatorname{rank}(\Sigma) < \sum_{i=1}^{q} \operatorname{rank}(\eta_i) = N$, which implies in particular that $\mathbf{J^0} \neq \mathbf{I}$. It is still possible to partition the network into clusters, but some clusters may be connected and the network topology within the cluster corresponding to the loop $\mathcal{L}_{\eta_j}$ will in general not coincide with the network topology predicted by the submatrix Σ_j of the corresponding simple cycle. Thus the consecutiveness requirement does not have an effect, whereas the minimality requirement takes care that the sub-matrices in $\mathbf{J^0}$ and $\mathbf{J}$ defining the connectivities within the clusters are non-singular. The following example illustrates these features.

Example 2.3.6. Consider the 10×12-cycle $\Sigma = (\Sigma_1^T, \Sigma_2^T, \Sigma_3^T)^T$, where

$$\Sigma_1^T = (\eta_1^T, (\eta_1\mathbf{P})^T, (\eta_1\mathbf{P}^2)^T, (\eta_1\mathbf{P}^3)^T)^T,$$
$$\Sigma_j^T = (\eta_j^T, (\eta_j\mathbf{P})^T, (\eta_j\mathbf{P}^2)^T)^T,\ j = 2, 3,$$

with

$$\eta_1 = (\ +\ +\ +\ -\ +\ +\ +\ -\ +\ +\ +\ -\ ),$$
$$\eta_2 = (\ -\ +\ +\ +\ -\ -\ -\ +\ +\ +\ -\ -\ ),$$
$$\eta_3 = (\ +\ -\ -\ +\ -\ -\ +\ -\ -\ +\ -\ -\ ).$$

This is a minimal inseparable admissible cycle with generator $G_\Sigma = \{\eta_1, \eta_2, \eta_3\}$. The connectivity matrix $\mathbf{J}$ is given by

$$\mathbf{J} = \frac{1}{8}\begin{pmatrix} 0 & 7 & 0 & -1 & 1 & -1 & 1 & -1 & -1 & -1 \\ -1 & 0 & 7 & 0 & -1 & 1 & -1 & -1 & -1 & -1 \\ 0 & -1 & 0 & 7 & 1 & -1 & 1 & -1 & -1 & -1 \\ 7 & 0 & -1 & 0 & -1 & 1 & -1 & -1 & -1 & -1 \\ 1 & -1 & 1 & -1 & 2 & 6 & 2 & 0 & 0 & 0 \\ -1 & 1 & -1 & 1 & -2 & 2 & 6 & 0 & 0 & 0 \\ 1 & -1 & 1 & -1 & 6 & -2 & 2 & 0 & 0 & 0 \\ -1 & -1 & -1 & -1 & 0 & 0 & 0 & -2 & 6 & -2 \\ -1 & -1 & -1 & -1 & 0 & 0 & 0 & -2 & -2 & 6 \\ -1 & -1 & -1 & -1 & 0 & 0 & 0 & 6 & -2 & -2 \end{pmatrix},$$

and $\mathbf{J^0}$ has the same block structure as $\mathbf{J}$ (with self-feedbacks of all neurons). From the form of $\mathbf{J}$ (and $\mathbf{J^0}$) we infer that the cluster corresponding to η_1 is connected to the clusters corresponding

to η_2 and η_3, while the latter two clusters are not directly connected. This connectivity structure is due to the fact that $\text{span}\{\mathcal{L}_{\eta_1}\}$ intersects $\text{span}\{\mathcal{L}_{\eta_2}\}$ and $\text{span}\{\mathcal{L}_{\eta_3}\}$ in the one-dimensional spaces spanned by $(+,-,+,-,\ldots,+,-)$ and $(+,+,+,\ldots,+)$, respectively, whereas $\text{span}\{\mathcal{L}_{\eta_2}\}$ and $\text{span}\{\mathcal{L}_{\eta_3}\}$ intersect trivially. The network topology for this example is shown in Figure 2.1**E**. In general, two clusters corresponding to two generators $\eta, \eta' \in G_\Sigma$ are connected, if there exists a sequence $\eta = \eta_1, \eta_2, \ldots, \eta_{s-1}, \eta_s = \eta'$ of generators such that $\text{span}\{\mathcal{L}_{\eta_j}\}$ and $\text{span}\{\mathcal{L}_{\eta_{j+1}}\}$ intersect nontrivially for $0 \leq j < s$.

2.3.4 Further Examples

The examples in this subsection serve to illustrate the possible effects of fewer essential generators than generators. Consider a cycle Σ with $EG_\Sigma = \{\epsilon_1, \ldots, \epsilon_r\}$. If $r < |G_\Sigma|$, the loop vectors of at least one generator are contained in the span of the loop vectors of another essential generator. Assuming $|\mathrm{R}(\Sigma)| = N$, this implies

$$\text{rank}(\Sigma) \leq \sum_{i=1}^{r} \text{rank}(\epsilon_i) < N,$$

and we encounter again a rank-deficiency that will destroy special structures in the clusters corresponding to the essential generators.

Example 2.3.7. The 6×6-cycle

$$\Sigma = \begin{pmatrix} + & + & - & - & + & - \\ + & - & - & + & - & + \\ - & - & + & - & + & + \\ - & + & - & + & + & - \\ + & - & + & + & - & - \\ + & - & + & - & + & - \end{pmatrix},$$

has two generators, $\text{row}_1(\Sigma)$ and $\text{row}_6(\Sigma)$, but $\text{row}_6(\Sigma) = \text{row}_1(\Sigma) + \text{row}_3(\Sigma) + \text{row}_5(\Sigma)$, thus there is only one essential generator, $\epsilon = \text{row}_1(\Sigma)$. Without the sixth row, Σ would be a simple MC-cycle

with ring-topology. The presence of the sixth row destroys this structure, which is revealed in the following forms of $\mathbf{J^0}$ and $\mathbf{J}$,

$$\mathbf{J^0} = \frac{1}{4}\begin{pmatrix} 3 & 0 & -1 & 0 & -1 & 1 \\ 0 & 4 & 0 & 0 & 0 & 0 \\ -1 & 0 & 3 & 0 & -1 & 1 \\ 0 & 0 & 0 & 4 & 0 & 0 \\ -1 & 0 & -1 & 0 & 3 & 1 \\ 1 & 0 & 1 & 0 & 1 & 3 \end{pmatrix}, \mathbf{J} = \frac{1}{4}\begin{pmatrix} 0 & 4 & 0 & 0 & 0 & 0 \\ -1 & 0 & 3 & 0 & -1 & 1 \\ 0 & 0 & 0 & 4 & 0 & 0 \\ -1 & 0 & -1 & 0 & 3 & 1 \\ -1 & -4 & -1 & -4 & -1 & -3 \\ -1 & 0 & -1 & 0 & -1 & -3 \end{pmatrix}.$$

Example 2.3.8. The cycle

$$\Sigma = \begin{pmatrix} 1 & -1 & 1 \\ -1 & 1 & -1 \\ 1 & 1 & 1 \end{pmatrix},$$

has three generators and one essential generator that can be chosen as the first or second row. Since Σ is non-singular, Σ is admissible and $\mathbf{J^0}$ is the identity matrix. A successfully retrieved cycle shows three consecutive phases 1, 2, and 3 during an oscillation. In phases 1 and 2, neuron 1 is "on" $(+)$ and in phase 3 it is "off" $(-)$, while neuron 2 is "on" in phase 1 and "off" in phases 2 and 3. Clearly, neuron 3 is "on" during all 3 phases. The matrix $\mathbf{J}$ is given by

$$\mathbf{J} = \begin{pmatrix} -1 & 1 & 1 \\ -1 & 0 & 0 \\ 0 & 0 & 1 \end{pmatrix},$$

and shows that neurons 1 and 2 form an excitatory/inhibitory pair, whereas neuron 3 acts excitatory on neuron 1. Without this third neuron the oscillations of neurons 1 and 2 as required by the first two rows of Σ could not be implemented, since the submatrix of Σ consisting of these rows is not admissible.

CHAPTER 3

MISALIGNMENT LENGTH ANALYSIS - QUALITATIVE AND QUANTITATIVE THEORY

In this chapter, we introduce a novel method for studying the relaxation dynamics of networks constructed from admissible cycles, which we refer to as *Misalignment Length Analysis* (MLA). The method consists of two parts, a qualitative theory on the evolution of binary patterns and a quantitative method for estimating the duration of the oscillation corresponding to a cycle stored in the Hopfield-type neural network. We begin, in Section 3.1, by explaining the motivation for the MLA method, before introducing the two parts of the method in detail in Sections 3.2 and 3.3.

3.1 Failures in Retrieving Admissible Cycles

Motivated by both biological nervous systems and analog electronic circuits, delays are introduced in continuous-time neural network models to model both finite inter-neuron transmission and (binary) state switching times. In our model, the delay coming from the finite inter-neuron transmission time is incorporated through a delay time τ in the coupling term imposing transition conditions in the network (1.10). The delay arising from the finite switching time is incorporated as the membrane constant in the network (1.1) and (1.10), and the membrane constant can be related to the gain scaling parameter λ [30] in both (1.1) and (1.10). Although in our networks, the gain scaling parameter λ is set uniformly throughout the whole network, starting from different initial values, the magnitude $|u_i(t)|$ will take different times to decrease to zero. The larger the initial magnitude $u_i(t)$ starts from, the longer $|u_i(t)|$ will take to decrease to zero. As not all blocks (*consecutive "+"s or "-"s in each row of a cycle* Σ *are called a* (temporal) block) have the same length (*the number of the same signs*), it follows that, even though all components of the initial data are taken with the same magnitude, the magnitudes of different $u_i(t)$'s will become different after just a few network state transitions (*we call the column vector of the signs of the membrane potentials of all neurons in the network at a time instant the* network state *at the time instant;*

and the change of the network state from $\xi^{(\mu)}$ *to* $\xi^{(\mu+1)}$ *a* network state transition*; a more precise definition of the start- and end-times of a network state transition is given in Subsection 3.3.1.2*). Thus, after just a few network state transitions, the membrane potentials of different neurons would need different times to switch from one sign to the other.

This time difference in state-switches, i.e. sign-changes, during one network state transition has two effects. First, if the Hamming distance between two successive patterns in the cycle is greater than one, then after a few network state transitions, the membrane potentials of different neurons will change their signs asynchronously, except for neurons which behave dynamically identical, i.e. $u_i(t) = u_j(t)$ or $u_i(t) = -u_j(t)$ for all $t \geq 0$. Thus, excluding dynamically identical behavior of two neurons, sign-changes of membrane potentials of different neurons occur one at a time during a network state transition.

Second, through the delayed inter-neuron couplings, membrane potential(s) that changed sign(s) in one network state transition earlier may force the membrane potentials that changed signs later in the same network state transition to start the state-switches earlier in the next network state transition. This leads to a consistent decrease in the magnitude of the membrane potential at the beginning of the first state-switch in successive network state transitions.

Next, in networks constructed from two different types of admissible cycles, we illustrate how asynchronous state-switches (sign-changes) cause retrieval fail.

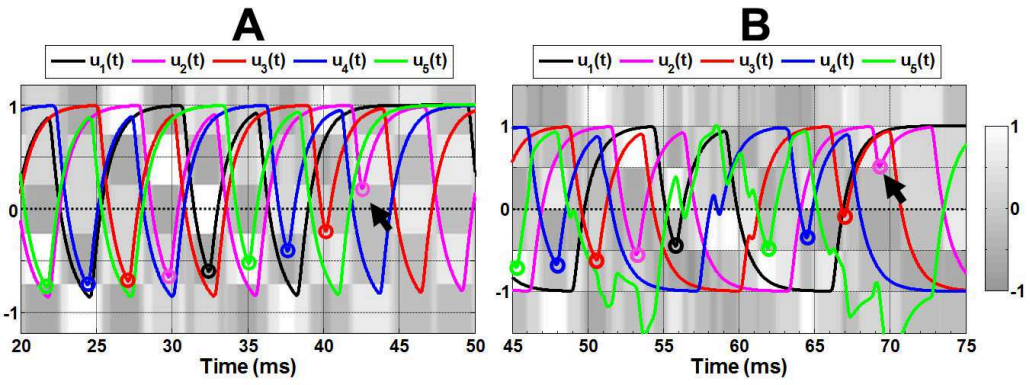

Figure 3.1: Retrieval failures caused by the second effect of the time difference in state-switches. **A** All *intermediate patterns* satisfy the transition conditions imposed by the prescribed cycle. **B** Not all *intermediate patterns* satisfy the transition conditions imposed by the prescribed cycle. The backgrounds in grayscales of both panels are the *overlaps* $m_i^{(\nu)}(t)$ [14, 26]. Parameters are set as: $\lambda = \beta = 10$, $\tau = 2.1$.

Example 3.1.1. In this example, we illustrate retrieval failure for two different types of admissible cycles. We choose the following typical cycles for each of the two types,

$$\Sigma = \begin{pmatrix} + & + & - & + & - \\ + & - & + & - & + \\ - & + & - & + & + \\ + & - & + & + & - \\ - & + & + & - & + \end{pmatrix}, \text{ and } \tilde{\Sigma} = \begin{pmatrix} + & + & - & + & - & - \\ + & - & + & - & - & + \\ - & + & - & - & + & + \\ + & - & - & + & + & - \\ - & - & + & + & - & + \end{pmatrix}. \tag{3.1}$$

The connectivity matrices of the two networks are constructed with the pseudoinverse learning rule (1.8) as follows,

$$\mathbf{J} = \begin{pmatrix} 0 & 1 & 0 & 0 & 0 \\ 0 & 0 & 1 & 0 & 0 \\ 0 & 0 & 0 & 1 & 0 \\ 0 & 0 & 0 & 0 & 1 \\ 1 & 0 & 0 & 0 & 0 \end{pmatrix}, \text{ and } \tilde{\mathbf{J}} = \begin{pmatrix} 0 & 1 & 0 & 0 & 0 \\ 0 & 0 & 1 & 0 & 0 \\ 0 & 0 & 0 & 1 & 0 \\ 0 & 0 & 0 & 0 & 1 \\ -1 & -1 & -1 & -1 & -1 \end{pmatrix}.$$

The network constructed from Σ is a unidirectional excitatory (also known as cooperative) ring network. This type of networks has drawn much attention in the past few years, and it has been well known that there is no stable periodic solution [37, 42], and the so called long-lasting transient oscillations have been observed in both numerical and analog electronic circuit simulations of such networks [16, 42]. In contrast, the network constructed from $\tilde{\Sigma}$ has more complicated network topology (see Chaper 2), and richer dynamics (see Chapter 5).

Figure 3.1 illustrates retrieval failures caused by the asynchronous state-switches in the networks constructed from these two cycles. While the relaxation dynamics of the two networks look very different (between the starting points of two successive state-switches, the membrane potentials in the network constructed form Σ (panel **A**) are smooth and monotone; but in some of the membrane potentials in the network constructed from $\tilde{\Sigma}$ (panel **B**), between the starting points of two successive state-switches, "humps" and "valleys" appear), retrievals in both networks fail in the same way, and the failures are both due to the above second effect of the asynchronous state-switches.

Taking panel **A** as example, at around $t = 25$ms, $u_4(t)$ (blue curve) acomplishes its state-switch first, and after approximately 2.1ms ($\tau = 2.1$ms), $u_3(t)$ (red curve) is forced to start its state-switch (reaches its turning point) first. At this starting point of the state-switch (red open circle) for retrieving $\xi^{(2)}$ (the overlap $m^{(\nu)}(t)$ in the background shows that over the interval from around $t = 28$ms to around $t = 31$ms, $\xi^{(2)}$ is successfully retrieved), the magitude is smaller than that at the starting point of the first state-switch (blue open circle at around $t = 24$ms) for retrieving $\xi^{(1)}$. As the simulation continues, this effect becomes more and more significant, and ultimately, it forces the retrieval of $\xi^{(2)}$ that is highlighted by a black arrow to fail. Panel **B** illustrates how the same effect forces the retrieval of $\xi^{(2)}$ (highlighted by a black arrow) to fail.

Remark 3.1.1. Although the retrievals of the two cycles fail in the same way, the dynamics of the two networks are not exactly the same. For example, while the membrane potential $u_i(t)$ of each neuron in the network shown in Figure 3.1**A** is monotone between the beginning of every state switch and that of the next state switch, there are some "humps" or "valleys" riding on the membrane potential curves shown in Figure 3.1**B** between the starting points of two successive state switches.

In the next section, motivated by the first effect described above, we develop a novel qualitative theory to characterize the dynamics of these three types of networks, and after establishing the quantitative method of the MLA in Section 3.3, we proceed to prove some important results described in Section 3.2.

3.2 Qualitative Theory of Binary Patterns Dynamics

Although the qualitative theory we are going to develop in this section can be applied to general simple cycles (and hence to separable composite cycles), rigorous proofs of the most important results provided in Section 3.3 will be restricted to simple MC-cycles. To keep both sections consistent, we confine ourselves in this section to simple MC-cycles too.

3.2.1 Interpolating Cycles with Intermediate Transitions

Definition 3.2.1. Let $\Sigma = (\xi^{(1)}, \ldots, \xi^{(p)})$ be any simple MC-cycle. The matrix $\mathbf{B} \in \mathbb{N}^{N \times p}$, called the *backward sequence matrix*, or for short, *BS-matrix* of Σ, is constructed as follows:

Step 1: Let $\Sigma' = (\xi^{(1)}, \ldots, \xi^{(p)}, \xi^{(1)}, \ldots, \xi^{(p)})$ and set $\mathbf{B'}_{i,1} = 1$ for all $i = 1, \ldots, N$;

Step 2: If $\Sigma'_{i,j}\Sigma'_{i,(j-1)} = 1$, then $\mathbf{B'}_{i,j} = \mathbf{B'}_{i,(j-1)} + 1$, otherwise $\mathbf{B'}_{i,j} = 1$ for all $i = 1, \ldots, N$ and $j = 2, \ldots, 2p$;

Step 3: Let $\mathbf{B}_{i,j} = \mathbf{B'}_{i,j+p}$ for all $i = 1, \ldots, N$ and $j = 1, \ldots, p$.

Remark 3.2.1. As Σ is a cycle, i.e., Σ represents an infinite cyclic (repeating) sequence of binary patterns, and Σ itself is a smallest block repeating in the sequence, it follows that the i-th row of the BS-matrix $\mathbf{B}$ represents the infinite sequence of positive integers associated to the i-th row of Σ, and the row vector in $\mathbf{B}$ is the corresponding repeating block in the sequence.

Definition 3.2.2. Let $\mathbf{B}$ be a BS-matrix. Then the left-infinite sequence $b_{i,j} = \ldots, \mathbf{B}_{i,(j-2)}, \mathbf{B}_{i,(j-1)}, \mathbf{B}_{i,j}$ is called the j-th *backward sequence* associated to the i-th neuron, where $\mathbf{B}_{i,k} = \mathbf{B}_{i,((k-1) \bmod p)+1}$. We define an ordering of the j-th backward sequences $b_{i,j}$ and $b_{k,j}$ associated to the i-th and k-th neurons with $i \neq k$ as follows:

Step 1:

$$\begin{cases} b_{i,j} < b_{k,j}, & \text{if } \mathbf{B}_{i,j} < \mathbf{B}_{k,j} \\ b_{i,j} > b_{k,j}, & \text{if } \mathbf{B}_{i,j} > \mathbf{B}_{k,j} \\ \text{Set the 0-th } \textit{parity } \pi_0 = 1 \text{ and jump to Step 2}, & \text{if } \mathbf{B}_{i,j} = \mathbf{B}_{k,j} \end{cases}$$

Step 2: Let $m \geq 1$ be the smallest integer such that $\mathbf{B}_{i,j-r} = \mathbf{B}_{k,j-r}$ for $r < m$ and $\mathbf{B}_{i,j-m} \neq \mathbf{B}_{k,j-m}$. For any $1 \leq r \leq m$ define the parity π_r by $\pi_r = -\pi_{r-1}$ if $\mathbf{B}_{i,j-r} \geq \mathbf{B}_{i,j-r+1}$ and $\pi_r = \pi_{r-1}$ otherwise, In this case, we define the ordering of $b_{i,j}$ and $b_{k,j}$ as

$$\begin{cases} b_{i,j} < b_{k,j}, & \text{if } \mathbf{B}_{i,j-m} < \mathbf{B}_{k,j-m} \text{ and } \pi_m = 1, \text{ or } \mathbf{B}_{i,j-m} > \mathbf{B}_{k,j-m} \text{ and } \pi_m = -1; \\ b_{i,j} > b_{k,j}, & \text{if } \mathbf{B}_{i,j-m} > \mathbf{B}_{k,j-m} \text{ and } \pi_m = 1, \text{ or } \mathbf{B}_{i,j-m} < \mathbf{B}_{k,j-m} \text{ and } \pi_m = -1. \end{cases}$$

Example 3.2.1. By the above definitions, the BS-matrices corresponding to Σ and $\tilde{\Sigma}$ in the example in Section 3.1 are derived as follows

$$\mathbf{B} = \begin{pmatrix} 1 & 2 & 1 & 1 & 1 \\ 2 & 1 & 1 & 1 & 1 \\ 1 & 1 & 1 & 1 & 2 \\ 1 & 1 & 1 & 2 & 1 \\ 1 & 1 & 2 & 1 & 1 \end{pmatrix}, \text{ and } \tilde{\mathbf{B}} = \begin{pmatrix} 1 & 2 & 1 & 1 & 1 & 2 \\ 2 & 1 & 1 & 1 & 2 & 1 \\ 1 & 1 & 1 & 2 & 1 & 2 \\ 1 & 1 & 2 & 1 & 2 & 1 \\ 1 & 2 & 1 & 2 & 1 & 1 \end{pmatrix}.$$

For demonstration purpose, we consider $\tilde{\mathbf{B}}$ and $i = 2$, $j = 2$, and $k = 3$ to construct two backward sequences $b_{i,j}$ and $b_{k,j}$ as follows

$$b_{2,2} = \cdots, 1, 1, 2, 1, 2, 1$$
$$b_{3,2} = \cdots, 1, 2, 1, 2, 1, 1$$

Since the first element in $b_{2,2}$ that is different from the one in $b_{3,2}$ appears at the second position counting leftward, and the corresponding parity is $\pi_1 = -1$, and $\tilde{\mathbf{B}}_{2,1} = 2 > 1 = \tilde{\mathbf{B}}_{3,1}$, it follows that $b_{2,2} < b_{3,2}$.

Remark 3.2.2. Observe that in the membrane potentials shown in Figure 3.1**B**, at around $t = 54$ms, $u_2(t)$ (purple curve) changes sign earlier than $u_3(t)$ (red curve). The network states right after the zeros of $u_2(t)$ and $u_3(t)$ can be recognized from the figure as $(+, +, +, -, -)^T$ and $(+, +, -, -, -)^T$ respectively. We call these two patterns intermediate patterns or network states. Note that the order in which the switches of $u_2(t)$ and $u_3(t)$ occur is consistent with the ordering of the two backward sequences $b_{2,2}$ and $b_{3,2}$. In the following, we will develop an "algorithm" to derive the intermediate binary network states that occur during the transitions from one prescribed cycle state to the next one, and order them using the ordering of the backward sequences $b_{i,j}$ such that a complete picture of the evolution of the binary network states can be obtained. In Section 3.3, we will rigorously prove that for cycles with intermediate patterns satisfying the transition conditions imposed by the cycles, the qualitative description of binary network states dynamics is indeed consistent with the actual binary network states dynamics. Next, before continuing to develop the algorithm, we show that for simple MC-cycles, the order we defined above is a total order.

Proposition 3.2.1. *Let Σ be any admissible cycle and assume that $\eta_i \neq \eta_k$ and $\eta_i \neq -\eta_k$ for all η_i, $\eta_k \in R(\Sigma)$ with $i \neq k$. Let the relation $<$ be as defined in Definition 3.2.2. Then $<$ is a total order.*

Proof: Assume $<$ is not a total order, then there exist η_i, η_k in $R(\Sigma)$ with $i \neq k$ such that the corresponding $b_{i,j} = b_{k,j}$ for some j. Accordingly, we have that $\mathbf{B}_{i,j-m} = \mathbf{B}_{k,j-m}$ for all $m \geq 0$. It follows that the i-th row and the k-th row in $\mathbf{B}$ are exactly the same, and this implies that either $\eta_i = \eta_k$ or $\eta_i = -\eta_k$.

Remark 3.2.3. Since for simple cycles, minimality is equivalent to linear independence of row vectors, it follows that the order defined in Definition 3.2.2 is a total order over the set of all simple MC-cycles.

Definition 3.2.3. Let Σ be a simple MC-cycle, and let $\xi^{(\mu)}$ and $\xi^{(\mu+1)}$ any two consecutive (column) patterns in Σ. Let $d_\mu = d(\xi^{(\mu)}, \xi^{(\mu+1)})$ be the Hamming distance of the two patterns. A binary (column) pattern $\tilde{\xi}^{(\mu,\nu)}$ is called an *intermediate pattern* between $\xi^{(\mu)}$ and $\xi^{(\mu+1)}$, if $\tilde{\xi}^{(\mu,\nu)}$ is interpolated as follows,

Step 1: If $\xi_i^{(\mu)} = \xi_i^{(\mu+1)}$, then $\xi_i^{(\mu,\nu)} = \xi_i^{(\mu)}$ for all $\nu = 1, \ldots, d_\mu - 1$;

Step 2: Let $\mathcal{A}_\mu$ be the set of row indices i with $\xi_i^{(\mu)} \neq \xi_i^{(\mu+1)}$ and order the $i \in \mathcal{A}_\mu$ as $i_1 < i_2 < \cdots < i_{d_\mu - 1}$ in accordance with the ordering of the backward sequences $b_{i,\mu}$. Set $\tilde{\xi}^{(\mu,0)} = \xi^{(\mu)}$ and define the ν-th intermediate pattern by $\tilde{\xi}_i^{(\mu,\nu)} = \tilde{\xi}_i^{(\mu,\nu-1)}$ if $i \neq i_\nu$ and $\tilde{\xi}_i^{(\mu,\nu)} = -\tilde{\xi}_i^{(\mu,\nu-1)}$ if $i = i_\nu$.

Definition 3.2.4. The cycle $\hat{\Sigma}$ is called the *interpolated cycle* of Σ, if $\hat{\Sigma}$ is the cycle with all the ordered intermediate patterns filled in between the corresponding prescribed patterns.

Next, we demonstrate how to find the interpolated cycle $\hat{\Sigma}_1$ for Σ in Example 3.1.1 step by step. The interpolated cycle $\hat{\Sigma}_2$ for $\tilde{\Sigma}$ can be obtained similarly.

Example 3.2.2 (Intermediate Transitions)**.** As by a cyclic permutation, any pattern in Σ can be shifted to the first column, for the convenience of discussion, we start from the first prescribed pattern $\xi^{(1)}$. Since $d(\xi^{(1)}, \xi^{(2)}) = 4$, only one entry in the pattern does not change sign during the network state transition between the first and second prescribed patterns, and there are three intermediate patterns.

Step 1: Since $\xi_1^{(1)} = \xi_1^{(2)}$, it follows that $\tilde{\xi}_1^{(1,1)} = \tilde{\xi}_1^{(1,2)} = \tilde{\xi}_1^{(1,3)} = 1$;

Step 2: The 2nd, 3rd, 4th and 5th entries of the pattern $\xi^{(1)}$ change signs during the network state transition to the next pattern $\xi^{(2)}$. Therefore, we need to order the four backward sequences

$$b_{2,1} = \ldots, 1, 1, 1, 1, 2$$
$$b_{3,1} = \ldots, 1, 1, 1, 2, 1$$
$$b_{4,1} = \ldots, 1, 1, 2, 1, 1$$
$$b_{5,1} = \ldots, 1, 2, 1, 1, 1$$

Following the algorithm for ordering backward sequences, we obtain:

$$b_{3,1} < b_{5,1} < b_{4,1} < b_{2,1}.$$

Step 3: According to the order of the backward sequences, we have that the third entry changes sign first, i.e. $\tilde{\xi}_3^{(1,1)} = -\xi_3^{(1)}$ and all other entries remain unchanged. The second, third and fourth patterns are determined similarly, and the fourth pattern turns out to be the second pattern in the prescribed cycle. Thus, we obtain the following three intermediate patterns

$$\tilde{\xi}^{(1,1)} = \begin{pmatrix} + \\ + \\ + \\ + \\ - \end{pmatrix}, \tilde{\xi}^{(1,2)} = \begin{pmatrix} + \\ + \\ + \\ + \\ + \end{pmatrix}, \tilde{\xi}^{(1,3)} = \begin{pmatrix} + \\ + \\ + \\ - \\ + \end{pmatrix}.$$

Step 4: Repeating the three steps above for the other 4 prescribed patterns, the interpolated cycle $\hat{\Sigma}_1$ is obtained as follows,

$$\hat{\Sigma}_1 = \left(\begin{array}{c|ccc|c|ccc|c|ccc|c|ccc|c|ccc} + & + & + & + & + & + & + & + & - & + & + & + & + & + & + & - & - & - & + & + \\ + & + & + & + & - & + & + & + & + & + & + & - & - & - & + & + & + & + & + & + \\ - & + & + & + & + & + & + & - & - & - & + & + & + & + & + & + & + & + & + & + \\ + & + & + & - & - & - & + & + & + & + & + & + & + & + & + & + & - & + & + & + \\ - & - & + & + & + & + & + & + & + & + & + & - & + & + & + & + & + & + & - \end{array}\right).$$

To emphasize the difference between prescribed and intermediate patterns, we use black and blue colors to label them respectively, and also use vertical lines to separate them. In each pattern (both

prescribed and intermediate) we use red color to highlight the entry at which the pattern changes sign.

Following exactly the same steps, the interpolated cycle $\hat{\Sigma}_2$ is obtained as follows,

$$\hat{\Sigma}_2 = \left(\begin{array}{c|cc|c|ccc|ccc|ccc|ccc|ccc} + & + & + & + & + & + & - & - & + & + & + & - & - & - & - & - & - & - & - & - \\ + & + & + & - & + & + & + & + & + & - & - & - & - & - & - & - & + & + & + & + \\ - & + & + & + & + & - & - & - & - & - & - & - & - & + & + & + & + & + & + & - \\ + & + & - & - & - & - & - & - & - & - & + & + & + & + & + & - & - & + & + & + \\ - & - & - & - & - & - & - & + & + & + & + & + & - & - & + & + & + & + & - & - \end{array}\right).$$

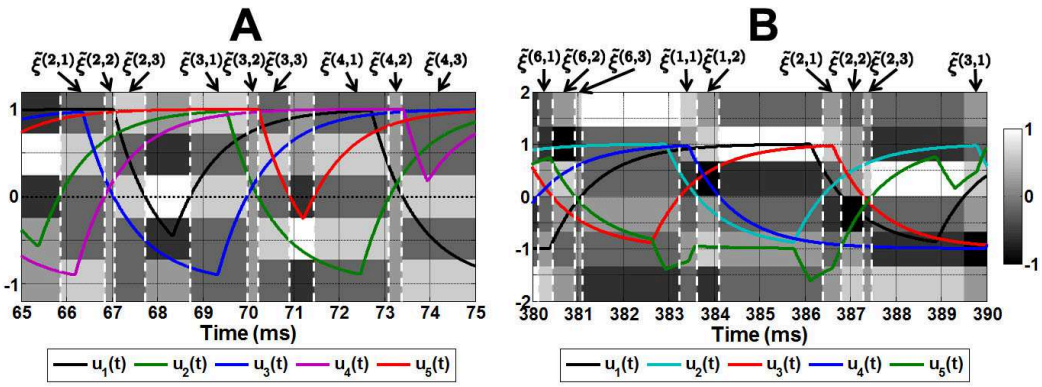

Figure 3.2: Network state transitions in actual simulations of the networks constructed from Σ (**A**) and $\tilde{\Sigma}$ (**B**) in Example 3.1.1. The backgrounds in both panels are raster plots of their overlaps $m^{(\nu)}(t)$ [14, 26] in grayscales. Above each panel, all intermediate patterns are labeled. Parameters for the simulations are set as: $\beta = \lambda = 100$, $\tau = 2.5$ms.

Figure 3.2 shows the actual simulations of the networks constructed from Σ (**A**) and $\tilde{\Sigma}$ (**B**) with both initial data taken as their first prescribed patterns. Above each panel, all the intermediate patterns are labeled. From the curves of the membrane potentials $u_i(t)$, every intermediate pattern can be very easily identified. For example, in panel **A**, the first intermediate pattern is $\tilde{\xi}^{(2,1)}$, and over the time interval between the first and second white dashed lines only the purple curve, i.e. $u_4(t)$, is below the horizontal axis, therefore, $\tilde{\xi}^{(2,1)} = (+,+,+,-,+)^T$. All other intermediate patterns can be identified similarly, and it can be easily checked that all of them are indeed exactly the same as the intermediate patterns determined above.

Remark 3.2.4. In Section 3.1, we have seen that if the prescribed cycle does not correspond to a stable periodic solution of the network (1.10), then the prescribed cycle will be retrieved as

relaxation oscillations, and will ultimately die out through one of the two scenarios illustrated in Figure 3.1**A** and **B**, respectively. In the first scenario, between successive starting points of any two state switches during two consecutive network state transitions, the membrane potentials $u_i(t)$ monotonically inscreases or decreases, which enables us to derive accurate results in the network corresponding to such a scenario. However, in the second scenario, between the starting points of two successive state-switches, some "humps" or "valleys" riding on the membrane potential curves occur. Although these "humps" or "valleys" make a quantitative description of the evolution of binary patterns difficult, a complete qualitative description of the evolution of the binary patterns, including the "humps" and "valleys" riding on the membrane potential curves, can be obtained. In the next subsection, we describe how to derive this complete qualitative description.

3.2.2 Qualitative Theory on Binary Patterns dynamics

Definition 3.2.5. The ν-th intermediate pattern $\tilde{\xi}^{(\mu,\nu)}$ between two successive patterns $\xi^{(\mu)}$ and $\xi^{(\mu+1)}$ of the prescribed cycle Σ is said to *satisfy the transition conditions* imposed by the prescribed cycle Σ, if

$$\mathbf{J}\tilde{\xi}^{(\mu,\nu)} = \tilde{\xi}^{(\mu+1,\nu)}, \tag{3.2}$$

where $\mathbf{J}$ is the connectivity matrix constructed from Σ with the pseudoinverse learning rule (1.9), and $\tilde{\xi}^{(\mu+1,\nu)}$ is the ν-th intermediate pattern between the prescribed pattern $\xi^{(\mu+1)}$ and $\xi^{(\mu+2)}$.

Example 3.2.3. Clearly, all the intermediate patterns of $\hat{\Sigma}_1$ in Example 3.2.2 satisfy the transition conditions (3.2) imposed by the prescribed cycle Σ. As an extreme simplification of the original system of delay differential equations (1.10) with $C_0 = 0$, we consider the following discrete dynamical system

$$\mathbf{x}_n = \mathbf{J}\text{sign}(\mathbf{x}_{n-1}) \tag{3.3}$$

and define the infinite sequence of binary patterns generated by repetitively applying the discrete dynamical system (3.3) on an initial binary pattern ξ^* as the *orbit* of ξ^* under the dynamical system (3.3). Then as the intermediate patterns of the cycle Σ satisfy the transition conditions imposed by Σ, the interdediate patterns in $\hat{\Sigma}_1$ themselves form orbits starting from any of them. Simple

computations show that these orbits consist of two periodic orbits and one fixed point listed as follows

$$\tilde{\xi}^{(1,1)} \xrightarrow{(3.3)} \tilde{\xi}^{(2,1)} \xrightarrow{(3.3)} \tilde{\xi}^{(3,1)} \xrightarrow{(3.3)} \tilde{\xi}^{(4,1)} \xrightarrow{(3.3)} \tilde{\xi}^{(5,1)} \xrightarrow{(3.3)} \tilde{\xi}^{(1,1)} \xrightarrow{(3.3)} \cdots$$

$$\tilde{\xi}^{(1,3)} \xrightarrow{(3.3)} \tilde{\xi}^{(2,3)} \xrightarrow{(3.3)} \tilde{\xi}^{(3,3)} \xrightarrow{(3.3)} \tilde{\xi}^{(4,3)} \xrightarrow{(3.3)} \tilde{\xi}^{(5,3)} \xrightarrow{(3.3)} \tilde{\xi}^{(1,3)} \xrightarrow{(3.3)} \cdots$$

and

$$\tilde{\xi}^{(1,2)} \xrightarrow{(3.3)} \tilde{\xi}^{(2,2)} = \tilde{\xi}^{(1,2)} \xrightarrow{(3.3)} \tilde{\xi}^{(3,2)} = \tilde{\xi}^{(1,2)} \xrightarrow{(3.3)} \tilde{\xi}^{(4,2)} = \tilde{\xi}^{(1,2)} \xrightarrow{(3.3)} \tilde{\xi}^{(5,2)} = \tilde{\xi}^{(1,2)} \xrightarrow{(3.3)} \cdots$$

Clearly, the two periodic orbits respectively starting from $\tilde{\xi}^{(m,1)}$ and $\tilde{\xi}^{(m,3)}$ for any m are exactly the same, and using matrix representation, the periodic orbit is given as follows

$$\Sigma' = \begin{pmatrix} + & + & + & + & - \\ + & + & + & - & + \\ + & + & - & + & + \\ + & - & + & + & + \\ - & + & + & + & + \end{pmatrix}. \tag{3.4}$$

It is also clear that some intermediate patterns in the interpolated cycle $\hat{\Sigma}_2$ must not satisfy the transition conditions imposed by $\tilde{\Sigma}$, as the Hamming distance between two successive prescribed patterns is not always the same. It is not difficult to check that the images of the intermediate patterns in $\hat{\Sigma}_2$ converge to the following two periodic orbits

$$\tilde{\Sigma}'_1 = \begin{pmatrix} + & + & - & - & - & + \\ + & - & - & - & + & + \\ - & - & - & + & + & + \\ - & - & + & + & + & - \\ - & + & + & + & - & - \end{pmatrix}, \text{ and } \tilde{\Sigma}'_2 = \begin{pmatrix} + & - & - & + & - & + \\ - & - & + & - & + & + \\ - & + & - & + & + & - \\ + & - & + & + & - & - \\ - & + & + & - & - & + \end{pmatrix}. \tag{3.5}$$

Remark 3.2.5. Since the network constructed from Σ is an excitatory (also known as cooperative) ring network, and it has been well known that there is no stable periodic solution in such a network [37, 42], it follows that all oscillatory solutions relax to one of the fixed point attractors, and the oscillatory solutions break via collisions of the boundaries between the adjacent blocks (*a consecutive*

set of neurons in a ring network with membrane potentials having the same sign at the same time is called a (spatial) block*, and the length of each block equals the number of neurons in the block*) of the oscillatory solutions [42]. Horikawa and Kitajima [42] pointed out that in the waves of oscillatory solutions traveling along a ring network, the bounary followed by a shorter block travels faster than that followed by a longer block. However, even in unidirectional ring networks, the prescribed cycle may have multiple shortest blocks, and these blocks may have different "priorities" to be "annihilated" via boundary collisions. Therefore, more information than just the length of the smallest blocks is needed, and this is the "duty" of the backward sequences. Next, we redefine a block as a temporal block, i.e. consecutive "+"s or "-"s in row vectors of the cycle-matrix Σ, and describe how to use the backward sequences to locate the blocks with the highest "priority" to be "annihilated" by boundary collisions.

Definition 3.2.6. Let $\Sigma \in \{-1,1\}^{N\times p}$ be an admissible cycle, and $\{b_{i,j} : i = 1,\dots,N,\ j = 1,\dots,p\}$ the set of all backward sequences associated to the entries of Σ. Let ξ' be the pattern derived from some $\xi^{(\mu)}$ in Σ by replacing $\xi_k^{(\mu)}$ by $-\xi_k^{(\mu)}$, where the associated backward sequence $b_{k,\mu} \in \min\{b_{i,j} : i = 1,\dots,N,\ j = 1,\dots,p\}$. Then the pattern ξ' is called a *derived pattern* and the cycle Σ' that is formed of the orbit of ξ' under (3.3) is referred to as a *derived cycle* of Σ.

Remark 3.2.6. Depending on ξ', the derived cycle Σ' may correspond to a fixed point attractor or stable periodic solution, or just another cycle satisfying the transition conditions imposed by Σ. If Σ' does not correspond to any fixed point attractor or stable periodic solution, then by repeating the same steps described in the above definition, a derived cycle Σ'' of the derived cycle Σ' can be obtained, and we call this derived cycle Σ'' a *second order derived cycle*. If Σ'' does not correspond to any fixed point attractor or stable periodic solution, then the above procedure can be continued until a derived cycle corresponding to some fixed point attractor or stable periodic solution is obtained.

Clearly $\xi' = \tilde{\xi}^{(m,1)}$ for some m, and if the intermediate patterns satisfy the transition conditions imposed by the prescribed cycle, then $\xi'' = \tilde{\xi}^{(m,2)}$ for some m. More generally, if the intermediate patterns satisfy the transition conditions imposed by the prescribed cycle, then the n-th order derived pattern is an n-th intermediate pattern of the prescribed cycle Σ. Therefore, the intermediate

patterns indeed tell the whole story of the qualitative dynamics of the network constructed from the prescribed cycle Σ.

If intermediate patterns do not satisfy the transition conditions imposed by the prescribed cycle Σ, then the network states may evolve into different "destinations".

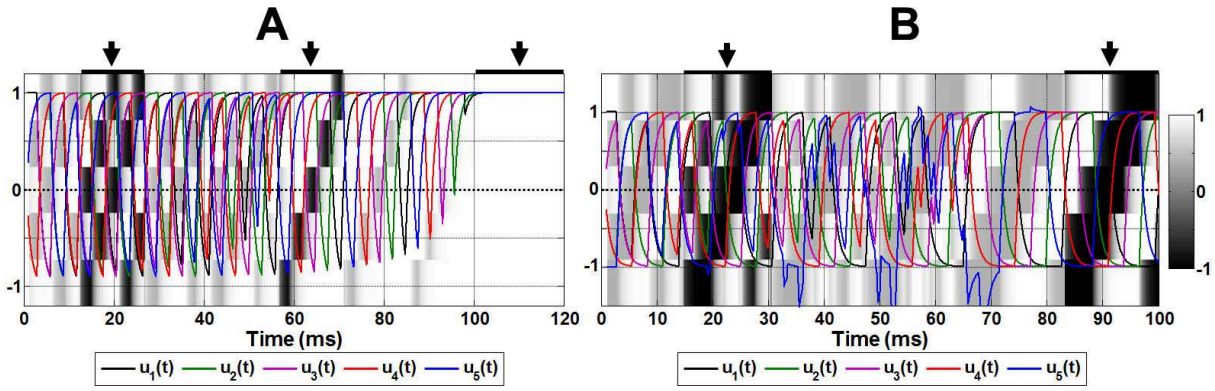

Figure 3.3: Qualitative description of the dynamics of the networks constructed from simple MC-cycles. Parameters are set as: $\beta = \lambda = 100$, $\tau = 2.3$.

Example 3.2.4. Figure 3.3**A** and **B** illustate actual simulations of the networks constructed from Σ and $\tilde{\Sigma}$ respectively. On the top of each panel, three and two thick black bars labelled with upside-down black arrows indicate the time intervals over which different phases of the qualitative dynamics of the network states are highlighted. The backgrounds in both panels are raster plots of the membrane potentials $\mathbf{u}(t)$. Comparing them with the derived cycles obtained in Example 3.2.3 shows that the derived cycles indeed capture the qualitative dynamics of the network states.

3.3 Quantitative Theory on Misalignment Length Dynamics

In the preceding Section, we have developed a novel qualitative method to fully describe the qualitative dynamics during the relaxation of the network states from the initial state to an attractor, either a fixed point attractor or a stable periodic solution. Based on this complete description of the transient network dynamics, in this section we develop the quantitative part of our MLA method, which captures the dynamics of the misalignment lengths through an iterated map. We begin by introducing the main "building blocks" needed for the quantitative MLA method.

3.3.1 Building Blocks - *Relaxation Times* and *Misalignment Lengths*

3.3.1.1 Hopfield-type Networks with $C_0 = 0$ and $\lambda = \beta \to \infty$

Neglecting the term for stabilizing the network in its current memory state, i.e. setting $C_0 = 0$, and introducing new variables $x_i(t) = \lambda u_i(t)$ and $s = t\lambda$, (1.10) can be rewritten as follows,

$$\dot{x}_i(s) = -\frac{1}{\lambda} x_i(s) + \beta_K \sum_{j=1}^{N} J_{ij} \tanh(x_j(s-\tau)) \tag{3.6}$$

This indicates that, from the point of view of biophysics, the gain scaling parameter λ can be related to the membrane time constant of the neurons in the network, and the membrane time constant of real neurons typically falls in the range from 10 to 100 ms [73]. In our studies on storage and retrieval of cycles of binary patterns in Hopfield-type networks, due to two reasons, we usually choose large values for the parameter λ. The first reason is that we interpret sequences of the binary states +1 and -1 traversed by single neurons in Hopfield-type networks as sequences of up and down states observed experimentally in cortical and CPG neurons [26], and the time scale of these subthreshold membrane bistable behaviors is much larger ($\sim$ 1 sec) than that of single potential actions [74]. The second reason is due to the simple fact that

$$\lim_{\lambda \to \infty} \tanh(\lambda u_j(t-\tau)) = \text{sign}(u_j(t-\tau))$$

and replacing $\tanh(\lambda u_j(t-\tau))$ by $\text{sign}(u_j(t-\tau))$ largely simplifies the process of solving the delay differential equations system (1.10). Therefore, for the convenience of introduction of the *MLA* method, we consider the systems with $\lambda \to \infty$ in this section, and in the next chapter, we demonstrate that the results obtained in networks with $\lambda \to \infty$ provide a decent approximation of the corresponding results in networks with λ large but finite.

Since $\beta_K = \beta/\lambda$ [14, 26], to avoid β_K approaching zero when λ approaches ∞, we take β to be a multiple of λ, i.e. $\beta = \alpha\lambda$, where α is some positive constant. Without loss of generality and also for simplicity, we set $\beta = \lambda$, i.e., $\beta_K = \alpha = 1$. Accordingly, we obtain the following network equations

$$\dot{u}_i(t) = -u_i(t) + \sum_{j=1}^{N} J_{ij} \text{sign}(u_j(t-\tau)), \tag{3.7}$$

which will form the basis for developping the quantitative MLA method.

3.3.1.2 Notations and Terminology

Suppose we choose the first pattern $\xi^{(1)}$ in the prescribed cycle Σ to set up an initial data as

$$\mathbf{u}(t) = a\xi^{(1)}, \text{ for all } t \in [-\tau, 0), \tag{3.8}$$

where the coefficient $a \in \mathbb{R}^+$ is an arbitrarily selected positive real number. Then starting from $t = 0$, as long as $\xi_i^{(2)} \neq \xi_i^{(1)}$, the membrane potential of the i-th neuron, $u_i(t)$, exponentially decreases or increases, and changes sign during the decrease or increase, and we call this sign-change process *state-switch* of the i-th neuron. When retrieving the second pattern $\xi^{(2)}$, no matter how many neurons change sign, they change it at the same time. If some pattern $\xi^{(\mu)}$ with $\mu > 1$ in the prescribed cycle Σ differ from the next pattern $\xi^{(\mu+1)}$ in Σ by more than one entries, i.e. the Hamming distance $d_\mu = d(\xi^{(\mu)}, \xi^{(\mu+1)}) > 1$, then some neurons will start changing signs asynchronously when retrieving the pattern $\xi^{(\mu+1)}$. We call these asynchronous sign-changes of the membrane potentials *misalignment of the zeros of the membrane potentials* (or for short, *misalignment*) during the network state transition from one prescribed pattern to the next, and refer to the smallest interval, on which all sign-changes switching the network states from one prescribed pattern to the next take place, as the *misalignment interval*.

Next, we formally define concepts and introduce the notations for the quantitative MLA method. First, we restate the concept of a network state used informally in Section 3.1.

Definition 3.3.1. Let $\mathbf{u}(t)$ be a solution of the network constructed from an admissible cycle Σ. If, for a given t, $u_i(t) \neq 0$ for all $1 \leq i \leq N$, then the (binary) column vector

$$\zeta(t) = \text{sign}(\mathbf{u}(t)), \tag{3.9}$$

is called the *network state* at time t.

Remark 3.3.1. Qualitatively, we denote the time interval during which the network state changes from prescribed cycle pattern to the next a network state transition. To make this qualitative description precise, we define distinguished times at which these transitions start and end.

Let $\mathbf{J}$ be the connectivity matrix constructed from any admissible cycle Σ with the pseudoinverse learning rule (1.8), and let the initial data be imposed as $\mathbf{u}(t) = a\xi^{(1)} \in \mathbb{R}^N$ with $a > 0$ and for all

$t \in [-\tau, 0)$. Then the corresponding initial value problem of nonlinear system of delay differential equations is formulated as

$$\begin{cases} \dot{u}_i(t) &= -u_i(t) + \sum_{j=1}^{N} J_{ij}\text{sign}(u_j(t-\tau)), \quad t \geq 0 \\ u_i(t) &= a\xi_i^{(1)}, \qquad\qquad\qquad\qquad\qquad\quad t \in [-\tau, 0) \end{cases} \tag{3.10}$$

Similar to the method of steps [75], we start solving the above initial value problem of delay differential equations by solving first its corresponding initial value problem of linear ordinary differential equations on the interval $[0, \tau)$,

$$\begin{cases} \dot{u}_i(t) &= -u_i(t) + \sum_{j=1}^{N} J_{ij}\xi_j^{(1)} \\ u_i(0) &= a\xi_i^{(1)} \end{cases} , \; t \in [0, \tau). \tag{3.11}$$

To emphasize the difference between the two different types of initial value problems in the forms of (3.10) and (3.11), respectively, we call (3.11) and analogous equations following from (3.10) *derived initial value problems.*

Since $\mathbf{J}\xi^{(\mu)} = \xi^{(\mu+1)}$, where $\mu = 1, \ldots, p$ and $\xi^{(p+1)} = \xi^{(1)}$, the derived initial value problem (3.11) becomes

$$\begin{cases} \dot{u}_i(t) &= -u_i(t) + \xi_i^{(2)} \\ u_i(0) &= a\xi_i^{(1)} \end{cases} , \; t \in [0, \tau)$$

The solution to this problem is easily obtained as

$$u_i(t) = e^{-t}[(e^t - 1)\xi_i^{(2)} + a\xi_i^{(1)}], \; t \in [0, \tau)$$

i.e.

$$u_i(t) = \begin{cases} \xi_i^{(2)}(1 - (1+a)e^{-t}), & \text{if } \xi_i^{(2)} \neq \xi_i^{(1)} \\ \xi_i^{(2)}(1 - (1-a)e^{-t}), & \text{if } \xi_i^{(2)} = \xi_i^{(1)} \end{cases} , \; t \in [0, \tau) \tag{3.12}$$

Different from the standard method of steps, instead of continuing to solve the derived initial value problem on the next interval $[\tau, 2\tau)$, we use the solution (3.12) to define the first variable time interval $\mathcal{I}_0$.

Designating the first zero of $u_i(t)$ by $t_i(0)$, provided that $\xi_i^{(1)} \neq \xi_i^{(2)}$, i.e.

$$t_i(0) = \min\{t > 0 : u_i(t) = 0, \text{ and } i \in \mathcal{A}_0\}, \tag{3.13}$$

where $\mathcal{A}_0$ is the set of row indices i with $\xi_i^{(1)} \neq \xi_i^{(2)}$ used in Definition 3.2.3, the first (variable) time interval $\mathcal{I}_0$ is defined as follows

$$\mathcal{I}_0 = [0, \check{t}(0) + \tau),$$

where

$$\check{t}(0) = \min_{i \in \mathcal{A}_0} \{t_i(0)\}.$$

If $\xi_i^{(1)} = \xi_i^{(2)}$, as in this case $u_i(t)$ moves towards $\xi_i^{(2)}$ from $a\xi_i^{(1)}$ without sign-change, i.e. $i \notin \mathcal{A}_0$, we say that $t_i(0)$ is not defined.

Similarly, we identify another important time point $\hat{t}(0)$ on the first interval $\mathcal{I}_0$ as

$$\hat{t}(0) = \max_{i \in \mathcal{A}_0} \left\{ t_i(0) : u_i(t_i(0)) = 0,\, \check{t}(0) \leq t_i(0) < \check{t}(0) + \tau \right\},$$

and define the first misalignment interval as $[t(0), \hat{t}(0)]$, i.e. the length of the first misalignment interval, ΔT_0, is computed as

$$\Delta T_0 = \hat{t}(0) - \check{t}(0), \tag{3.14}$$

which we refer to as the first *misalignment length*. Clearly, as $|u_i(0)| = a$ for every $i = 1, \ldots, N$, it follows that $t_i(0) = \ln(1 + a)$ provided $t_i(0)$ is defined, i.e. $\xi_i^{(1)} \neq \xi_i^{(2)}$. Thus, we have that $\check{t}(0) = \hat{t}(0) = \ln(1 + a)$, and accordingly,

$$\Delta T_0 = 0,$$

and

$$\mathcal{I}_0 = [0, \ln(1 + a) + \tau). \tag{3.15}$$

We note that, since (3.15) always holds as $\Delta T_0 = 0$, we don't have to take intermediate patterns into account yet. But as we continue to define the subsequent (variable) intervals $\mathcal{I}_n$ with $n \geq 1$, ΔT_n may become positive. In this case, if any intermediate pattern appearing in this subinterval does not satisfy the transition conditions imposed by the prescribed cycle Σ, it may change the time course of the membrane potentials in the next interval $\mathcal{I}_{n+1}$. To avoid this complication, in this dissertation, we develop the MLA method for admissible cycles with intermediate patterns satisfying the transition conditions they impose only, and extend it to more general admissible cycles in forthcoming work. Next, we extend notations related to the first interval $\mathcal{I}_0$ to any interval $\mathcal{I}_n$, and proceed to obtain the general formula for these intervals.

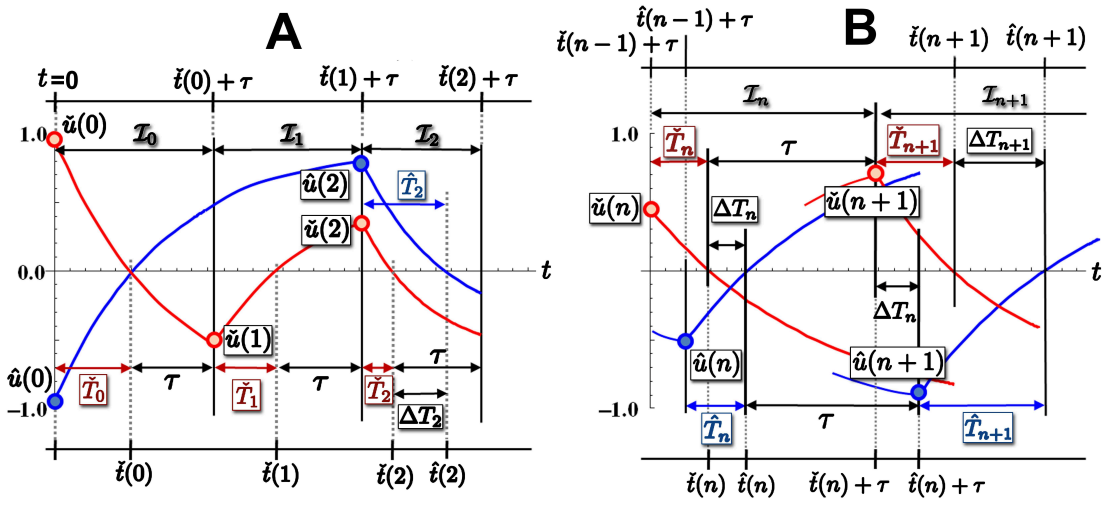

Figure 3.4: Illustration of the notations and definitions related to the *misalignment lengths* ΔT_n in timing diagrams. Panel (**A**) illustrates how non-trivial misalignment arises in the two components $u_1(t)$ (blue curve) and $u_2(t)$ (red curve) of a sketched solution $\mathbf{u}(t)$ starting from a "uniform" initial data $u_1(t) = -1$ and $u_2(t) = 1$ for all $t \in [-\tau, 0]$. Among quantities with the same value, only one is labeled. For example, as $\check{t}(0) = \hat{t}(0)$, only $\check{t}(0)$ is labeled. Quantities with zero value are not labeled either. For example, as $\Delta T_0 = \Delta T_1 = 0$, these two quantities are not labeled. Panel (**B**) illustrates how the *misalignment length* ΔT_n changes with increasing n.

Definition 3.3.2. Assuming that the n-th interval $\mathcal{I}_{n-1}$ and all relevant quantities, i.e. $t_i(n-1)$, $\check{t}(n-1)$, and $\hat{t}(n-1)$, have been defined, and, for $t > \check{t}(n-1)+\tau$, at least one component of the solution $\mathbf{u}(t)$ changes sign, we define the $(n+1)$-th *(variable) time interval* $\mathcal{I}_n$ and all its relevant quantities $t_i(n)$, $\check{t}(n)$, $\hat{t}(n)$ as follows

$$t_i(n) = \min\{t > \hat{t}(n-1) : u_i(t) = 0,\ i \in \mathcal{A}_n\}, \tag{3.16}$$

where $\mathcal{A}_n$ is the set of row indices i with $\xi_i^{(n+1)} \neq \xi_i^{(n+2)}$ and $\xi^{(\nu)} = \xi^{((\nu-1) \bmod p)+1}$ for any $\nu > 0$;

$$\check{t}(n) = \min_{i\in\mathcal{A}_n} \{t_i(n)\}\,, \text{ and } \hat{t}(n) = \max_{i\in\mathcal{A}_n} \{t_i(n)\}\,; \tag{3.17}$$

and

$$\mathcal{I}_n = [\check{t}(n-1)+\tau, \check{t}(n)+\tau). \tag{3.18}$$

Defining the $(n+1)$-th misalignment interval as $[\check{t}(n), \hat{t}(n)]$, the length of this interval, referred to as the $(n+1)$-th *misalignment length*, is computed as

$$\Delta T_n = \hat{t}(n) - \check{t}(n). \tag{3.19}$$

Definition 3.3.3. With the notation from Definition 3.3.2, we define the start- and end-times of the n-th state transition $\xi^{(n)} \to \xi^{(n+1)}$ as $\check{t}(n-1)+\tau$ and $\hat{t}(n)$, respectively. Moreover, for any $i \in \mathcal{A}_n$, we define the initial values of the state-switches during the n-th network state transition as $u_{i,n} = u_i(\tilde{t}_i(n))$, where

$$\tilde{t}_i(n) = \min\{\tilde{t} : \tilde{t} < t_i(n) \text{ and } \dot{u}_i(\tilde{t}_i(n)) \text{ is continuous in } (\tilde{t}, t_i(n))\}. \tag{3.20}$$

Then, letting $j, k \in \mathcal{A}_n$ be defined by

$$j = \arg\min_{i\in\mathcal{A}_n}\{|u_{i,n}|\}, \text{ and } k = \arg\max_{i\in\mathcal{A}_n}\{|u_{i,n}|\},$$

we set

$$\check{u}(n) = u_{j,n},\ \hat{u}(n) = u_{k,n},\ \check{T}_n = t_j(n) - \tilde{t}_j(n),\ \hat{T}_n = t_k(n) - \tilde{t}_k(n) \tag{3.21}$$

and call $\check{T}_n$ and $\hat{T}_n$ the $(n+1)$-th minimal and maximal relaxation times, respectively.

Figure 3.4**A** illustrates how a non-trivial misalignment length ΔT_2 arises. The figure illustrates the two components $u_1(t)$ (blue curve) and $u_2(t)$ (red curve) of a sketched solution $\mathbf{u}(t)$ starting from the "uniform" initial data $\mathbf{u}(t) = \xi^{(1)}$ (i.e. $a = 1$) for all $t \in [-\tau, 0]$. Since in the first interval $\mathcal{I}_0$, $t_2(0) = t_1(0) = \ln(1+a) = \ln 2$, and in the second interval $\mathcal{I}_1$, only the component $u_2(t)$ (red curve) changes sign, it follows that $\Delta T_0 = \Delta T_1 = 0$. Since the component $u_1(t)$ (blue curve) does not change sign in the second interval $\mathcal{I}_1$, its magnitude at the end of $\mathcal{I}_1$, $\underline{\hat{u}}(2)$, becomes larger than that of the component $u_2(t)$ (red curve), $\underline{\check{u}}(2)$, it follows that in the third interval $\mathcal{I}_2$, $u_1(t)$ (blue curve) will need longer time to reach its zero, i.e. $\hat{t}(2) > \check{t}(2)$. So in this example, the first non-trivial misalignment $\Delta T_2 = \hat{t}(2) - \check{t}(2) > 0$ arises in the third interval $\mathcal{I}_2$.

Figure 3.4**B** illustrates how the misalignment length ΔT_n changes with increasing n in the timing diagram of a sketched solution $\mathbf{u}(t)$ in two successive time intervals $\mathcal{I}_n$ and $\mathcal{I}_{n+1}$. From this figure, we can see that

$$\begin{cases} \Delta T_0 = \hat{T}_0 - \check{T}_0, & \text{if } n = 0 \\ \Delta T_n = \hat{T}_n - \check{T}_n + \Delta T_{n-1} & \text{if } n > 0 \end{cases}, \tag{3.22}$$

and the first minimal and maximal relaxation times are $\check{T}_0 = \check{t}(0)$ and $\hat{T}_0 = \hat{t}(0)$ respectively. In the next subsection, we prove this important relation, and based on this relation, we develop the quantitative method.

3.3.2 Recurrence Equations and Duration of the Delay-Induced Relaxation Oscillations

Before proving the relation (3.22), we first prove two other important results.

Lemma 3.3.1. *Let $\Sigma = (\xi^{(1)}, \ldots, \xi^{(p)})$ be a simple MC-cycle with its intermediate patterns satisfying the transition conditions imposed by Σ. Let $\mathbf{u}(t)$ be a solution of the network of the form (3.7) constructed from Σ and starting from $\mathbf{u}(t) = a\xi^{(\mu)}$ for some $a \in \mathbb{R}^+$ and $1 \leq \mu \leq p$. Let $b_{i,k}$ and $b_{j,k}$ be the backward sequences introduced in Section 3.2 with the total ordering "$<$". Then $b_{i,k} < b_{j,k}$ implies that*

$$t_i(n) < t_j(n) \tag{3.23}$$

and

$$|u_{i,n}| < |u_{j,n}| \tag{3.24}$$

for any k, and i, $j \in \mathcal{A}_n$ with $n > 0$.

Proof: Recalling the definition of the order of the backward sequences in Definition 3.2.2, we have that $b_{i,k} < b_{j,k}$ implies one of the following holds true,

- $\mathbf{B}_{i,k} < \mathbf{B}_{j,k}$;
- $\mathbf{B}_{i,k-m} < \mathbf{B}_{j,k-m}$ and $\pi_m = 1$;
- $\mathbf{B}_{i,k-m} > \mathbf{B}_{j,k-m}$ and $\pi_m = -1$.

We prove the statement for first case in detail, for the other two cases the proof proceeds similarly.

Recall that in Section 3.1 we defined the set of consecutive "+"s or "-"s in each row of a cycle Σ represented as a loop a temporal block. For example, suppose $\eta_3 = (+,+,+,-,+,+,-,-,+) \in R(\Sigma)$ is the 3rd row vector of a given cycle Σ, then the temporal blocks in η_3 are $(+,+,+,+)$, $(-)$, $(+,+)$, and $(-,-)$. According to the definition of the BS-matrix, it is clear that the entry $\mathbf{B}_{i,k}$ counts the number of "+" or "-" in the "current" block before and including the k-th element in the i-th row. For example, still consider the row vector η_3 given above, $\mathbf{B}_{3,2} = 3$, because in the "current" block[1], the entry $\Sigma_{3,2} = +$ is the third "+". Also, if $\mathbf{B}_{i,k} = 1$, then the membrane

[1] *"current"* in this example means in time we are at the second column, and *"current" block* means the temporal block containing the current entry $\Sigma_{3,2} = +$

potential $u_i(t)$ has a zero at a time point corresponding to the block boundary right before the "current" entry $\Sigma_{i,k}$. Based on this, it follows that $\mathbf{B}_{i,k} < \mathbf{B}_{j,k}$ implies that the last zero of $u_j(t)$ is located at some point in a variable time interval $\mathcal{I}_{n_j}$ which appears, in time, before the last zero of $u_i(t)$ that is located at some point in another variable time interval $\mathcal{I}_{n_i}$, and we have that $n_i - n_j = \mathbf{B}_{j,k} - \mathbf{B}_{i,k}$.

Now, consider the corresponding derived initial value problem of the form (3.11). Since here we only care about the magnitude, and the initial value is 0, the corresponding derived initial value problem can be simplified as follows,

$$\begin{cases} \dfrac{d|u_i|}{dt} = -|u_i| + 1 \\ |u_i(t_i(n_i))| = 0 \end{cases} . \tag{3.25}$$

It is straightforward to see that the solution to this initial value problem is:

$$|u_i(t)| = 1 - e^{-(t - t_i(n_i))}.$$

Similarly, we can obtain

$$|u_j(t)| = 1 - e^{-(t - t_j(n_j))}.$$

Since $\mathbf{B}_{i,k} < \mathbf{B}_{j,k}$ implies that $t_i(n_i) < t_j(n_j)$, it follows that $|u_i(t)| < |u_j(t)|$.

Since the intermediate patterns of Σ satisfy the transition conditions imposed by Σ, following from the Definitions 3.2.3 and 3.2.4, we have that $d_{i,k} < d_{j,k}$ implies that the i-th component of the prescribed pattern $\xi^{(n)}$ changes sign before the j-th component forms the corresponding intermediate pattern $\xi^{(n,\nu_i)}$, where $\xi^{((n-1) \bmod p)+1} = \xi^{(k)}$, and the two corresponding intermediate patterns are $\xi^{(n,\nu_i)}$ and $\xi^{(n,\nu_j)}$ with $\nu_i < \nu_j$. It follows that $|u_{i,n}| < |u_{j,n}|$.

Since $u_{i,n}$ is reached earlier than $u_{j,n}$, and $|u_{i,n}| < |u_{j,n}|$, it follows that the two zeros $t_i(n)$ and $t_j(n)$ also satisfy the order $t_i(n) < t_j(n)$. This completes the proof.

Lemma 3.3.2. *Let $\check{T}_n$ and $\hat{T}_n$ be the $(n+1)$-th minimal and maximal relaxation times of a solution $\mathbf{u}(t)$ of the network constructed from a simple MC-cycle $\Sigma = (\xi^{(1)}, \ldots, \xi^{(p)})$ with the intermediate patterns satisfying the transition conditions imposed by Σ, and assume the solution starts from a uniform initial condition, i.e. $\mathbf{u}(t) = a\xi^{(\mu)}$ for some $a \in \mathbb{R}^+$ and $1 \le \mu \le p$ and all $t \in [-\tau, 0)$. Then*

$$\check{T}_n = \check{t}(n) - \check{t}(n-1) - \tau, \tag{3.26}$$

and

$$\hat{T}_n = \hat{t}(n) - \hat{t}(n-1) - \tau, \tag{3.27}$$

Proof: Since the intermediate patterns of Σ satisfy the transition conditions imposed by Σ, following from the Definitions 3.2.3 and 3.2.4, we have that, if $t_i(n) = \check{t}(n)$, then the i-th neuron is the first neuron starting its state-switch on the $(n+1)$-th interval $\mathcal{I}_n$. It follows that $\check{T}_n = \check{t}(n) - \check{t}(n-1) - \tau$. The formula (3.27) is obtained analogously. This completes the proof.

Proposition 3.3.3. *Let $\check{T}_n$, $\hat{T}_n$ and ΔT_n be defined as above, and the initial data for retrieving the prescribed cycle be uniform in magnitude, i.e. $\mathbf{u}(t) = a\xi^{(\mu)}$ for some $1 \leq \mu \leq p$, $a \in \mathbb{R}^+$, and $t \in [-\tau, 0)$. Then we have that the relation (3.22) holds true.*

Proof: The relation (3.22) is an immediate consequence of the Lemma 3.3.2.

Since if the Hamming distance between any two consecutive patterns of a cycle is 1, the cycle does not have any intermediate pattern and the misalignment length is always 0, it follows that using the MLA terminology, this case is trivial. So next, we consider more general cases, i.e., the Hamming distance between two consecutive patterns is always greater than or equal to 2, and demonstrate in an example how to use the relation (3.22) of misalignment lengths to find a recurrence equation. This recurrence equation is then used to find a lower bound for the duration of the delay-induced relaxation oscillations.

Example 3.3.1. Consider the simple admissible cycle Σ with the connectivity matrix $\mathbf{J}$,

$$\Sigma = \begin{pmatrix} + & + & + & - \\ + & + & - & + \\ + & - & + & + \\ - & + & + & + \end{pmatrix}, \mathbf{J} = \Sigma \mathbf{P} \Sigma^+ = \begin{pmatrix} 0 & 1 & 0 & 0 \\ 0 & 0 & 1 & 0 \\ 0 & 0 & 0 & 1 \\ 1 & 0 & 0 & 0 \end{pmatrix}.$$

This network is an excitatory, unidirectional ring of four neurons. A simulated solution of the network equations starting from the inital data $\mathbf{u}(t) = \xi^{(1)}$ for all $t \in [-\tau, 0)$ is shown in Figure 3.6.

In general, if the i-th neuron changes sign first during the n-th network state transition and the j-th neuron changes sign last during this transition, then the i-th neuron changes sign at $\check{t}(n)$ and

the j-th neuron changes sign at $\hat{t}(n) = \check{t}(n) + \Delta T_n$, and both $\check{T}_n$ and $\hat{T}_n$ can be explicitly derived as

$$\check{T}_n = \ln(1 + |\check{u}(n)|), \text{ where } \check{u}(n) = u_i(\check{t}(n-1) + \tau), \tag{3.28}$$

and

$$\hat{T}_n = \ln(1 + |\hat{u}(n)|), \text{ where } \hat{u}(n) = u_j(\check{t}(n-1) + \Delta T_{n-1} + \tau). \tag{3.29}$$

Since in this example, we have

$$|\check{u}(n)| = |u_i(\check{t}(n-1) + \tau)| = 1 - e^{-(\tau - \Delta T_{n-1})} \tag{3.30}$$

and

$$|\hat{u}(n)| = |u_j(\check{t}(n-1) + \Delta T_{n-1} + \tau)| = 1 - e^{-(3\tau + \check{T}_{n-2} + \check{T}_{n-1} + \Delta T_{n-1})}, \tag{3.31}$$

it follows that

$$\check{T}_n = \ln(2 - e^{-(\tau - \Delta T_{n-1})}) \tag{3.32}$$

and

$$\hat{T}_n = \ln(2 - e^{-(3\tau + \check{T}_{n-2} + \check{T}_{n-1} + \Delta T_{n-1})}). \tag{3.33}$$

Applying (3.32) to $\check{T}_{n-1}$ and $\check{T}_{n-2}$ yields

$$\check{T}_{n-1} = \ln(2 - e^{-(\tau - \Delta T_{n-2})}), \text{ and } \check{T}_{n-2} = \ln(2 - e^{-(\tau - \Delta T_{n-3})}),$$

and substituting this into (3.33) gives

$$\hat{T}_n = \ln\left(2 - \frac{e^{-(\tau + \Delta T_{n-1})}}{(2e^{\tau} - e^{\Delta T_{n-2}})(2e^{\tau} - e^{\Delta T_{n-3}})}\right). \tag{3.34}$$

Thus, substituting both (3.32) and (3.34) into (3.22) gives a recurrence equation

$$\Delta T_n = \ln\left(2e^{\Delta T_{n-1}} - \frac{e^{-\tau}}{(2e^{\tau} - e^{\Delta T_{n-2}})(2e^{\tau} - e^{\Delta T_{n-3}})}\right) - \ln(2 - e^{-(\tau - \Delta T_{n-1})}). \tag{3.35}$$

By direct computations, the "initial condition" for this recurrence equation is derived as

$$\begin{cases} \Delta T_0 &= 0 \\ \Delta T_1 &= \ln\left(2 - \dfrac{(1-a)e^{-\tau}}{1+a}\right) - \ln(2 - e^{-\tau}) \\ \Delta T_2 &= \ln\left(2 - \dfrac{(1-a)e^{-\tau}}{2(1+a)e^{\tau} - (1-a)}\right) - \ln(2 - e^{-\tau}) + \Delta T_1 \end{cases} \tag{3.36}$$

where a is the coefficient of the initial data (3.8), and in this example we set $a = \beta_1 = 0.9999$. With the above initial condition (3.36), any misalignment ΔT_n, can be computed iteratively using (3.35). Figure 3.5 illustrates both the update function $f(x) = \ln\left(2e^x - \frac{e^{-\tau}}{(2e^{\tau}-e^x)^2}\right) - \ln\left(2 - e^{-(\tau-x)}\right)$ with $\tau = 1$, 2, and 5 respectively (**A**), and iterations of the recurrence equation (3.35) with the initial condition (3.36) (**B**).

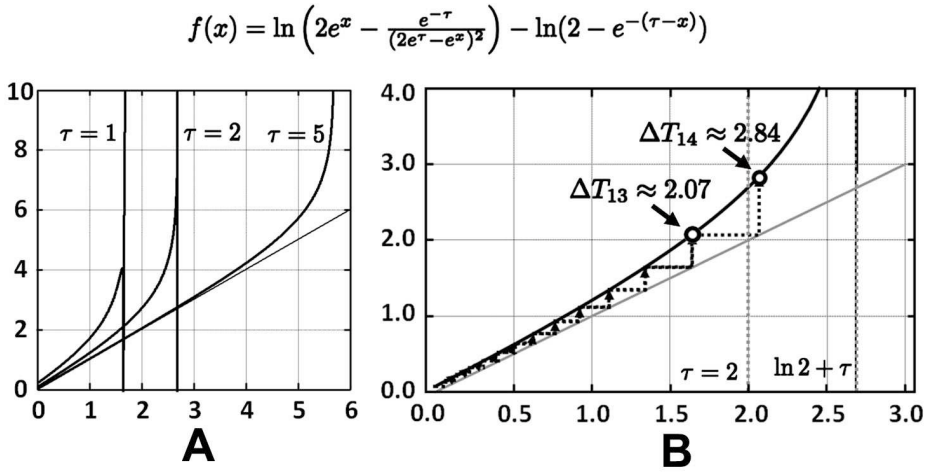

Figure 3.5: Illustration of the recurrence equation (3.35). **A** Graph of the function $f(x)$ with $\tau = 1$, $\tau = 2$, and $\tau = 5$ respectively. **B** Cobweb diagram of the iterates of the recurrence equation (3.35) with the initial condition (3.36). The two gray dotted vertical lines locate τ and $\ln 2 + \tau$ on the horizontal axis.

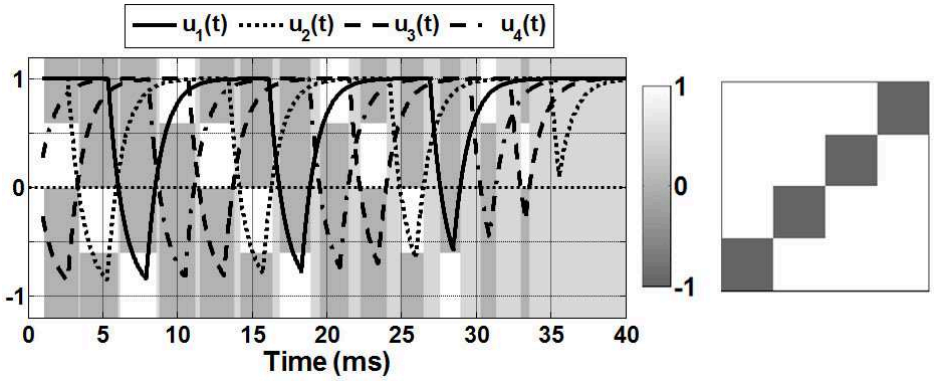

Figure 3.6: Delay-induced relaxation oscillation converging to a stable fixed point $(1, 1, 1, 1)^T$. The background in the left panel is the raster plot of the overlaps $m^{(\mu)}(t)$. The right panel plots the prescribed cycle Σ generated by the row vector $\eta = (+, +, +, -)$.

Since the $(n+1)$-th transition starts at $\check{t}(n)+\tau$, it follows that if $\hat{n}>0$ is the smallest integer such that $\Delta T_{\hat{n}} \geq \tau$, then the sign vector of the coupling term $\mathbf{J}\text{sign}(\mathbf{u}(t-\tau))$ of the network (3.7) for $t > \check{t}(\hat{n})+\tau$ will be different from the next prescribed pattern. Therefore, the $(\hat{n}+1)$-th pattern will not be retrieved successfully. In other words, the condition for failure in retrieving the $(\hat{n}+1)$-th patterns is

$$\Delta T_{\hat{n}} \geq \tau. \tag{3.37}$$

Figure 3.5**B** shows that the first iteration for which the misalignment exceeds $\tau = 2$ is the 13th, i.e. $\hat{n} = 13$. Therefore, in the network with $\tau = 2$, 13 prescribed patterns can be retrieved successfully. Figure 3.6 illustrates retrieval of this cycle with the above parameter values, showing that indeed 13 consecutive patterns are retrieved successfully. Since $\check{t}(n+1) - \hat{t}(n) > \tau$, $\hat{n}\tau$ can be used as an approximate lower bound for the duration of the transient oscillations.

CHAPTER 4

RETRIEVABILITY OF ADMISSIBLE CYCLES

In Chapter 3 we developed a novel method for analyzing the relaxation dynamics of networks constructed from admissible cycles, referred to as *Misalignment Length Analysis* (MLA). The method consists of qualitative and quantitative parts. In this chapter, with the help of the quantitative MLA method, we prove that simple MC-cycles with intermediate patterns satisfying the transition conditions imposed by the cycles are weakly retrievable. Then, starting from this result, we study retrievability of general admissible cycles.

4.1 Retrieving Admissible Cycles in Networks with $C_0 = 0$

The network constructed from the cycle Σ given in Example 3.3.1 is an excitatory unidirectionally coupled ring network. It has been well-known that such networks have no stable periodic solution, and the delay-induced long lasting transient oscillations exist for a large set of parameter values and initial conditions. In Example 3.3.1, with the sigmoid-shaped gain function approximated by the signum function, we have derived the recurrence equation (3.35) for the misalignment lengths, and demonstrated, by iteratively solving this recurrence equation for the largest misalignment length $\Delta T_{\hat{n}}$, how an approximate lower bound $\hat{n}\tau$ for the duration of the long lasting transient oscillations can be obtained. Actually, following exactly the same procedure, a recurrence equation can be obtained for every network constructed from a simple MC-cycle if the intermediate patterns satisfy the transition conditions imposed by the cycle. For composite cycles, we will show that a lower bound for the duration of the delay-induced transient oscillations in networks constructed from them is the smallest of the lower bounds of the simple cycle components of the composite cycle.

Although the results in Chapter 3 were obtained in the limit when the gain scaling parameter $\lambda \to \infty$, with $\tanh(\lambda x)$ approximated by sign(x), they can be extended to networks with finite but still large λ by applying the method of singular perturbations [76]. In this chapter, we assume that

λ is sufficiently large such that the properties of the networks are qualitatively identical to those of networks with $\lambda \to \infty$.

From (3.35), we can see that when $\tau \to \infty$, the misalignment length ΔT_n will approach its initial value. In other words, the larger the delay τ, the longer the misalignment ΔT_n will be stuck around its initial value, and hence, the more prescribed patterns the network will retrieve. If we denote the largest number of the prescribed patterns the network can retrieve by $\hat{n}$, then $\hat{n} \to \infty$, as $\tau \to \infty$. Next, motivated by this simple observation, we introduce the concepts of weak and strong retrievability of admissible cycles, and prove that every admissible cycle is weakly retrievable.

Definition 4.1.1. Let $\Sigma = (\xi^{(1)}, \ldots, \xi^{(p)})$ be an admissible cycle, and $\mathbf{u}(t)$ a solution of the network (1.10) constructed from Σ starting from an initial data $\mathbf{u}(t) = a\xi^{(\mu)}$ for all $t \in [-\tau, 0]$, $\xi^{(\mu)} \in \Sigma$ and $a \in \mathbb{R}^+$. We say that $\mathbf{u}(t)$ **satisfies the transition conditions imposed by** Σ over an interval $(0, T)$, if $\mathbf{u}(t)$ satisfies

$$\operatorname{sign}(\mathbf{u}(t)) = \xi^{((\mu+n+1) \bmod p)+1}, \tag{4.1}$$

for $t \in (\hat{t}(n), \check{t}(n+1))$, and all n for which $\check{t}(n+1) < T$.

Definition 4.1.2. An admissible cycle Σ is **strongly retrievable**, if the system (1.10) has a stable periodic solution $\mathbf{u}(t)$ satisfying the transition conditions imposed by Σ.

Definition 4.1.3. An admissible cycle Σ is **weakly retrievable**, if for any integer $m > 0$, there exists a $\tau_0 > 0$, such that the largest number $\hat{n}$ of prescribed patterns every network constructed from Σ with $\tau \geq \tau_0$ retrieves is greater than m.

Next, we prove that every admissible cycle is weakly retrievable in the network constructed from it with $C_0 = 0$, and λ sufficiently large. For $C_0 > 0$, the prescribed admissible cycles may or may not be retrieved in the networks constructed from them. We will discuss the retrieval of admissible cycles in such networks in examples in Section 4.2.

Lemma 4.1.1. *Let ΔT_n and $\Delta \tilde{T}_n$ be the misalignment lengths of two networks constructed from admissible cycles. If $\Delta T_n \leq \Delta \tilde{T}_n$ for all n, and the network associated to $\Delta \tilde{T}_n$ is weakly retrievable, then the network associated to ΔT_n is weakly retrievable too.*

Proof: This is clear, as $\Delta T_n < \tau$ is the condition for successful retrieval of the n-th prescribed pattern.

Theorem 4.1.2. *Every simple MC-cycle Σ with intermediate patterns satisfying the transition conditions imposed by Σ is weakly retrievable in the network constructed from it for λ sufficiently large.*

Proof: Let $\tilde{\Sigma}$ be the simple MC-cycle generated by the following first row: $\tilde{\eta}_1 = (+,+,\ldots,+,-) \in \{-1,1\}^p$. The backward sequence $\tilde{b}_{1,p}$ of this row is the smallest possible backward sequence that can occur in any simple MC-cycle $\Sigma \in \{-1,1\}^{N\times p}$, thus we have that $\tilde{b}_{1,p} \leq b_{i,j}$ for all backward sequences in Σ. It then follows from Lemma 3.3.1 that

$$\Delta T_n \leq \Delta \mathcal{T}_n$$

for all n, where ΔT_n and $\Delta \mathcal{T}_n$ are the n-th misalignment lengths of Σ and $\tilde{\Sigma}$, respectively. According to Lemma 4.1.1, it is sufficient to show that $\tilde{\Sigma}$ is weakly retrievable.

Now, following exactly the preceding used in Example 3.3.1, a recurrence equation for $\Delta \mathcal{T}_n$ is obtained as follows

$$\Delta \mathcal{T}_{n+p-1} = \ln\left(2e^{\Delta \mathcal{T}_{n+p-2}} - e^{-\tau}\prod_{k=2}^{p-1}(2e^{\tau} - e^{\Delta \mathcal{T}_{n+p-1-k}})^{-1}\right) - \ln(2 - e^{\Delta \mathcal{T}_{n+p-2}-\tau}). \tag{4.2}$$

From this recurrence equation, it can be seen that $\Delta \mathcal{T}_{n+p-1} = \Delta \mathcal{T}_{n+p-2}$ for all $n \in \mathbb{N}$ as $\tau \to \infty$. Moreover, as $\tau \to \infty$, the difference $|\hat{u}(k) - \check{u}(k)| \to 0$ for all $k \leq p-1$, and accordingly, $|\check{T}_k - \hat{T}_k| \to 0$, which implies that $|\Delta T_k - \Delta T_{k-1}| \to 0$. Since $\Delta \mathcal{T}_0 \equiv 0$, there exists τ^* such that $\Delta \mathcal{T}_{p-1} < \tau$ if $\tau \geq \tau^*$. By continuity, we can find for any $\tilde{n} \in \mathbb{N}$ and $\tilde{\tau} > \tau^*$ such that $\Delta \mathcal{T}_n < \tau$ for all $n \leq \tilde{n}$ if $\tau \geq \tilde{\tau}$, that is, $\tilde{\Sigma}$ is weakly retrievable.

Corollary 4.1.3. *For a given $\mathbf{J} \in \mathbb{R}^{N\times N}$, all simple MC-cycles $\Sigma \in \{-1,1\}^{N\times p}$ satisfying $\mathbf{J}\Sigma = \Sigma\mathbf{P}$ are weakly retrievable.*

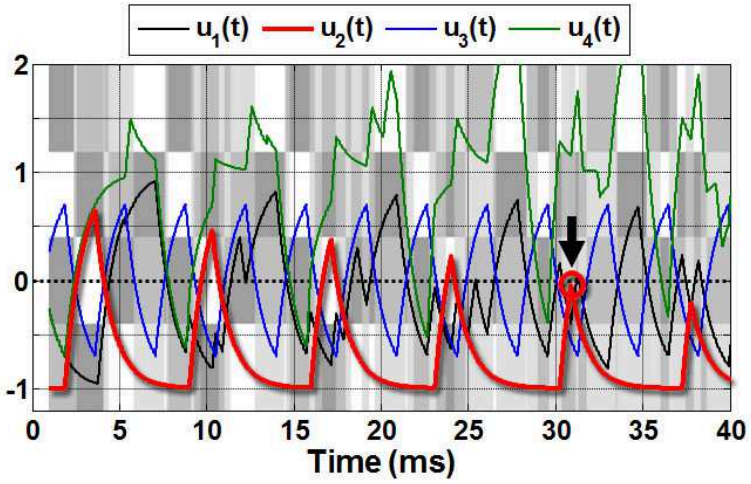

Figure 4.1: Retrieval of the inseparable composite admissible cycle Σ from Example 4.1.1. Parameters for the simulation are set as: $C_0 = 0$, $\lambda = \beta = 100$, $\tau = 1.2$ms.

Example 4.1.1. Consider the following inseparable composite admissible cycle Σ and its connectivity matrix $\mathbf{J}$

$$\Sigma = \begin{pmatrix} + & - & - & + \\ - & - & + & - \\ - & + & - & + \\ + & - & + & + \end{pmatrix}, \mathbf{J} = \Sigma \mathbf{P} \Sigma^{+} = \begin{pmatrix} 0 & 1 & 1 & 1 \\ 0 & 0 & 0 & -1 \\ 0 & 0 & -1 & 0 \\ -1 & 0 & 1 & 1 \end{pmatrix},$$

This cycle is an inseparable composite cycle, and the network constructed from it is neither excitatory nor a ring network. But simulations show that Σ is indeed stored and retrieved as delay-induced long lasting transient oscillations. Since the longest block in Σ is of length 3, it can be expected that its misalignment lengths are bounded by $\Delta T_n \leq \Delta \mathcal{T}_n$, where $\Delta \mathcal{T}_n$ are the misalignment lengths for the cycle from Example 3.3.1. We have already seen that, with $C_0 = 0$, $\tau = 2$, the network from Example 3.3.1 can retrieve exactly 13 prescribed patterns. Figure 4.1 shows a simulated solution of the network constructed from the composite cycle Σ above. Obviously the number of prescribed patterns the network retrieves is actually much larger than 13, illustrating that the bound from Theorem 4.1.2 is really a worst case scenario.

Remark 4.1.1. Similar behavior as shown in Example 4.1.1 has been found in networks constructed from other admissible cycles even if they were not simple MC-cycles. We conjecture that for a given

$\mathbf{J}$, all cycles Σ satisfying $\mathbf{J}\Sigma = \Sigma\mathbf{P}$ are weakly retrievable. A proof of this more general conjecture is still pending and will be the subject of future research.

In the following, given an admissible cycle Σ with connectivity matrix $\mathbf{J}$ constructed from Σ, we call any other cycle Σ' satisfying $\mathbf{J}\Sigma' = \Sigma'\mathbf{P}$ a derived cycle.

Although Theorem 4.1.2 requires Σ to be the cycle prescribed in the network, i.e., the network is constructed from it, we emphasize that Σ is not the only cycle that can be retrieved in the network. In Corollary 4.1.3, we have shown that any simple MC-cycle Σ' satisfying the transition condition imposed by Σ can be retrieved in the network constructed from Σ, and numerical obervations indicate that this is indeed true for any admissible cycle Σ! In the next example, we demonstrate that in the network constructed from a randomly chosen prescribed admissible simple cycle

$$\Sigma = \begin{pmatrix} + & + & - & + & - & - \\ + & - & + & - & - & + \\ - & + & - & - & + & + \\ + & - & - & + & + & - \\ - & - & + & + & - & + \end{pmatrix}, \tag{4.3}$$

in addition to Σ, three other cycles are successfully retrieved.

Example 4.1.2. Consider the network constructed from the cycle (4.3) using the pseudoinverse learning rule. The connectivity matrices $\mathbf{J^0}$ and $\mathbf{J}$ are respectively constructed as $\mathbf{J^0} = \Sigma\Sigma^+$ and $\mathbf{J} = \Sigma\mathbf{P}\Sigma^+$, and $\mathbf{J}\Sigma = \Sigma\mathbf{P}$ as Σ is admissible. In order to reveal how many other cycles satisfy the transition conditions imposed by Σ, we investigate the evolutions of all binary state patterns $\xi \in \{-1, 1\}^5$ under the transition operation $\xi \mapsto \mathrm{sgn}(\mathbf{J}\xi)$. In Figure 4.2, we illustrate the evolution graphs of the binary state patterns. Following [56], we represent each binary column vector $\xi \in \{-1, 1\}^N$ by a decimal integer. Before converting binary vectors to decimal integers, the digit -1 in ξ is replaced by 0. For instance, $\xi = (+, +, -, +, -)^T$ is replaced by $(1, 1, 0, 1, 0)$ first, then converted to $2^4 + 2^3 + 2^1 = 26$.

The evolution graphs exhibit four loops. Direct calculations show that these four loops correspond to four cycles satisfying the transition conditions imposed by Σ. Labeling these four cycles by Σ_1, Σ_2, Σ_3 and Σ_4 respectively (see Figure 4.2), all four cycles satisfy $\mathbf{J}\Sigma_i = \Sigma_i\mathbf{P}$, $i = 1, 2, 3, 4$,

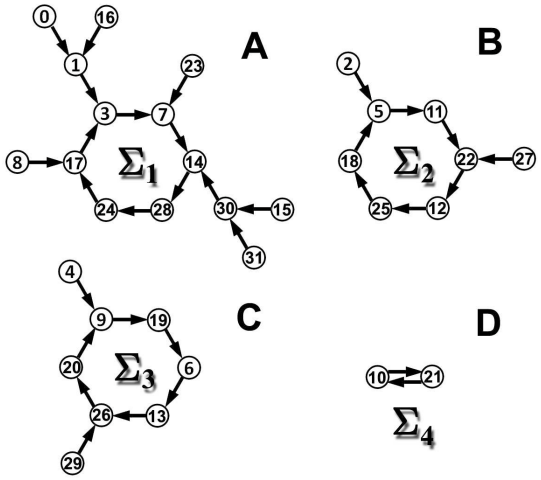

Figure 4.2: Graphs of evolution of the state patterns $\xi^{(\mu)}$ in the state space $\{-1, 1\}^5$ under the transition operation $\xi^{(\mu)} \mapsto \text{sgn}(\mathbf{J}\xi^{(\mu)})$, where $\mathbf{J}$ is constructed from the cycle (4.3) using the pseudoinverse learning rule.

where $\mathbf{P}$ is the cyclic permutation matrix of the form (1.5). For $i \neq 4$, $\mathbf{P}$ is of order 6, and for $i = 4$, $\mathbf{P}$ is of order 2. Note that Σ_4 is not a simple MC-cycle. Clearly, the cycle Σ_3 is the prescribed cycle Σ.

Figure 4.3**A** and **B** respectively illustrate the retrieved time series in raster plots of the four cycles and the projections of their phase trajectories onto the three-dimensional (u_2, u_3, u_4) phase subspace. Both illustrations suggest that the four cycles are retrieved successfully. This confirms Corollary 4.1.3.

In the next section, we discuss retrieval of prescribed and derived admissible cycles in networks with $C_0 > 0$.

4.2 Retrieving Admissible Cycles in the Networks with $C_0 > 0$

In general, the connectivity of a network (1.10) contains two components [14, 26], $\mathbf{J^0}$ and $\mathbf{J}$. One is for stabilizing individual patterns in Σ as fixed points of the system, and the other is for imposing the transitions among patterns prescribed by the cycle Σ. We use the two parameters C_0 and $C_1 = 1 - C_0$ to control the relative contributions of these two components in shaping the dynamics of the network. In Section 4.1, we proved in Theorem 4.1.2 that when only the transition component $\mathbf{J}$ is included, i.e. $C_0 = 0$, every prescribed simple MC-cycle can be retrieved with both

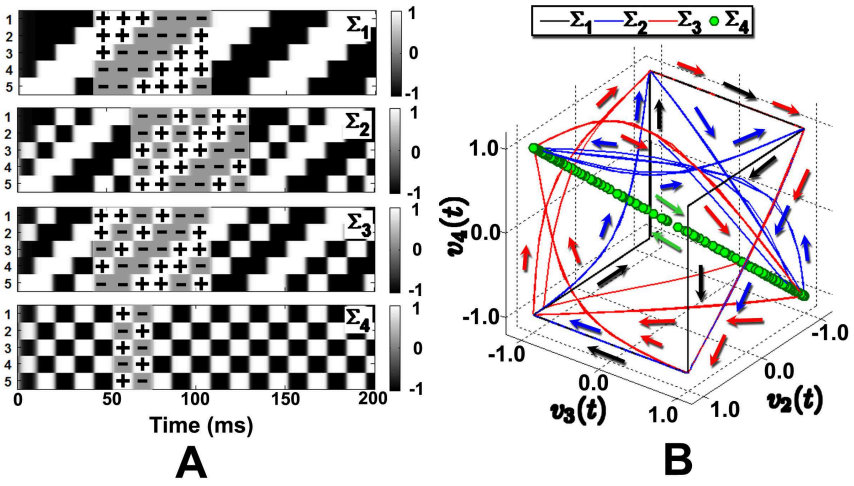

Figure 4.3: Retrieval of the 4 coexisting derived cycles. **A** Raster plots of the time series of the four retrieved cycles, Σ_1, Σ_2, Σ_3, and Σ_4. The network is constructed from the cycle (4.3). Clearly, the prescribed cycle $\Sigma = \Sigma_3 = -\Sigma_2$, and $\Sigma_1 = (\hat{\eta}^T, (\hat{\eta}\mathbf{P})^T, \ldots, (\hat{\eta}\mathbf{P}^5)^T)^T$, with $\hat{\eta} = (+,+,+,-,-,-)$. The cycle Σ_4 is of length two and $\mathbf{J}\Sigma_4 = \Sigma_4\mathbf{P} = -\Sigma_4$. The i-th row in each raster plot represents the firing rates $v_i(t)$ of the i-th neuron. The parameters are set as $\beta = 3$, $C_0 = 0$, $\tau = 10$ms, and $\lambda = 20$. **B** Projections of the phase trajectories of the four cycles onto the (u_2, u_3, u_4) phase subspace.

λ and τ sufficiently large. For $C_0 = 1$, the transition conditions imposed by the prescribed cycle Σ are completely removed. Consequently, no cycle is stored in such networks [56], and we will not consider this type of networks here. In this section, we consider networks with $0 < C_0 < 1$, and discuss retrieval of prescribed admissible cycles.

Theorem 4.2.1. *Suppose a network of the form (1.10) is constructed from an admissible cycle* $\Sigma = (\xi^{(1)}, \xi^{(2)}, \ldots, \xi^{(p)})$, *and in the* $(n+1)$*-th time interval* $[n\tau, (n+1)\tau)$, *the solution of the network (1.10) satisfies* $\mathrm{sgn}(\mathbf{u}(t)) = \xi^{(\mu)}$ *for some* $1 \le \mu \le p$. *Then in the next time interval* $t \in [(n+1)\tau, (n+2)\tau)$, $\beta_K\beta_1\xi^{(\mu+1)}$ *is an asymptotically stable equilibrium point of (1.10).*

Proof: Since $\mathrm{sgn}(\mathbf{u}(t)) = \xi^{(\mu)}$ for all $t \in [n\tau, (n+1)\tau)$, for λ sufficiently large, we may assume $\mathbf{v}(t) = \beta_1\xi^{(\mu)}$, or equivalently, $\mathbf{u}(t) = \mathrm{arctanh}(\beta_1\xi^{(\mu)})/\lambda = \beta_K\beta_1\xi^{(\mu)}$. Thus, constraining ourselves to the $(n+2)$-th time interval, i.e., $t \in [(n+1)\tau, (n+2)\tau)$, and substituting $\mathbf{u}(t-\tau) = \beta_K\beta_1\xi^{(\mu)}$ into (1.10), we obtain a nonlinear system of ordinary different equations,

$$\dot{\mathbf{u}}(t) = -\mathbf{u}(t) + C_0\beta_K\mathbf{J}^{\mathbf{0}}\tanh(\lambda\mathbf{u}(t)) + C_1\beta_K\mathbf{J}\beta_1\xi^{(\mu)}.$$

Since $\mathbf{J}\xi^{(\mu)} = \xi^{(\mu+1)}$ [14, 26], we have

$$\dot{\mathbf{u}}(t) = -\mathbf{u}(t) + C_0\beta_K\mathbf{J^0}\tanh(\lambda\mathbf{u}(t)) + C_1\beta_K\beta_1\xi^{(\mu+1)}. \tag{4.4}$$

Assuming $\mathbf{u}^*$ is an equilibrium solution of (4.4), substituting $\mathbf{u}(t) = \mathbf{u}^*$ into (4.4) gives

$$\mathbf{u}^* = C_0\beta_K\mathbf{J^0}\tanh(\lambda\mathbf{u}^*) + C_1\beta_K\beta_1\xi^{(\mu+1)}.$$

Let $\mathbf{v}^* = \tanh(\lambda\mathbf{u}^*)$, then

$$\frac{1}{\lambda}\text{arctanh}(\mathbf{v}^*) = C_0\beta_K\mathbf{J^0}\mathbf{v}^* + C_1\beta_K\beta_1\xi^{(\mu+1)}.$$

Direct substitution shows that $\mathbf{v}^* = \beta_1\xi^{(\mu+1)}$ is a solution of the above equations. This shows that $\mathbf{u}^* = \beta_K\beta_1\xi^{(\mu+1)}$ is an equilibrium solution of (4.4).

Next, we show that the equilibrium solution $\mathbf{u}^* = \beta_K\beta_1\xi^{(\mu+1)}$ is asymptotically stable on $[(n+1)\tau, (n+2)\tau)$. Let $\mathbf{u}(t)$ be a perturbed solution around the equilibrium solution $\mathbf{u}^*$, that is, $\mathbf{u}(t) = \mathbf{u}^* + \delta\mathbf{u}(t)$. Thus, $\dot{\mathbf{u}}(t) = \delta\dot{\mathbf{u}}(t)$. Linearizing the right hand side of the inhomogeneous system (4.4) around $\mathbf{u}^*$ and substituting $\mathbf{u}^* = \beta_K\beta_1\xi^{(\mu+1)}$ into the linearized system yield

$$\delta\dot{\mathbf{u}}(t) = C_0\beta\mathbf{J^0}\Xi\delta\mathbf{u}(t) - \delta\mathbf{u}(t),$$

where $\beta = \beta_K\lambda$, and $\Xi = \text{diag}(1 - \tanh^2(\lambda\beta_K\beta_1\xi_1^{(\mu+1)}), \ldots, 1 - \tanh^2(\lambda\ \beta_K\beta_1\xi_N^{(\mu+1)}))$. Since $\xi_i^{(\mu+1)} \in \{-1, 1\}$ for every i, and $\lambda\beta_K\beta_1 = \text{arctanh}(\beta_1)$, it follows that $\Xi = (1-\beta_1^2)\mathbf{I}$. Therefore, we get

$$\delta\dot{\mathbf{u}}(t) = \mathbf{A}\delta\mathbf{u}(t), \tag{4.5}$$

where $\mathbf{A} = C_0\beta(1-\beta_1^2)\mathbf{J^0} - \mathbf{I}$. Since the connectivity matrix $\mathbf{J^0}$ and the identity matrix $\mathbf{I}$ commute, they are simultaneously diagonalizable. That is, if $\mathbf{Q}$ diagonalizes $\mathbf{A}$, i.e. $\mathbf{Q}^{-1}\mathbf{A}\mathbf{Q} = \Lambda = \text{diag}(\sigma_1, \sigma_2, \ldots, \sigma_N)$, with $\Re(\sigma_1) \geq \Re(\sigma_2) \geq \cdots \geq \Re(\sigma_N)$, where $\Re(x)$ designates the real part of the complex number x, then

$$\Lambda = C_0\beta(1-\beta_1^2)\mathbf{Q}^{-1}\mathbf{J^0}\mathbf{Q} - \mathbf{I}. \tag{4.6}$$

Since $\mathbf{J^0} = \Sigma\Sigma^+$ is idempotent, the eigenvalues of $\mathbf{J^0}$ are either 0 or 1. Thus,

$$\sigma_i = C_0\beta(1-\beta_1^2) - 1 \text{ or } -1$$

Since $\beta = \dfrac{\operatorname{arctanh}(\beta_1)}{\beta_1}$, and $0 < \beta_1 < 1$, it follows that

$$\sigma_i = C_0 \frac{\operatorname{arctanh}(\beta_1)(1-\beta_1^2)}{\beta_1} - 1 \text{ or } -1 \tag{4.7}$$

Since $C_0 \leq 1$, $\dfrac{\operatorname{arctanh}(\beta_1)(1-\beta_1^2)}{\beta_1}$ is a monotonically decreasing function of β_1 over the open interval $(0,1)$, and moreover,

$$\lim_{\beta_1 \to 0} \frac{\operatorname{arctanh}(\beta_1)(1-\beta_1^2)}{\beta_1} = 1, \ \lim_{\beta_1 \to 1} \frac{\operatorname{arctanh}(\beta_1)(1-\beta_1^2)}{\beta_1} = 0,$$

it follows that $\Re(\lambda_i) < 0$ for all i. This shows that $\mathbf{u}^* = \beta_K \beta_1 \xi^{(\mu+1)}$ is asymptotically stable over the interval $t \in [(n+1)\tau, (n+2)\tau)$, which completes the proof.

Suppose the pattern $\xi^{(\mu)}$ has been retrieved successfully in the $(n+1)$-th time interval, i.e. $\operatorname{sgn}(\mathbf{u}(t)) = \xi^{(\mu)}$ for $t \in [n\tau, (n+1)\tau)$, neglecting the transient transitions. Substituting $\mathbf{u}(t-\tau) = \beta_K \beta_1 \xi^{(\mu)}$ into (1.10) and taking the continuity of the solution at $t = (n+1)\tau$ into account, we obtain the following derived initial value problem

$$\begin{cases} \dot{\mathbf{u}}(t) &= -\mathbf{u}(t) + C_0 \beta_K \mathbf{J^0} \tanh(\lambda \mathbf{u}(t)) + C_1 \beta_K \beta_1 \xi^{(\mu+1)} \\ \mathbf{u}((n+1)\tau) &= \beta_K \beta_1 \xi^{(\mu)} \end{cases} . \tag{4.8}$$

Theorem 4.2.1 guarantees that in the next time interval, $\mathbf{u}^* = \beta_K \beta_1 \xi^{(\mu+1)}$ is an asymptotically stable equilibrium point. Therefore, if in the $(n+1)$-th time interval, the solution $\mathbf{u}(t)$ entered the basin of attraction of $\mathbf{u}^*$ in the $(n+2)$-th time interval, then $\mathbf{u}(t)$ would be attracted to $\mathbf{u}^*$ in the $(n+2)$-th time interval. Accordingly, the next pattern $\xi^{(\mu+1)}$ in the cycle Σ would be retrieved successfully. Next we follow Cheng et al. [46, 47] to adopt a similar geometry-based method to analyze the basin of attraction of the stable equilibria of the above derived nonlinear system (4.8).

Let the right-hand side of (4.8) be denoted by $\mathbf{f}(\mathbf{u}) = (f_1(\mathbf{u}), \ldots, f_N(\mathbf{u}))^T$, where for every $i = 1, 2, \ldots, N$,

$$f_i(\mathbf{u}) = -u_i + C_0 \beta_K \sum_{j=1}^{N} J_{ij}^0 \tanh(\lambda u_j) + C_1 \beta_K \beta_1 \xi_i^{(\mu+1)}. \tag{4.9}$$

We prove two simple but useful results.

Lemma 4.2.2. *Let $\mathbf{J^0}$ be constructed from any admissible cycle $\Sigma \in \{-1, 1\}^{N \times p}$ using the pseudoinverse learning rule (1.7). Then $J_{ii}^0 \geq 0$ for every $i = 1, 2, \ldots, N$.*

Proof: Let $\Sigma = U\Lambda V^*$ be the singular value decomposition of Σ, where Λ is an $N \times p$ diagonal matrix, and V^* is the adjoint of V. Then $\Sigma^+ = V\Lambda^+ U^*$, where Λ^+ is the $p \times N$ diagonal matrix obtained from Λ by taking the reciprocal of each non-zero element on the diagonal of Λ, leaving the zeros in place, and transposing the resulting matrix. Thus, if $\Lambda = \text{diag}(\sigma_1, \sigma_2, \ldots, \sigma_k, 0, \ldots, 0)$ with $\sigma_i \neq 0$ for every $i \leq k$, and $k \leq \min\{N, p\}$, then $\Lambda^+ = \text{diag}(\sigma_1^{-1}, \sigma_2^{-1}, \ldots, \sigma_k^{-1}, 0, \ldots, 0)$ and $\Lambda\Lambda^+ = \text{diag}(1, 1, \ldots, 1, 0, \ldots, 0)$. Since $\mathbf{J^0} = \Sigma\Sigma^+ = U\Lambda\Lambda^+ U^*$, it follows that $J_{ii}^0 = \sum_{j=1}^{k} U_{ij} U_{ji}^*$, where U_{ij} and U_{ji}^* are the entries in the place (i, j) and (j, i) in the matrices U and U^* respectively. Since $U_{ji}^* = (U_{ij})^*$, it follows that $U_{ij} U_{ji}^* = \|U_{ij}\|^2$, where $\|U_{ij}\|$ is the modulus of the complex number U_{ij}. Therefore, we have that

$$J_{ii}^0 = \sum_{j=1}^{k} \|U_{ij}\|^2.$$

Since $\|U_{ij}\|^2 \geq 0$ for every $j \leq k$, it follows that $J_{ii}^0 \geq 0$ for every i.

Lemma 4.2.3. *Let $i = 1, \ldots, N$ be fixed. If $C_0 \beta J_{ii}^0 > 1$, then there exist two values p_i and q_i of the i-th component u_i of the membrane potential function $\mathbf{u}$ with $p_i < 0 < q_i$, such that $\partial_i f_i(\mathbf{u})|_{u_i = p_i} = 0$ and $\partial_i f_i(\mathbf{u})|_{u_i = q_i} = 0$ for $i = 1, \ldots, N$.*

Proof: Since $\partial_i f_i(\mathbf{u}) = C_0 \beta_K J_{ii}^0 \lambda(1 - \tanh^2(\lambda u_i)) - 1$, setting $\partial_i f_i(\mathbf{u}) = 0$ and replacing $\beta_K \lambda$ by β gives $C_0 \beta J_{ii}^0 (1 - \tanh^2(\lambda u_i)) = 1$, it follows that

$$\tanh^2(\lambda u_i) = \frac{C_0 \beta J_{ii}^0 - 1}{C_0 \beta J_{ii}^0}, \tag{4.10}$$

which implies that the equation $\partial_i f_i(\mathbf{u}) = 0$ has two distinct solutions p_i and q_i with $p_i < 0 < q_i$ only when $C_0 \beta J_{ii}^0 > 1$. This completes the proof.

Remark 4.2.1. The last equality (4.10) implies that if $C_0 \beta J_{ii}^0 > 1$, then there exist two distinct real values p_i and q_i with $p_i < 0 < q_i$ such that $\partial_i f_i(\mathbf{u})|_{u_i = p_i} = 0$ and $\partial_i f_i(\mathbf{u})|_{u_i = q_i} = 0$. Moreover, if $C_0 \beta J_{ii}^0 = 1$, then $\partial_i f_i(\mathbf{u}) = 0$ only at $u_i = 0$, and if $C_0 \beta J_{ii}^0 < 1$, then $\partial_i f_i(\mathbf{u}) < 0$ for all $u_i \in \mathbb{R}$. Therefore, if $C_0 \beta J_{ii}^0 < 1$ for every i, then the equation for equilibrium points $\mathbf{f}(\mathbf{u}) = \mathbf{0}$ will have only one solution. Direct substitution of $\mathbf{u} = \beta_K \beta_1 \xi^{(\mu+1)}$ into the equation $\mathbf{f}(\mathbf{u}) = \mathbf{0}$ shows that $\beta_K \beta_1 \xi^{(\mu+1)}$ is the solution. Since in this case $\partial_i f_i(\mathbf{u}) < 0$ for all i and $\mathbf{u} \in \mathbb{R}^N$, it follows that the unique equilibrium $\mathbf{u}^* = \beta_K \beta_1 \xi^{(\mu+1)}$ is globally asymptotically stable. Accordingly, we have the

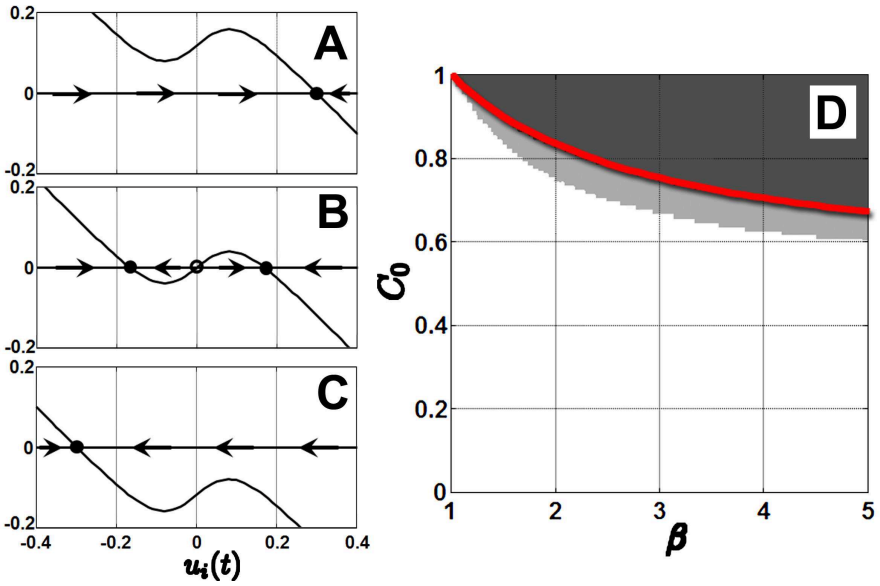

Figure 4.4: The graphs for $\hat{f}_i(u_i)$ (**A**), $\bar{f}_i(u_i)$ (**B**), and $\check{f}_i(u_i)$ (**C**). The parameters for the three curves are set as follows, $C_0 = 0.6$, $\beta = 3$, $\lambda = 10$, $J^0_{ii} = 1$ and $J^0_{ij} = 0$ for all $i \neq j$ (this corresponds to Σ being separable, minimal and consecutive [26]). The red curve in **D** is the solution curve of the equation (4.12). The white, light gray and dark gray backgrounds in **D** correspond to the regions in the parameter plane where the system (1.10) with ring topology with one inhibitory connection has 1, 3 or 1, and 3^N equilibria respectively. On the boundary between light-gray region and dark-gray region, which coincides with the solution curve (red curve in **D**) of (4.12), both the multiple saddle-nodes on limit cycle bifurcations and saddle-node bifurcations occur. The former bifurcation breaks the limit cycle, and both bifurcations create all the rest equilibria.

that, if $C_0\beta J^0_{ii} < 1$ and τ is sufficiently large in comparison to the time span of the transients, then any admissible cycle is retrievable, and any cycle satisfying the transition condition imposed by the prescribed cycle can be retrieved in the network constructed from the prescribed cycle.

For $C_0\beta J^0_{ii} > 1$, since $\xi^{(\mu)} \in \{-1, 1\}^N$ for all $\mu \in \mathbb{N}$, and the "forcing term" $C_1\beta_K\beta_1\xi_i^{(\mu+1)}$ in (4.9) vertically shifts the curve of the function (see Figure 4.4**A**, **B** and **C**)

$$\bar{f}_i(u_i) = -u_i + C_0\beta_K J^0_{ii}\tanh(\lambda u_i), \tag{4.11}$$

we have that $\check{f}_i(u_i) \leq f_i(\mathbf{u}) \leq \hat{f}_i(u_i)$ for every $i = 1, 2, \ldots, N$, where

$$\check{f}_i(u_i) = -u_i + C_0\beta_K J^0_{ii}\tanh(\lambda u_i) + k_i^-,\ \hat{f}_i(u_i) = -u_i + C_0\beta_K J^0_{ii}\tanh(\lambda u_i) + k_i^+$$

with

$$k_i^- = -C_0\beta_K \sum_{j=1, j\neq i}^{N} |J^0_{ij}| - C_1\beta_K\beta_1,\ k_i^+ = C_0\beta_K \sum_{j=1, j\neq i}^{N} |J^0_{ij}| + C_1\beta_K\beta_1.$$

If $\hat{f}_i(p_i) < 0$ and $\check{f}_i(q_i) > 0$, then the function $f_i(\mathbf{u})$ must intersect with the horizontal axis at three distinct points. Accordingly, if $\hat{f}_i(p_i) < 0$ and $\check{f}_i(q_i) > 0$ for every i, then the derived system in (4.8) has 3^N equilibria. Moreover, with further constraints on the parameters, 2^N of these 3^N equilibria become asymptotically stable. A similar results has been proved in [46], and using the same arguments as in [46], we can prove the two lemmas below. We summarize the three parameter conditions as

$$\begin{aligned}
(\mathbf{H_1}): &\quad C_0\beta J_{ii}^0 > 1;\\
(\mathbf{H_2}): &\quad \check{f}_i(q_i) > 0 \text{ and } \hat{f}_i(p_i) < 0;\\
(\mathbf{H_3}): &\quad C_0\beta \sum_{j=1}^{N} |J_{ij}^0|(1-\tanh^2(\lambda\eta_j)) < 1,
\end{aligned}$$

where η_j is chosen such that $\tanh^2(\lambda\eta_j) = \min\{\tanh^2(\lambda u_j)|u_j = \check{c}_j, \hat{a}_j\}$, with $\check{c}_j$ and $\hat{a}_j$ defined exactly as in [46], and $i = 1, 2, \ldots, N$.

Lemma 4.2.4. *Under ($\mathbf{H_1}$) and ($\mathbf{H_2}$), the derived nonlinear system in (4.8) has 3^N equilibria.*

Lemma 4.2.5. *Under ($\mathbf{H_1}$), ($\mathbf{H_2}$) and ($\mathbf{H_3}$), the derived nonlinear system in (4.8) has 2^N asymptotically stable equilibria.*

Clearly, $\hat{f}_i(u_i)$ and $\check{f}_i(u_i)$ are respectively the upper and lower bounds for the function $f_i(\mathbf{u})$. Depending on the values of C_0 and β, the curve $f_i(\mathbf{u})$ may intersect with the $u_i(t)$ axis in one, two or three points. For $C_0\beta J_{ii}^0 > 0$, let $u_i = p_i$ and take $\xi_i^{(\mu+1)} = 1$, then setting $f_i(\mathbf{u}) = 0$ and substituting $p_i = -\frac{1}{\lambda}\text{arctanh}\left(\sqrt{\frac{C_0\beta-1}{C_0\beta}}\right)$ yield the following transcendental equation for the curve of the saddle-node bifurcations of the system (4.8) occuring at $u_i = p_i$,

$$\text{arctanh}\left(\sqrt{\frac{C_0\beta-1}{C_0\beta}}\right) - \sqrt{C_0\beta(C_0\beta-1)} + C_1\text{arctanh}(\beta_1) = 0, \tag{4.12}$$

where $\beta = \text{arctanh}(\beta_1)/\beta_1$, and $\beta_1 \in (0,1)$. For the saddle-node bifurcations of the derived system in (4.8) occuring at $u_i = q_i$, the equation for the bifurcation curve can be obtained similarly by taking $u_i = q_i = -p_i$ and $\xi_i^{(\mu+1)} = -1$. A simple direct calculation shows this result in equation (4.12). Therefore, we use it for finding the parameter values of both saddle-node bifurcations.

We numerically solve the above equation (4.12) for C_0 with values of β between 1 and 5. The red curve in Figure 4.4**D** illustrates the solutions (β, C_0) for $\beta \in (1, 5]$. It is interesting to note that numerically this curve coincides with the curves of the multiple saddle-nodes on limit cycle

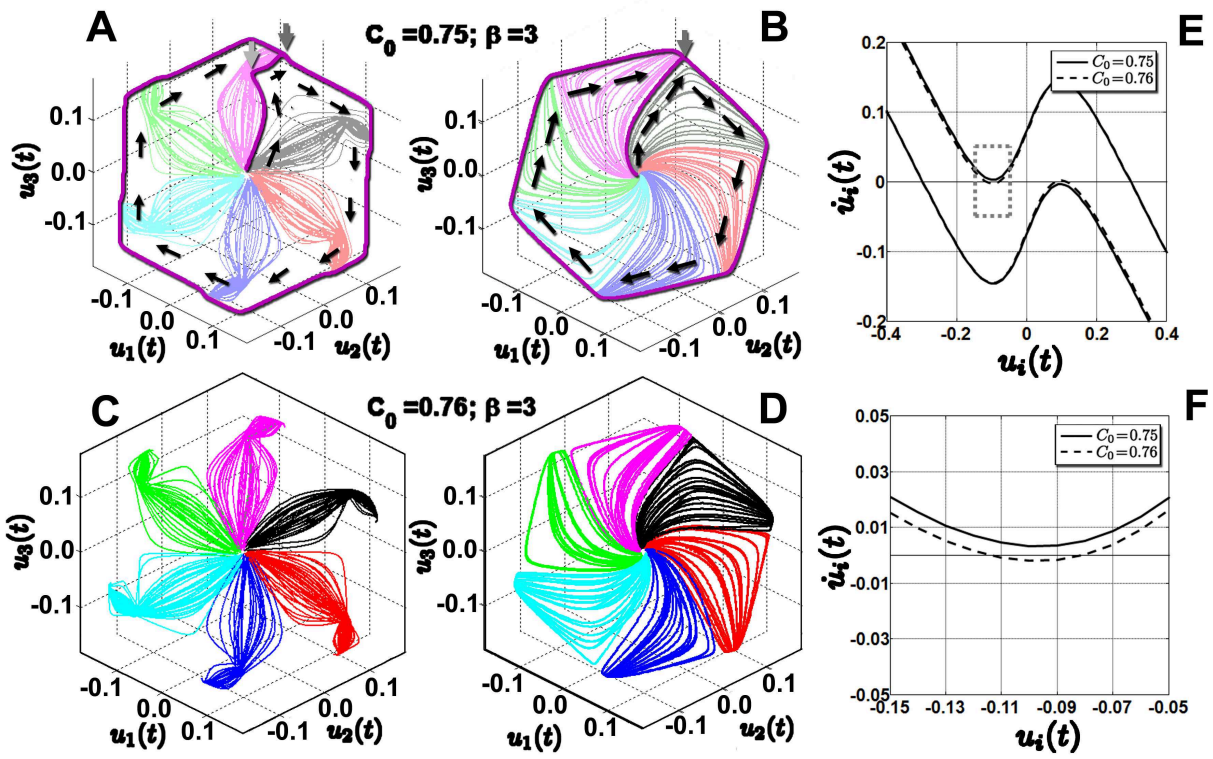

Figure 4.5: Breaking the cycles in the networks with (**A** and **C**) and without delay (**B** and **D**). The curves in **E** and **F** illustrate the occurrence of the saddle-node bifurcation in the derived system in (4.8).

bifurcations in the networks (1.10) with ring topology with one inhibitory connection and without transmission time delay. In Figure 4.4**D**, we use the background with different grayscales to indicate the regions in the β-C_0 parameter plane in which the corresponding networks (1.10) with ring topology with one inhibitory connection have 1 (white background), 3 or 1 (light gray backgound), and 3^N (dark gray backgound) equilibria. As we will see in Chapter 5, a *multiple saddle-nodes on limit cycle bifurcation* [77] and several *saddle-note bifurcations* occur on the boundary between the light-gray and dark-gray regions. The multiple saddle-nodes on the limit cycle bifurcation breaks the limit cycle, and both bifurcations create all of the remaining equilibria in the networks without transmission delay. We will discuss this in more detail in Chapter 5. In the next example we show that it is the saddle-node bifurcation in the system (4.8) that breaks the successful retrievals of the prescribed cycles, and we also compare this bifurcation with the multiple saddle-nodes on limit cycle bifurcation in the corresponding network without transmission delay.

Example 4.2.1. In order to compare the saddle-node bifurcation of the derived system in (4.8) with the multiple saddle-nodes on limit cycle bifurcation in the corresponding network without transmission time delay, we consider the networks constructed using the pseudoinverse learning rule from the following admissible cycle,

$$\Sigma = \begin{pmatrix} + & + & + & - & - & - \\ + & + & - & - & - & + \\ + & - & - & - & + & + \end{pmatrix}. \tag{4.13}$$

The network equations for this cycle are

$$\begin{cases} \dot{u}_1(t) = -u_1(t) + C_0\beta_K \tanh(\lambda u_1(t)) + C_1\beta_K \tanh(\lambda u_2(t-\tau)) \\ \dot{u}_2(t) = -u_2(t) + C_0\beta_K \tanh(\lambda u_2(t)) + C_1\beta_K \tanh(\lambda u_3(t-\tau)) \\ \dot{u}_3(t) = -u_3(t) + C_0\beta_K \tanh(\lambda u_3(t)) - C_1\beta_K \tanh(\lambda u_1(t-\tau)) \end{cases}. \tag{4.14}$$

It is easy to verify that only two cycles are stored in this network, one is the prescribed cycle (4.13), the other is the cycle of the two patterns, $(-,+,-)^T$ and $(+,-,+)^T$. In Chapter 5, we will show in numerical continuation computations that in this network the prescribed cycle Σ is stored as an attracting limit cycle. In Figure 4.5 **A**, **B**, **C** and **D**, we respectively illustrate 180 phase trajectories starting from randomly chosen initial data which are very close to the origin in simulations in networks with (**A**, **C**) and without (**B**, **D**) transmission delay. The trajectories converging to the same first binary pattern are plotted in the same color. The light-gray arrow in Figure 4.5**A** indicates the point at which $t = \tau$. At this point the delay term $C_1\beta_K \mathbf{J} \tanh(\lambda \mathbf{u}(t-\tau))$ in the system (1.10) ceases being fixed, and the trajectory starts to evolve towards the point corresponding to the binary pattern $(-,+,+)^T$, labeled with a dark-gray arrow. Here, we avoid calling the point equilibrium, because although after the saddle-node bifurcation in the derived system (4.8) an attracting node does exist around this point, it does not exist before the bifurcation. However, in the region around this point, the system behaves like that in the neighborhood of a saddle, i.e. the trajectory approaches the point, and then moves away from it. In contrast, in the network without delay, there is no such a period as in the network with delay before $t = \tau$ (the arch between the starting point and the point labelled with the light-gray arrow). The phase trajectories of the networks without delay directly approach the point at which a saddle-node on limit cycle

bifurcation occurs when the parameter values move across the bifurcation curve. Therefore, in Figure 4.5**B** along the purple representative phase trajectory, there is no point corresponding to that labelled with a light-gray arrow in Figure 4.5**A**. This is the most significant difference between the corresponding phase trajectories in the two networks. Using the Matlab packages for numerical continuation computations and bifurcation analysis, DDE-BIFTOOL and Matcont, we verified that each of the two purple representative phase trajectories in Figure 4.5**A** and **B** converges to an attracting limit cycle (see Chapter 5 for details). In Figure 4.5**C** and **D** we illustrate the phase trajectories (180 trajectories in each panel) in the same two networks with the parameter C_0 increased from 0.75 (**A** and **B**) to 0.76. Clearly, both networks stop retrieving the prescribed cycle. In Chapter 5, we will see that a multiple saddle-nodes on limit cycle bifurcation [77] occurs during the increase of C_0 in the network both with and without delay, which breaks the limit cycle corresponding to the prescribed cycle into 6 pairs of saddles and nodes. In Figure 4.5**E**, we illustrate the curves of the function (4.9) with $\xi_i^{(\mu+1)} = 1$ (the upper solid and dashed curves) and -1 (the lower solid and dashed curves) respectively. When C_0 increases from 0.75 to 0.76, the graphs of the functions (4.9) move from the solid curves to the dashed curves, while the points $f_i(p_i)$ and $f_i(q_i)$ move across the horizontal axis, indicating that a saddle-node bifurcation occurs in the derived system (4.8). In order to visualize the portion of the curves close to the horizontal axis more clearly, in Figure 4.5**F** we illustrate the portion of the solid and dashed curves in the region enclosed by a dashed gray box in Figure 4.5**E**.

CHAPTER 5

BIFURCATIONS IN NETWORKS CONSTRUCTED FROM ADMISSIBLE CYCLES

Having investigated the retrievability of admissible cycles in Chapter 4, in this Chapter we continue to study how these cycles stored in a network. Through a systematic bifurcations analysis, we show that the local bifurcations of the trivial equilibrium in networks constructed from admissible cycles are determined by the structural features of these cycles, and that admissible cycles are stored and retrieved either as attracting limit cycles, unstable periodic solutions or as so called long-lasting transient oscillations, which are suggested to be consequences of interactions between unstable periodic solutions and stable and unstable equilibria. We begin our study with a linear stability analysis of the trivial equilibrium solution.

5.1 Scenarios for Possible Local Bifurcations of the Trivial Equilibrium Solution

Consider the nonlinear system of delay differential equations (1.10). Since the delay-time τ is treated as a parameter, we rescale time t as $t = \tilde{t}\tau$ and set $\mathbf{w}(\tilde{t}) = \mathbf{u}(\tilde{t}\tau)$ to obtain

$$\dot{\mathbf{w}}(\tilde{t}) = \tau\Big[-\mathbf{w}(\tilde{t}) + C_0\beta_K\mathbf{J^0}\tanh(\lambda\mathbf{w}(\tilde{t})) + C_1\beta_K\mathbf{J}\tanh(\lambda\mathbf{w}(\tilde{t}-1))\Big].$$

Dropping the tilde to simplify the notation, the rescaled system of delay differential equations studied in this chapter takes the form

$$\dot{\mathbf{w}}(t) = \tau\Big[-\mathbf{w}(t) + C_0\beta_K\mathbf{J^0}\tanh(\lambda\mathbf{w}(t)) + C_1\beta_K\mathbf{J}\tanh(\lambda\mathbf{w}(t-1))\Big]. \tag{5.1}$$

For systems without transmission delay, $\tau = 0$, we set $\mathbf{w}(t) = \mathbf{u}(t)$ and study bifurcations in the system of ordinary differential equations

$$\dot{\mathbf{w}} = -\mathbf{w} + C_0\beta_K\mathbf{J^0}\tanh(\lambda\mathbf{w}) + C_1\beta_K\mathbf{J}\tanh(\lambda\mathbf{w}). \tag{5.2}$$

Clearly, $\mathbf{w}^* = \mathbf{0}$ is an equilibrium solution, referred to as trivial equilibrium, of both systems (5.1) and (5.2). By expanding the right-hand side of (5.1) into a Taylor series in the neighborhood of $\mathbf{w}^* = \mathbf{0}$ and neglecting the nonlinear terms, the linearization of (5.1) about the trivial equilibrium is derived as follows

$$\delta\dot{\mathbf{w}}(t) = \mathbf{A}_1\delta\mathbf{w}(t) + \mathbf{A}_2\delta\mathbf{w}(t-1), \tag{5.3}$$

where $\mathbf{A}_1 = \tau(C_0\beta\mathbf{J^0} - \mathbf{I})$ and $\mathbf{A}_2 = \tau C_1\beta\mathbf{J}$. Suppose (5.3) has a solution of the form $\delta\mathbf{w}(t) = e^{\sigma t}\phi$ with $\sigma \in \mathbb{C}$ and $\phi \in \mathbb{R}^N$, and accordingly $\delta\mathbf{w}(t-1) = e^{\sigma(t-1)}\phi$. Substituting these two functions back into (5.3) gives

$$\sigma e^{\sigma t}\phi = \tau(C_0\beta\mathbf{J^0} - \mathbf{I})e^{\sigma t}\phi + \tau C_1\beta\mathbf{J}e^{\sigma(t-1)}\phi. \tag{5.4}$$

The equation (5.4) reduces to a linear, homogeneous system of algebraic equations, $\Delta(\sigma)\phi = 0$, where $\Delta(\sigma)$ is called the *characteristic matrix* of the linearized system (5.3),

$$\Delta(\sigma) = (\sigma + \tau)\mathbf{I} - \tau C_0\beta\mathbf{J^0} - \tau e^{-\sigma}C_1\beta\mathbf{J}.$$

Thus, (5.4) has a nontrivial solution if and only if

$$\det(\Delta(\sigma)) = 0, \tag{5.5}$$

which is called the *characteristic equation* of (5.3). The solution set of (5.5) forms the *spectrum* of the *infinitesimal generator* $\mathcal{A}$ of the strongly continuous semigroup $\{\mathcal{T}(t)|t \geq 0\}$ of the solution maps $\mathcal{T}(t) : \mathcal{C} \to \mathcal{C}$, where for every $t \geq 0$, the solution map $\mathcal{T}(t)$ is defined by the relation $\mathbf{w}_t(\theta) = \mathcal{T}(t)\varphi(\theta)$ with the initial data $\varphi(\theta) \in \mathcal{C}$ [61, 62].

As the connectivity matrices $\mathbf{J^0}$ and $\mathbf{J}$ are constructed from the prescribed cycle Σ with the pseudoinverse learning rule (1.7) and (1.9), we have that $\mathbf{J^0}$ and $\mathbf{J}$ commute [26], and accordingly, $\mathbf{J^0}$ and $\mathbf{J}$ are simultaneously diagonalizable [78]. Suppose $\mathbf{Q}$ is a nonsingular matrix which simultaneously diagonalizes the connectivity matrices $\mathbf{J^0}$ and $\mathbf{J}$. Thus, if the characteristic matrix has the diagonalization $\Delta(\sigma) = \mathbf{QKQ}^{-1}$, where $\mathbf{K} = \mathrm{diag}(\kappa_1, \kappa_2, \ldots, \kappa_N)$, then

$$\det(\Delta(\sigma)) = \det(\mathbf{K}) = \prod_{i=1}^{N} \kappa_i$$

and

$$\mathbf{K} = (\sigma + \tau)\mathbf{I} - \tau C_0\beta\mathbf{Q}^{-1}\mathbf{J^0}\mathbf{Q} - \tau e^{-\sigma}C_1\beta\mathbf{Q}^{-1}\mathbf{J}\mathbf{Q}.$$

Suppose the prescribed admissible cycle Σ is simple, minimal and consecutive, then $\mathbf{J^0} = \mathbf{I}$ [26], and

$$\mathbf{K} = (\sigma + \tau(1 - C_0\beta))\mathbf{I} - \tau e^{-\sigma} C_1 \beta \mathbf{Q}^{-1}\mathbf{J}\mathbf{Q}.$$

Since $\mathbf{J}^p = \mathbf{I}$, it follows that $\tilde{\mathbf{K}} = \mathrm{diag}(\tilde{\kappa}_1, \tilde{\kappa}_2, \ldots, \tilde{\kappa}_N)$ with $\tilde{\kappa}_i = e^{2n_i\pi\mathbf{i}/p}$, where $\tilde{\mathbf{K}} = \mathbf{Q}^{-1}\mathbf{J}\mathbf{Q}$, $\mathbf{i} = \sqrt{-1}$, $0 \le n_1 < n_2 < \cdots < n_N \le p-1$, and $N \le p$. Accordingly, we get

$$\kappa_i = \sigma + \tau(1 - C_0\beta) - \tau C_1 \beta e^{-\sigma + 2n_i\pi\mathbf{i}/p}. \tag{5.6}$$

Thus, the characteristic equation (5.5) becomes

$$\prod_{i=1}^{N} \Big(\sigma - \tau C_1 \beta e^{2n_i\pi\mathbf{i}/p - \sigma} + \tau(1 - C_0\beta)\Big) = 0. \tag{5.7}$$

For networks of the form (5.2) without transmission delay, the same procedure leads to

$$\prod_{i=1}^{N} \Big(\sigma - C_1 \beta e^{2n_i\pi\mathbf{i}/p} + (1 - C_0\beta)\Big) = 0. \tag{5.8}$$

For the linear stability analysis, we set $\sigma = \alpha + \mathbf{i}\omega$ with α, $\omega \in \mathbb{R}$. From (5.7), it then follows that

$$\begin{cases} \alpha + \tau(1 - C_0\beta) &= \tau(1 - C_0)\beta e^{-\alpha}\cos(\tilde{\omega}) \\ \omega &= \tau(1 - C_0)\beta e^{-\alpha}\sin(\tilde{\omega}) \end{cases} \tag{5.9}$$

where $\tilde{\omega} = 2n_i\pi/p - \omega$. Since a local bifurcation from the trivial equilibrium requires neutral stability, we set $\alpha = 0$ in (5.9). Accordingly, a necessary condition for a local bifurcation from $\mathbf{w}^* = \mathbf{0}$ is that

$$\begin{cases} \tau(1 - C_0\beta) &= \tau(1 - C_0)\beta\cos(\tilde{\omega}) \\ \omega &= \tau(1 - C_0)\beta\sin(\tilde{\omega}) \end{cases} \tag{5.10}$$

holds for at least one of the possible N values of $\tilde{\omega}$. Adding the first equation squared to the second equation squared in (5.10) gives

$$C_0 = \frac{\beta + 1}{2\beta} - \frac{\omega^2}{2\tau^2(\beta - 1)\beta}. \tag{5.11}$$

Solving the first equation in (5.10) for ω yields

$$\omega = \frac{2n_i\pi}{p} - \arccos\frac{1 - C_0\beta}{(1 - C_0)\beta}. \tag{5.12}$$

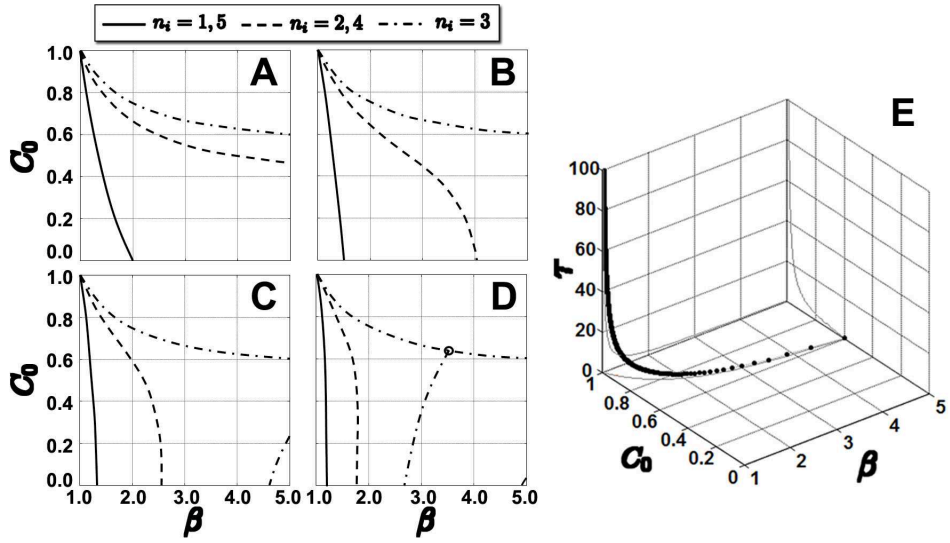

Figure 5.1: Curves of characteristic roots with zero real part (**A**-**D**) and the curve of the double-zero characteristic roots (**E**). In **A**, **B**, **C** and **D**, the solid curves correspond to $n_i = 1$ or 5; the dashed curves correspond to $n_i = 2$ or 4; and the dash-dot curves correspond to $n_i = 3$. For $n_i = 0$, $\Re(\sigma) > 0$ for all $0 \le C_0 \le 1$ and $1 < \beta$, therefore no curve corresponding to $n_i = 0$ is shown for $\beta > 1$ and $0 \le C_0 \le 1$. In both **C** and **D** the dash-dot curve consists of two parts. On the top part, the characteristic roots σ move across the imaginary axis along the real axis, and on the right part, the characteristic roots σ move across the imaginary axis off the real axis. The open circle in **D** is the intersection of the two parts of the dash-dot curve, which is a double zero and suggests a Bogdanov-Takens bifurcation [58, 59, 79]. The dotted curve in **E** corresponds to the double zeros of the characteristic equation (5.7). The parameters for the curves shown in this figure are set as follows, $p = 6$, $\tau = 0$ (**A**), $\tau = 0.2$ (**B**), $\tau = 0.4$ (**C**), and $\tau = 0.8$ (**D**).

Substituting then (5.12) into (5.11) provides an implicit equation for the curves of the characteristic roots with zero real part,

$$C_0 - \frac{\beta+1}{2\beta} + \frac{1}{2\tau^2(\beta-1)\beta}\left(\frac{2n_i\pi}{p} - \arccos\frac{1-C_0\beta}{(1-C_0)\beta}\right)^2 = 0. \tag{5.13}$$

Preceding in the same way for networks without transmission delay, equation (5.8), the above implicit equation reduces to

$$C_0 = \frac{1-\beta\cos(2n_i\pi/p)}{(1-\cos(2n_i\pi/p))\beta}. \tag{5.14}$$

Since $\mathbf{P}$ is the cyclic permutation matrix (1.5), the eigenvalues of $\mathbf{P}$ are the p-th roots $\rho^k = e^{2k\pi\mathbf{i}/p}$ of unity, and its $(k+1)$-th eigenvector corresponding to ρ^k has the general form $v^{(k)} = (1, \rho^k, \ldots, \rho^{(p-1)k})^T$. In Chapter 2, we have seen that the indices n_i in the characteristic equations (5.7) and (5.8) are determined by the structural features of Σ. Specifically, if the cycle Σ annihilates the $(k+1)$-th eigenvector, i.e. $\Sigma v^{(k)} = \mathbf{0}$, then k will not appear in the set of the N indices

$\{n_i | i = 1, 2, \ldots, N\}$. Thus, the structural features of a cycle Σ determine the linear stability of the equilibrium points of the networks constructed from it by selecting the indices n_i that appear in the corresponding characteristic equation (5.7) or (5.8), and hence indirectly determine the local dynamics of the networks with and without transmission delay.

Therefore, in general, for a given p, depending on how the characteristic roots move across the imaginary axis on the curves defined by (5.13) or (5.14), a scenario of all possible local bifurcations of the trivial equilibrium solution of a network constructed from a simple cycle of length p can be determined. As an illustrative example, we show the scenario of all possible local bifurcations of the trivial equilibrium solution of the networks constructed from simple cycles of length $p = 6$ in Figure 5.1.

The curves in panels **A**, **B**, **C** and **D** respectively illustrate the characteristic roots with zero real part for the transmission delays $\tau = 0$, 0.2, 0.4, and 0.8. The solid and dashed curves correspond to purely imaginary characteristic roots, and $n_i = 1$ or 5 and $n_i = 2$ or 4, respectively. If the index $n_i = 1, 5$ or $n_i = 2, 4$ is "chosen" by the prescribed cycle, then when parameters of the network move across the corresponding solid or dashed curve transversely, a Hopf bifurcation will occur.

The dash-dot curve on the top of each of the four panels corresponds to zero characteristic roots and $n_i = 3$. Since no quadratic term appears in the Taylor expansion of the right-hand side of (5.1) around the trivial solution $\mathbf{w}^* = \mathbf{0}$, it follows that if the prescribed cycle "selects" $n_i = 3$ (i.e. $\mathbf{J}$ has an eigenvalue with $n_i = 3$), and the parameters of the network move across the dash-dot curve on the top transversely, a pitchfork bifurcation will occur.

It is necessary to mention that the curve of zero characteristic roots is independent of the transmission delay τ. A direct calculation shows that the explicit formula for this curve is

$$C_0 = \frac{1 + \beta}{2\beta}, \tag{5.15}$$

and in this case $n_i = p/2$, where p is not only just 6, it could be any even natural number with $p/2$ being odd. It is also not difficult to see that for $n_i = p/2$, in addition to the dash-dot curve (5.15) on the top in every panel **A**, **B**, **C** and **D**, the equation (5.13) has other solutions. These "extra" solutions correspond to purely imaginary characteristic roots too. In **C** and **D**, these "extra" solutions are plotted as dash-dot curves on the right. Accordingly, if $n_i = 3$ is chosen,

then when the parameters (C_0, β) move across the curve of these "extra" solutions transversely, also a Hopf bifurcation will occur. As the "extra" solutions change with the transmission delay τ, the curve of these solutions moves together with other curves corresponding to purely imaginary characteristic roots, and intersects with the dash-dot curve on the top at one single point (open circle in Figure 5.1**D**). At this point, the curve of the first (i.e. leftmost) "extra" solution terminates. Since the intersection point corresponds to a double zero of the characteristic equation (5.7), it can be verified through direct computations that at this point a codimension-two Bogdanov-Takens bifurcation takes place [58, 59, 79]. The points on the dotted curve in **E** correspond to these double zeros.

In general, for networks constructed from admissible cycles with p even, Figure 5.1 provides an overview of the scenario of all possible local bifurcations of the trivial equilibrium solution. If $n_i = p/2$ is "chosen", then at the trivial equilibrium solution of the corresponding network, Hopf bifurcations, pitchfork bifurcation, and Bogdanov-Takens bifurcation will occur. If $n_i = p/2$ is not "chosen", then at the trivial equilibrium solution, only Hopf bifurcations can occur. If $n_i = 0$ is "selected", then all the solutions bifurcating from the trivial equilibrium, including the trivial equilibrium itself, are unstable.

Directly substituting $\omega = 0$ into (5.11) and (5.12) gives $n_i = p/2$. Since for networks constructed from admissible cycles with p odd, $p/2$ is not an integer, it follows that no index n_i can be $p/2$, and accordingly, when the characteristic roots move across the imaginary axis, none of them passes through the origin. Thus, in such networks, no pitchfork bifurcation can take place, and only Hopf bifurcations occur at the trivial equilibrium solution.

Considering composite cycles, since every network constructed from a separable composite cycle consists of isolated clusters, and each of these clusters corresponds to a simple cycle associated with a generator of the cycle according to Chapter 2 or [26], it follows that the local bifurcations of the trivial equilibrium of such networks are determined by the structural features of its simple cycle components, which are as described above. By contrast, in networks constructed from inseparable composite cycles, the local bifurcations from the trivial equilibrium solution are much more complicated.

In the next section, we demonstrate how the structural features of the prescribed cycles determine the local bifurcation structures through characteristic examples. We demonstrate that prescribed cycles are stored and retrieved in the corresponding networks as different mathematical objects. Anti-symmetric simple MC-cycles (see Chapter 2 or [26]) of size $N \times p$ with $N = p/2$ are stored and retrieved as attracting limit cycles created from the Hopf bifurcation which occurs when the pair of the conjugate complex characteristic roots with the largest real part move across the imaginary axis transversely from the left. Simple MC-cycles of size $N \times p$ with $N = p$ are stored and retrieved as transient oscillations that are exclusively due to the effects of the transmission delay. More complicated cycles, including general simple cycles and inseparable composite cycles, both prescribed and derived, are stored and retrieved as either attracting limit cycles or transient oscillations induced by the delay.

5.2 Bifurcations in Networks Constructed from Admissible Cycles

In Section 5.1, we have explained how the structural features of an admissible cycle prescribed in a network can be used to determine the local bifurcations from the trivial equilibrium. In this section, we discuss the structure of these bifurcations in more detail for different types of admissible cycles, and study how they are connected with bifurcations from nontrivial equilibria using numerical continuation techniques.

We first recall two definitions from Chapter 2 and [26].

Definition 5.2.1. A cycle Σ is called *simple*, if it is generated by one single binary row vector η, in other words, its rows are cyclic permutations of a binary row vector η. That is, if η_i is the i-th row of Σ, then $\eta_i = \eta \mathbf{P}^k$ for some $k \in \mathbb{N}$.

Definition 5.2.2. A binary row vector $\eta = (\eta_1, \eta_2, \ldots, \eta_p) \in \{-1, 1\}^p$ is said to be *anti-symmetric*, if it has the following two properties: (a) p is even; (b) $\eta = (\zeta, -\zeta)$, where $\zeta = (\zeta_1, \zeta_2, \ldots, \zeta_{p/2}) \in \{-1, 1\}^{p/2}$. A cycle Σ of size $N \times p$ is called *anti-symmetric simple MC*, if it has the following four properties: (a) Σ is simple; (b) η_i is anti-symmetric for every i, where η_i designates the i-th row of Σ; (c) $\mathrm{rank}(\Sigma) = N$; (d) $\eta_{i+1} = \eta_i \mathbf{P}$ for all $1 \leq i < N$, where $\mathbf{P}$ is the cyclic permutation matrix defined by (1.5).

Remark 5.2.1. For example, the admissible cycle (4.13) discussed in Example 4.2.1 is an anti-symmetric simple MC-cycle of size $N \times p$ with $N = p/2$. Gencic et al. [14] have considered the storage and retrieval of such cycles. Both numerical simulations and analog electronic circuit experiments demonstrated successful storage and retrieval of such cycles in Hopfield-type neural networks without delay. In Chapter 2 and [26], we showed that networks constructed from such cycles are rings of unidirectionally coupled neurons (see Figure 5.2). In such ring networks of N neurons, the connection from the first neuron to the N-th neuron is inhibitory, and except for this connection, all other connections are excitatory. It has been well known that for ring networks of unidirectionally coupled neurons, if the number of inhibitory couplings is odd, the ring networks can generate sustained oscillations, and such ring networks have been widely used in different areas ranging from digital circuits for variable-frequency oscillations [80] to models of nervous systems for generating rhythmic movements [81, 82].

5.2.1 Bifurcations in Networks Constructed from Anti-symmetric Simple MC-Cycles with $N = p/2$

We now give a complete description of the local bifurcations from the trivial equilibrium for antisymmetric simple MC-cycles with $N = p/2$ (p even). In particular, we show that in such networks a Hopf bifurcation occurs creating a stable limit cycle that evolves into the prescribed cycle stored in the networks both with and without delay. We first discuss the bifurcations for the case of the cycle (4.13) in detail. For this cycle, $\mathbf{J^0} = \mathbf{I}$ and

$$\mathbf{J} = \begin{pmatrix} 0 & 1 & 0 \\ 0 & 0 & 1 \\ -1 & 0 & 0 \end{pmatrix}$$

Example 5.2.1. Due to its anti-symmetric structure, the cycle Σ defined in (4.13) annihilates the first, third, and fifth eigenvectors $v^{(0)} = (1, 1, 1, 1, 1, 1)^T$, $v^{(2)} = (1, \rho^2, \rho^4, 1, \rho^2, \rho^4)^T$, and $v^{(4)} = (1, \rho^4, \rho^2, 1, \rho^4, \rho^2)^T$ of the cyclic permutation matrix $\mathbf{P}$, where $\rho = e^{\pi \mathbf{i}/3}$. Accordingly, it "selects" the indices $n_1 = 1$, $n_2 = 3$, and $n_3 = 5$ for the characteristic equation (5.7) or (5.8) of the network constructed from it both with and without delay, corresponding to the complex conjugate pair of roots $\tilde{x}_1 = e^{\mathbf{i}\pi/3}$, $\tilde{x}_5 = e^{-\mathbf{i}\pi/3}$ and the real root $\tilde{x}_3 = -1$. Figure 5.3**A** shows the bifurcation curves

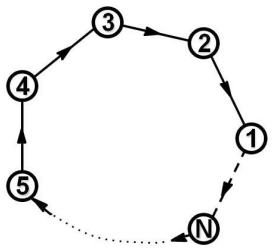

Figure 5.2: Topology of the networks constructed from anti-symmetric simple MC-cycles of size $N \times p$ with $p = 2N$. Such networks have topology of unidirectionally coupled neurons. All connections, except for the one from the neuron 1 to the neuron N which is inhibitory (dashed line), are excitatory (solid lines).

of the network without delay. The solid curve is the Hopf bifurcation corresponding to $n_1 = 1$ and $n_3 = 5$, and the dashed curve is the pitchfork bifurcation corresponding to $n_2 = 3$. Since 0, 2, and 4 are not the n_i indices in the characteristic equation (5.8), it follows that the limit cycle created from the Hopf bifurcation corresponding to $n_1 = 1$ and $n_3 = 5$ may be stable, and the Hopf bifurcation corresponding to $n_i = 2$ and 4 cannot occur in this network. Using the MatLab package MatCont 3.1, we numerically continued both the equilibrium solutions and the periodic solution created from the trivial solution via the Hopf bifurcation. Both the analytic computations and numerical simulations confirm that the limit cycle created from the trivial solution via the Hopf bifurcation is stable. Numerical simulations (see Figure 1.4 in Chapter 1 or Figure 1 in [26]) show that the limit cycle satisfies the transition conditions imposed by the prescribed cycle (4.13). Moreover, numerical continuation (Figure 5.3**C** and **D**) also indicate that the prescribed cycle is retrieved as attracting limit cycle (see the six nodes labelled by dark green pentagrams in panel **D**).

Figure 5.3**E-H** illustrate the results of the same analysis implemented in the network with delay. From the distribution of the characteristic roots (**F**) and the bifurcation curves (**E**), it is apparent that the delay changes the structure of the local bifurcations of the trivial solution significantly. Especially, due to the interaction between the Hopf bifurcation (**K**,**L**) corresponding to $n_2 = 3$ and the complex conjugate characteristic roots with the second largest real part (**J**) and the pitchfork bifurcation, a codimension two Bogdanov-Takens bifurcation occurs in the network with delay, while this bifurcation does not happen without delay. We recall from Section 4.2 that for the matrices

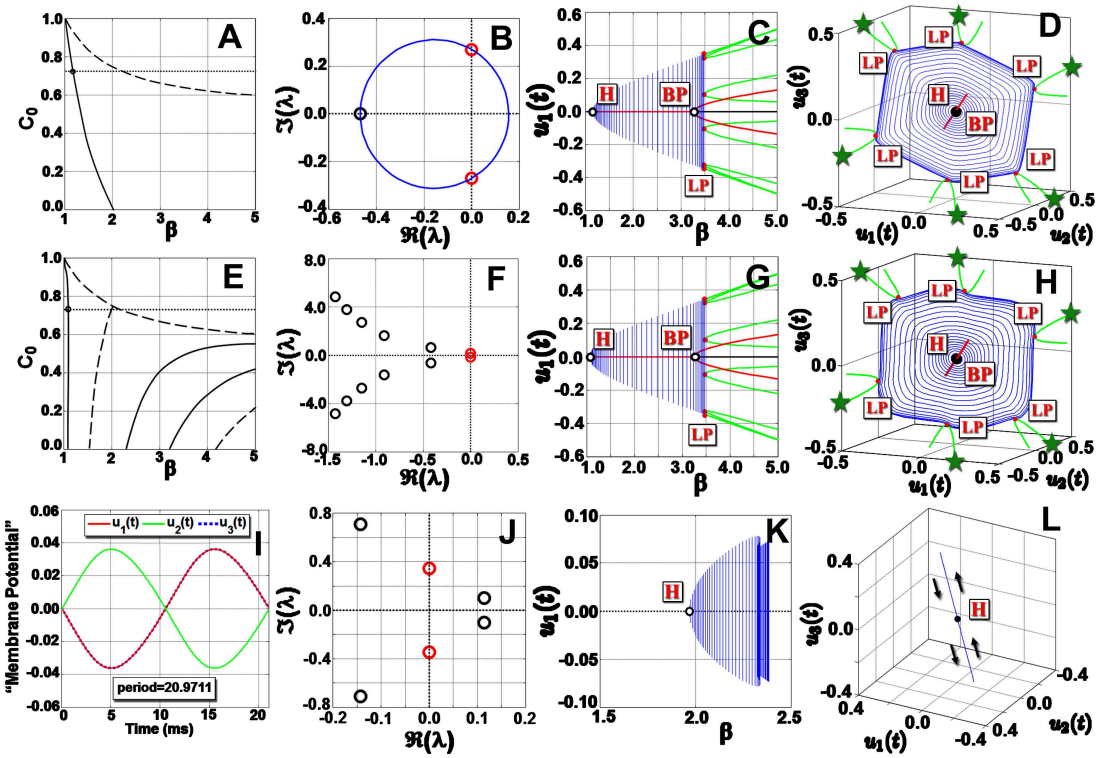

Figure 5.3: Local bifurcations of the trivial solution of the network constructed from the anti-symmetric simple MC-cycle (4.13). Panels from **A** to **D** are for the network without delay, and panels from **E** to **F** are for the network with delay ($\tau = 2.0$ms). Panels **A** and **E** show the bifurcation curves of the two networks respectively. In both panels, the solid curves are the bifurcation curves corresponding to $n_1 = 1$ and $n_3 = 5$, and the dashed curves are those of the bifurcations corresponding to $n_2 = 3$. The horizontal dotted line in each of **A** and **E** indicates the path ($C_0 = 0.73$) in parameter space along which the numerical continuation computations were carried out. The intersection between the dotted line and the solid curve indicates where the Hopf bifurcation occurs, and in both networks, this bifurcation creates the attracting limit cycle corresponding to the prescribed cycle (4.13). In both panels, the dashed curve on the top is the curve corresponding to the pitchfork bifurcation, and all other (dashed and solid) curves are Hopf bifurcation curves. Panels **B**, **F** and **J** show the location of the characteristic roots when the conjugate pair of roots with the largest (**B**,**F**) and second largest (**J**) real parts move across the imaginary axis from the left transversely, which indicates a Hopf bifurcation. Panels **C** and **D** show the results of numerical continuations of the trivial and non-trivial equilibria and the periodic solution bifurcating from the trivial solution. In panels **C**, **D**, **G**, **H**, **K** and **L**, we adopt the notations of MatCont [83], and use **H** to label **H**opf bifurcations, **BP** to label **B**ranch (pitchfork bifurcation) **P**oints, and **LP** to label **L**imit **P**oint (fold or saddle-node) bifurcations, respectively. The dark green pentagrams in panels **D** and **H** label the branches of nodes continued from the multiple saddle-nodes on limit cycle bifurcation. Panel **I** displays the unstable periodic solution ($\beta = 2.0345$) bifurcating from the trivial solution via the first "extra" Hopf bifurcation corresponding to $n_2 = 3$, and **K** and **L** display numerical continuations of this periodic solution. The continuation computations shown in **C** and **D** were implemented in MatCont 3.1. The continuation computations shown in **G** **H**, **K** and **L** were implemented in DDE-BIFTOOL 2.03.

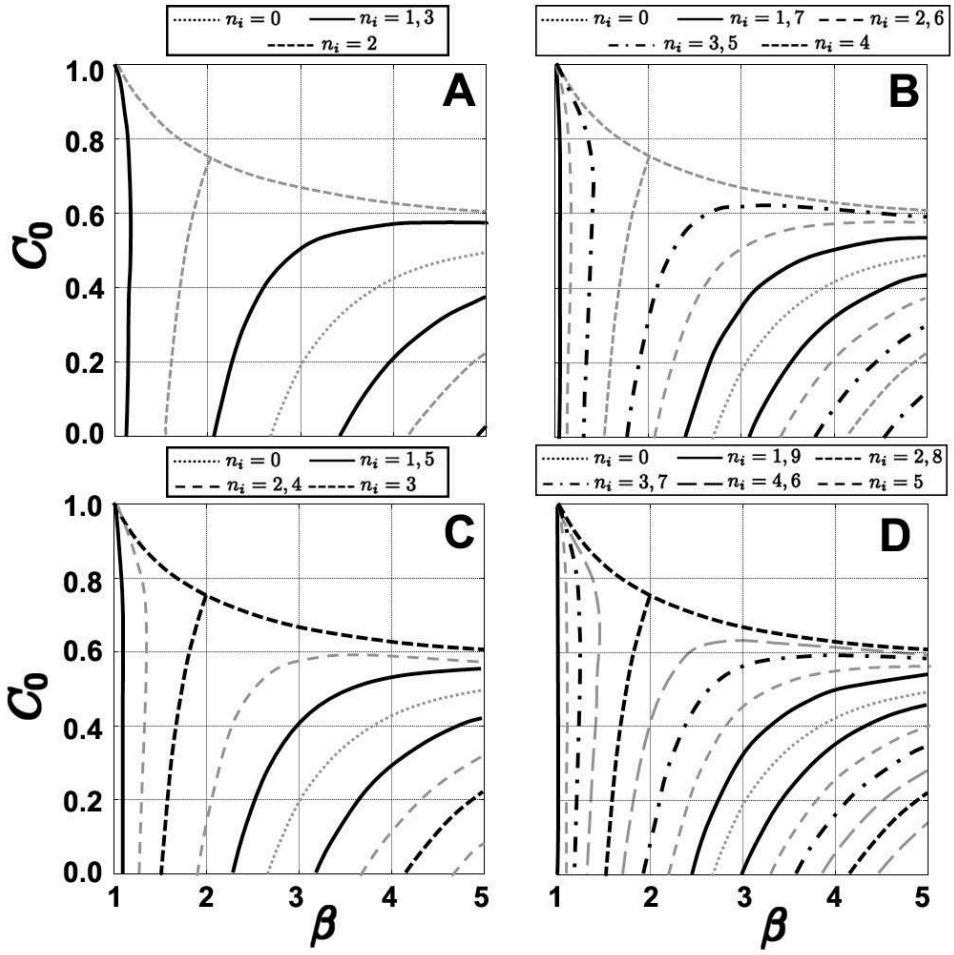

Figure 5.4: Curves of possible local bifurcations (in both black and gray) of networks constructed from simple MC-cycles of period $p = 4$ (**A**), 8 (**B**), 6 (**C**), and 10 (**D**) respectively. The black curves in the four panels are those respectively chosen by the four prescribed cycles, Σ_1 (**A**), Σ_2 (**B**), Σ_3 (**C**), and Σ_4 (**D**) (see text for the generators of these four cycles). For Σ_1 (**A**) and Σ_2 (**B**), the numbers of neurons in the two networks are $N = 2$ and $N = 4$. Clearly, in this case, $p/2$, which is 2 and 4 respectively, is not "chosen" by the prescribed cycles. Therefore, the pitchfork bifurcation (short dashed "horizontal" curve on the top of each panel) does not occur, and accordingly, the Bogdanov-Takens bifurcation (intersection between the short dashed "horizontal" curve on the top and the short dashed "vertical" curve on the left of each panel) does not occur either. For Σ_3 (**C**) and Σ_4 (**D**), the numbers of neurons in the two networks are $N = 3$ and $N = 5$. Thus, $p/2$, which is 3 and 5 respectively, is "chosen" by the prescribed cycles. Therefore, in these two networks, both Hopf bifurcations and pitchfork bifurcation occur at the trivial equilibrium solution. Since the networks shown in this figure are with transmission delay ($\tau = 2.0$ms), it follows that the Bogdanov-Takens bifurcation occurs at the trivial equilibrium solution in these two networks too. All the curves are obtained by numerically continuing Hopf bifurcations and steady-state bifurcations with DDE-BIFTOOL 2.03. Parameters for the computations were set as $\lambda = 10$, $\tau = 2.0$.

$\mathbf{J^0}$ and $\mathbf{J}$ derived from the cycle (4.13) with $p = 6$, the transition and fixed point conditions are also satisfied for the cycle

$$\Sigma = \begin{pmatrix} + & - \\ - & + \\ + & - \end{pmatrix},$$

with $p = 2$ (referred to as "derived cycle"). This cycle is retrieved as unstable periodic solution in the network with delay, but does not induce a periodic solution without delay. Figure 5.3**I** illustrates the profile of this unstable periodic solution at $C_0 = 0.73$ and $\beta = 2.0345$. Figure 5.3**K** and **L** illustrate the numerical continuation of this periodic solution.

Despite the dramatic differences between networks with and without delay, in terms of the "principal" Hopf bifurcation associated with the complex conjugate characteristic roots pair with the largest real part, which corresponds to $n_1 = 1$ and 5 for the cycle (4.13), delay does not change the qualitative structure of the local bifurcations of the trivial equilibrium. Numerical simulations and continuation results (see panels **G** and **H**) show that a limit cycle is created from the trivial solution via the "principal" Hopf bifurcation. By checking the direction of the Hopf bifurcation, it can be seen that this limit cycle is stable, and by computing the overlap [14, 26], it is found that it corresponds to the prescribed cycle (4.13).

Remark 5.2.2. We conclude this subsection with a complete description of the local bifurcations from the trivial equilibrium for general simple, anti-symmetric MC-cycles with $N = p/2$. For these cycles, we have that $\mathbf{J^0} = \mathbf{I}$ and

$$\mathbf{J} = \begin{pmatrix} 0 & 1 & 0 & 0 & \cdots & 0 & 0 \\ 0 & 0 & 1 & 0 & \cdots & 0 & 0 \\ \vdots & \vdots & \vdots & \vdots & \ddots & \vdots & \vdots \\ 0 & 0 & 0 & 0 & \cdots & 0 & 1 \\ -1 & 0 & 0 & 0 & \cdots & 0 & 0 \end{pmatrix}.$$

The eigenvalues of this matrix are the roots of $\tilde{x}^N = -1$, i.e. $\tilde{x}_i = e^{n_i \pi \mathbf{i}/N}$, $\tilde{x}_{2N-i} = 1/\tilde{x}_i$, with n_i odd and $1 \leq n_i \leq N-1$, whereas for N odd we have these complex conjugate root pairs for $1 \leq n_i \leq N-2$ (n_i odd) and there is the additional real root $\tilde{x}_N = -1$ corresponding to $n_N = N$.

In the next two paragraphs we discuss these two cases and illustrate them for the four cycles Σ_1, Σ_2, Σ_3, Σ_4 with $p = 4, 8, 6, 10$ ($N = 2, 4, 3, 5$), respectively. All of these cycles are generated by $\eta = (\zeta, -\zeta)$ with $\zeta = (+, +, +, \ldots, +) \in \{-1, 1\}^N$. Note that Σ_3 is the cycle (4.13) discussed in detail in Example 5.2.1. Bifurcation curves for these cycles in networks with delay ($\tau = 2.0$ms) are shown in Figure 5.4. A nonlinear local bifucation analysis near these bifurcations using center manifold and normal theory has not been pursued yet and will be presented elsewhere.

If N is even, only Hopf bifurcations occur at the trivial equilibrium. For networks without delay, only $N/2$ Hopf bifurcations occur, and the one corresponding to $n_i = 1$ and $p-1$ creates the attracting limit cycle corresponding to the prescribed cycle. For networks with delay, corresponding to each pair of n_i's, there are infinitely many Hopf bifurcations at the trivial equilibrium solution, and among those corresponding to $n_i = 1$ and $p - 1$, the first that occurs when β increases from $\beta = 1$ creates the attracting limit cycle corresponding to the prescribed cycle.

If N is odd, both Hopf bifurcations and a pitchfork bifurcation occur at the trivial equilibrium. For networks without delay, only $(N - 1)/2$ Hopf bifurcations occur, and the one corresponding to $n_i = 1$ and $p - 1$ creates the attracting limit cycle corresponding to the prescribed cycle. For networks with delay, there are again infinitely many Hopf bifurcations at the trivial equilibrium, and among those corresponding to $n_i = 1$ and $p - 1$, the first that occurs when β increases creates the attracting limit cycle corresponding to the prescribed cycle. In networks both with and without delay, a pitchfork bifurcation occurs when parameters move accross the curve (5.15), which is independent of the transmission delay τ. For networks with delay, corresponding to $N = p/2$, in addition to the pitchfork bifurcation, infinitely many "extra" Hopf bifurcations occur too. The first (for increasing β) of these "extra" Hopf bifurcations terminates at a Bogdanov-Takens point on the pitchfork curve, depicted in Figure 5.1**E** for Σ_3.

5.2.2 Bifurcations in Networks Constructed from Simple MC-Cycles with $N = p$

In addition to networks constructed from anti-symmetric simple MC-cycles with $N = p/2$, there is another type of networks which are rings of unidirectionally coupled neurons, which are constructed from simple MC-cycles with $N = p$. The only difference in terms of the network connections is that while every network constructed from an anti-symmetric simple MC-cycle with

$N = p/2$ has one inhibitory connection, all connections in networks constructed from simple MC-cycles with $N = p$ are excitatory.

This type of excitatory unidirectional ring networks have been extensively investigated recently (see for example [37, 41, 42, 84] etc.). Pakdaman et al. [37] showed that the long lasting oscillations shown by such networks, referred to as *transient oscillations*, can not be explained by the analysis of the asymptotic behavior of the system. They considered the system of difference equations derived from the original system of delay differential equations. Such a system of difference equations can be used to approximate the original system of delay differential equations when the time scale under consideration is much larger than the characteristic charge-discharge time of the network. Pakdaman et al. showed that the long lasting oscillations presented in the original network correspond to attracting periodic orbits in the descretized system of difference equations. Accordingly, they argued that the long lasting transient behavior observed in the original system of delay differential equations is due to the competition between the antagonistic asymptotic behavior of the original system and that of its descretized system. Both the properties of the transient oscillations and the bifurcation structures of excitatory unidirectional ring networks were investigated by many other authors in the past few years too (see for example [41, 42, 84] etc.).

Here, we consider the networks investigated by Pakdaman et al [37] and others as a special case of our networks constructed from simple MC-cycles with $N = p$ and $C_0 = 0$. We claim that the cycles retrieved in such networks corresponding to the prescribed cycles are the transient oscillations described by Pakdaman et al [37]. Next, we briefly discuss how the prescribed cycles determine the local bifurcation structures of the trivial equilibrium in such networks.

Since the networks here are constructed from simple MC-cycles with $N = p$, all integers from 0 to $p-1$ are indices appearing in the characteristic equations (5.7) and (5.8) of networks both with and without delay. As we have shown in Section 5.1, pitchfork bifurcation, Hopf bifurcations, and Bogdanov-Takens bifurcation may occur in such networks. From the characteristic equations (5.7) and (5.8), one can see by setting $n_i = 0$, that the characteristic root $\sigma = 0$ can occur only when $\beta = 1$, but since $\beta = \text{arctanh}(\beta_1)/\beta_1$ and $\beta_1 \in (0, 1)$, we have that $\beta > 1$ [26]. It follows naturally that for $n_i = 0$, throughout the whole parameter space, there is always one characteristic root with positive real part. Therefore, all the solutions bifurcating from the trivial equilibrium, including

the trivial equilibrium itself, are unstable [61]. Accordingly, the periodic solutions bifurcating from the trivial equilibrium are unstable as well.

Next, we prove two useful results.

Lemma 5.2.1. *Any network constructed from a simple MC-cycle with $N = p$ has at least three equilibrium solutions.*

Proof: Any network constructed from a simple MC-cycle has the following general form

$$\frac{du_i}{dt}(t) = -u_i(t) + C_0\beta_K \tanh(\lambda u_i(t)) + C_1\beta_K \tanh(\lambda u_{i+1}(t-\tau)) \tag{5.16}$$

where $\tau = 0$ for networks without delay, and following [37], the index i is taken modulo $N+1$, i.e. $u_{N+1} = u_1$. We show that this network has at least the following three equilibria, $\mathbf{u}^* = \pm(u^*, u^*, \ldots, u^*)^T \in \mathbb{R}^N$ and $\mathbf{0} \in \mathbb{R}^N$. Since obviously $\mathbf{0}$ is an equilibrium, we only need to consider the non-trivial equilibrium. Substituting then $\mathbf{u}(t) = \mathbf{u}^*$ into the network (5.16) gives a scalar equation

$$\mathbf{0} = -\mathbf{u}^* + \beta_K \tanh(\lambda \mathbf{u}^*).$$

Setting $f(x) = x - \beta_K \tanh(\lambda x)$, we have that $\lim_{x\to-\infty} f(x) = -\infty$, $\lim_{x\to\infty} f(x) = \infty$, and $f(0) = 0$. Also, since $df(x)/dx = 1 - \beta(1 - \tanh^2(\lambda x))$, $df/dx = 0$ leads to

$$\tanh^2(\lambda x) = \frac{\beta - 1}{\beta}.$$

Since $\beta > 1$, $f(x)$ has two distinct critical points $x^+ > 0$ and $x^- = -x^+$. Since $f(0) = 0$, $df(0)/dx < 0$, and $\lim_{x\to\pm\infty} df(x)/dx = 1 > 0$, it follows from the intermediate value theorem that $f(x^-) > 0$ and $f(x^+) < 0$, and this implies that $f(x)$ has three roots. This proves the assertion.

For the convenience of discussion, we denote the two non-trivial equilibrium solutions by $\mathbf{u}^-$ and $\mathbf{u}^+$ respectively. Next, we prove that these two non-trivial equilibrium solutions are asymptotically stable.

Lemma 5.2.2. *Let $u^* > 0$ be the positive solution of the equation $x - \beta_K \tanh(\lambda x) = 0$. Then the non-trivial equilibrium solutions $\mathbf{u}^- = -(u^*, u^*, \ldots, u^*)^T \in \mathbf{R}^N$ and $\mathbf{u}^+ = (u^*, u^*, \ldots, u^*)^T \in \mathbf{R}^N$ are asymptotically stable for $\beta < 1/(1 - \tanh^2(\lambda u^*))$.*

Proof: Here we only analyze the local stability of the equilibrium $\mathbf{u}^+$, because the local stability analysis for $\mathbf{u}^-$ is exactly the same.

Linearizing the system (5.16) around the equilibrium $\mathbf{u}^+$ gives

$$\dot{\mathbf{u}}(t) = \mathbf{A_1}(\mathbf{u}^+)\mathbf{u}(t) + \mathbf{A_2}(\mathbf{u}^+)\mathbf{u}(t-\tau)$$

where $\mathbf{A_1}(\mathbf{u}^+) = (C_0\beta(1-\tanh^2(\lambda u^*))-1)\mathbf{I}$ and $\mathbf{A_2}(\mathbf{u}^+) = C_1\beta(1-\tanh^2(\lambda u^*))$. Substituting the ansatz $\mathbf{u} = \phi e^{\sigma t}$ with $\phi \in \mathbb{R}^N$ into the above linearized equation leads to the following characteristic equation

$$\det(\Delta(\sigma)) = \prod_{i=1}^{N}(\sigma + 1 - C_0\beta(1-\tanh^2(\lambda u^*)) - C_1\beta(1-\tanh^2(\lambda u^*))e^{2n_i\pi\mathbf{i}/p-\sigma\tau}) = 0.$$

The factor with $n_i = 0$ in this equation reduces to

$$\sigma + 1 - C_0\beta(1-\tanh^2(\lambda u^*)) - C_1\beta(1-\tanh^2(\lambda u^*))e^{-\sigma\tau} = 0.$$

Letting $\sigma = \alpha + \mathbf{i}\omega$, this equation becomes

$$\begin{cases} \alpha &= (C_0 + C_1 e^{-\alpha\tau}\cos(\omega\tau))\beta(1-\tanh^2(\lambda u^*)) - 1 \\ \omega &= C_1\beta(1-\tanh^2(\lambda u^*))e^{-\alpha\tau}\sin(\omega\tau) \end{cases}$$

If $\alpha = 0$, then $\beta = 1/((C_0+C_1\cos(\omega\tau))(1-\tanh^2(\lambda u^*)))$. It follows that for $\beta < 1/(1-\tanh^2(\lambda u^*))$, $\Re(\sigma) = \alpha < 0$.

Thus, for networks constructed from simple MC-cycles, the situation is very similar to that Pakdaman et al described in [37], and the unstable limit cycles bifurcating from the trivial equilbrium solution will stay in the boundary between the respective basins of attraction of the two non-trivial equilibrium points $\mathbf{u}^-$ and $\mathbf{u}^+$, which has been proved to be a codimension one locally Lipschitz manifold containing the unstable equilibrium point $\mathbf{u} = \mathbf{0}$ and its stable manifold [37].

5.2.3 Bifurcations in Networks Constructed from More Complicated Admissible Cycles

In the above two different cases, we have discussed the local bifurcations of the trivial solution of the two types of ring networks of unidirectionally coupled neurons. We showed that the prescribed cycles in the two different types of networks are retrieved as different objects. In the networks with

one inhibitory connection, i.e., in those constructed from anti-symmetric simple MC-cycles with $N = p/2$, the prescribed cycles are retrieved as attracting limit cycles bifurcating from the trivial equilibrium via Hopf bifurcations. In the networks without inhibitory connection, i.e., in those constructed from simple MC-cycles with $N = p$, the prescribed cycles are retrieved as so called long lasting *transient oscillations*. In this subsection, we continue to discuss the local bifurcations of the trivial solution of the networks constructed from more general and complicated cycles, and show that, in more general cases, both the prescribed cycles and the derived cycles stored in the same networks may be retrieved as either attracting limit cycles or long lasting transient oscillations.

Although in general, the network constructed from a generic simple cycle may have complicated network topology, the way the prescribed cycle determines the structures of local bifurcations of the trivial equilibrium solution of the network by its structural features remains exactly the same. We illustrate this for two examples. The first example is a network constructed from a simple cycle for which an anti-symmetric derived cycle is retrieved as attracting limit cycle, and the prescribed cycle is retrieved as long lasting transient oscillations.

Example 5.2.2. Consider the cycle Σ_3 from Example 4.1.2. Figure 5.5 illustrates the evolution of the attracting limit cycle bifurcating from the trivial equilibrium. Since Σ_3 only annihilates the first eigenvector $v^{(0)} = (1, 1, \ldots, 1)^T \in \mathbb{C}^6$ of the cyclic permutation matrix $\mathbf{P}$, it follows that the indices n_i in the characteristic equation (5.7) are $1, 2, \ldots, 5$. Therefore, both Hopf bifurcations, and pitchfork bifurcation may occur. In Figure 5.5**E**, the curves on which these bifurcations are located are shown as gray curves and the black curve on the left. On the black curve on the left, the complex conjugate characteristic roots pair with the largest real part moves across the imaginary axis transversely. Therefore, when parameters move across this curve, an attracting limit cycle may bifurcate from the trivial solution. In panels **A** and **B**, we numerically compute solution trajectories starting from randomly chosen constant initial data $\varphi(\theta) \in C([-1.0, 0], \mathbb{R}^5)$, and in panel **F** we track both the periodic solution and the non-trivial equilibrium solutions corresponding to the binary patterns in the derived admissible cycle Σ_1 from Example 4.1.2 with DDE-BIFTOOL. Both the simulations (**A**-**D**) and the numerical continuations (**F**) confirm the appearance of the attracting limit cycle, and illustrate that the attracting limit cycle corresponds to the anti-symmetric,

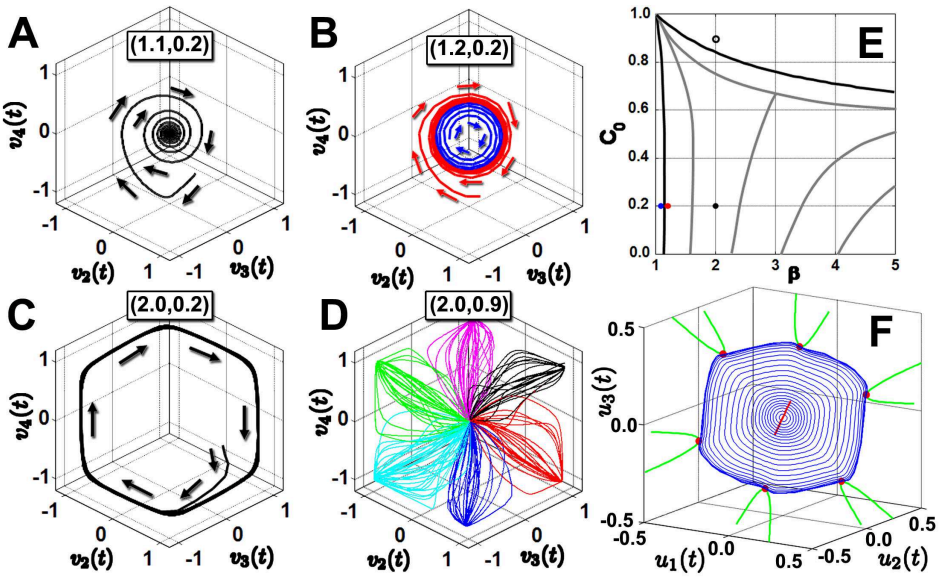

Figure 5.5: The attracting limit cycle bifurcating from the trivial equilibrium solution of the network constructed from Σ_3 in Example 4.1.2. In the four panels on the left, simulated solution trajectories starting from randomly chosen constant initial data with different (β, C_0) parameter values (**A**: $(1.1, 0.2)$, **B**: $(1.2, 0.2)$, **C**: $(2.0, 0.2)$, and **D**: $(2.0, 0.9)$) are displayed. The blue, red, black solid circles and the open circle in panel **E** indicate the locations of the (β, C_0) parameter values for the simulations shown in the four panels on the left. The black curve on the left in **E** and the gray curves are curves on which conjugate complex and real characteristic roots move across the imaginary axis indicating possible Hopf and pitchfork bifurcations. The black curve on the top of **E** is the curve corresponding to the *multiple saddle-nodes on limit cycle bifurcation* [77], which destroys the attracting limit cycle bifurcating from the trivial solution. Panel **F** shows the numerical continuations of the equilibrium solutions and the periodic solution bifurcating from the trivial solution. The little red dots on the green curves mark where the multiple saddle-nodes on limit cycle bifurcation occurs, and the green curves are branches of the saddles and nodes created from the destroyed limit cycle. The red line in the middle are the two branches of the symmetric equilibria $(u, -u, u, -u, u)$ and $(-u, u, -u, u, -u)$ respectively, and these two equilibria arise from the trivial equilibrium via the pitchfork bifurcation. Both the simulations (**A**-**D**) and the numerical continuations (**F**) confirm the occurence of the predicted bifurcations (**E**). The parameters are set as follows: $\tau = 1.0$ms, and $\lambda = 10$.

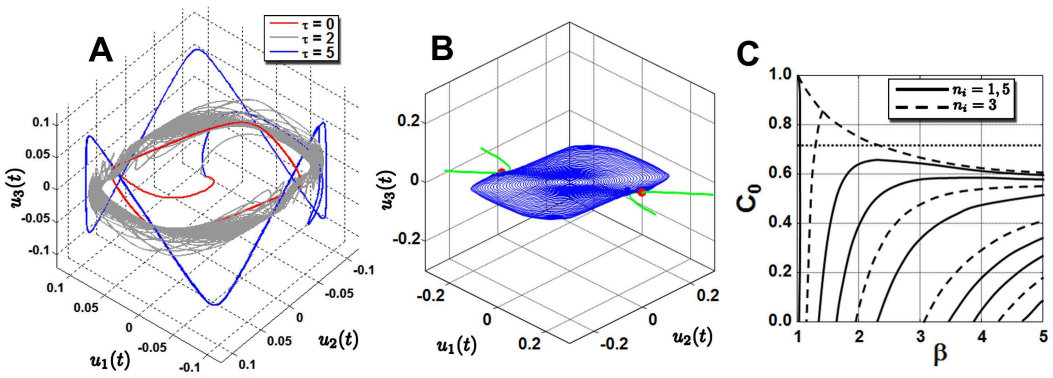

Figure 5.6: Retrieving an inseparable composite cycle and the local bifurcation structures. The curves in **A** are simulated solution trajectories with parameter values $C_0 = 0.71$, $\beta = 2$ and different delay values: $\tau = 0$ms (red curve), $\tau = 2$ms (gray curve), $\tau = 5$ms (blue curve). Panel **B** illustrates the numerical continuations (along $C_0 = 0.71$, see dotted line in **C**) of both the periodic solution (blue curves) bifurcating from the trivial equilibrium and the two pairs of saddles and nodes (green curves) bifurcating from the periodic solution via the multiple saddle-nodes on limit cycle bifurcation. The two saddle-nodes are plotted as the two small solid red circles on the two green curves. We note that all curves are actually on the plane $u_3(t) = 0$. Panel **C** illustrates curves of all possible local bifurcations of the trivial solution. All but the top dashed curve, which is that of the pitchfork bifurcation, are Hopf bifurcation curves. The numerical continuation computations and the bifurcation curves are implemented and obtained in Matlab with the package DDE-BIFTOOL 2.03.

simple, and consecutive but not minimal cycle [26] Σ_1 in Example 4.1.2. Meanwhile (see also Example 5.2.1), as the Hopf bifurcation corresponding to $n_3 = 5 = p/2$ does occur in this network, the cycle Σ_4 shown in Figure 4.3**A** is retrieved successfully in this network too, and it is retrieved as the unstable periodic solution along the symmetric diagonal line $\{\mathbf{u} \in \mathbb{R}^5 | \mathbf{u} = (u, -u, u, -u, u)\}$.

In Chapter 2 and [26], we have seen that networks constructed from separable cycles consist of isolated clusters, and each cluster corresponds to a simple cycle component. Accordingly, not only the local bifurcation structures of the trivial equilibrium solution, but also the dynamics of the networks are completely determined by its simple cycle components. Therefore, we complete our discussions of the local bifurcation structures of the trivial equilibrium with a network constructed from an inseparable admissible cycle.

Example 5.2.3. Consider the network constructed from the following cycle

$$\Sigma = \begin{pmatrix} 1 & 1 & -1 & -1 & -1 & 1 \\ 1 & -1 & -1 & -1 & 1 & 1 \\ -1 & 1 & -1 & 1 & -1 & 1 \end{pmatrix}. \tag{5.17}$$

Since the vector space spanned by the set of all cyclic permutations of the third row η_3, which is called the loop generated by η_3 (see Chapter 2 and [26]), is contained in the vector space spanned by the set of all cyclic permutations of the first two rows η_1 and η_2, and η_3 is linearly independent of η_1 and η_2, it follows that Σ is an inseparable composite cycle [26].

Direct computations show that the prescribed cycle is the only cycle satisfying the transition conditions imposed by the prescribed cycle itself. Figure 5.6 illustrates the simulated solutions (**A**), continuation of the limit cycle bifurcating from the trivial solution via the "principal" Hopf bifurcation (**B**), and the curves of all possible local bifurcations of the trivial solution (**C**). For $C_0 = 0.71$, $\beta = 2.0$, and without delay, $\tau = 0$, the solution trajectory approaches the attracting limit cycle created by the "principal" Hopf bifurcation. When τ increases, the solution trajectory starts deviating from the attracting limit cycle (gray curve in panel **A** for example), and becomes more and more close to the prescribed cycle (see the blue curve in panel **A**). However, during this process, only one "extra" Hopf bifurcation occurs, which creats one unstable limit cycle, and four non-trivial equilibria are created via one pair of saddle-node bifurcations. We compared the successfully retrieved cycle, which corresponds to the prescribed cycle Σ, with both the attracting limit cycle created via the "principal" Hopf bifurcation corresponding to $n_1 = 1$ and $n_3 = 5$, and the unstable limit cycle created via the "extra" Hopf bifurcation corresponding to $n_2 = 3$. The retrieved cycle corresponds to none of them. We argue that this retrieved cycle may be the transient oscillation described by Pakdaman et al and others [37,42,84], and it may be the consequence of the competition among the attracting limit cycle, the unstable limit cycle and the saddles and nodes.

CHAPTER 6

CONCLUSIONS AND DISCUSSIONS

In this dissertation, we have systematically studied the storage and retrieval of cyclic patterns in Hopfield-type neural networks. In this chapter, we summarize and discuss our main methods and results developed and obtained in Hopfield-type neural networks on three topics: admissibility of cyclic patterns and topology of the networks constructed from admissible cycles; relaxation dynamics of the networks constructed from simple MC-cycles; retrievability of admissible cycles and bifurcations of the networks constructed from admissible cycles.

6.1 Admissibility and Network Topology

In this part, we studied the structural features of admissible cycles and their relation to the topology of the corresponding networks. While our main motivation in this part was the storage of cycles in continuous-time Hopfield-type networks, the results apply to other networks as well, including the discrete networks considered by [56] and [1] and networks of spiking neurons exhibiting up-down states. In particular, we have formulated and proved conditions on binary cyclic patterns that guarantee the existence of a network with connectivity satisfying the transition conditions imposed by the cycle, independent of the specific dynamics of the individual neurons.

We showed that if and only if the discrete Fourier transform $\hat{\Sigma} = \Sigma V$ of a cycle matrix Σ contains exactly r nonzero columns, where $r = \text{rank}(\Sigma)$, then a network can be constructed from Σ with the pseudoinverse learning rule. Based on the structural analysis of the invariant subspaces of the row space of Σ, the admissible cycles have been classified into simple cycles, and separable and inseparable composite cycles. This classification was based on the decomposition of the row space of Σ into subsets corresponding to disjoint loops. The admissibility of a cycle implied that all vectors of a loop are in the row space of Σ if Σ contains some of these loop vectors. If no loop-space associated with Σ is a subspace of another loop-space (the generators are essential generators), we have identified for each loop the neurons associated with the loop vectors contained in Σ with

a cluster. For general admissible cycles the clusters are connected, and the connectivity of the clusters depends on the intersections of their loop-spaces. Two clusters are directly connected if their indecomposable invariant subspaces intersect non-trivially. They are "indirectly" connected if they are part of a chain of directly connected clusters.

If an admissible cycle is separable, the clusters are completely isolated. In this case each cluster corresponds to a simple cycle associated with a generator of Σ. If the simple cycle is minimal and consecutive, the cluster has the form of a feedforward chain from the last neuron to the first neuron with feedbacks to the last neuron from the other neurons. If in addition the length of the cycle, p, is even and the rank of the generator is $p/2$, we generically find a ring structure with excitatory or inhibitory connection from the first neuron to the last neuron, but we cannot exclude that special loops with these properties exist for which no ring-structure occurs. If the simple cycle is minimal but non-consecutive, we find more than one feedforward chains.

Regarding non-minimal simple as well as composite cycles, it would be interesting to find equivalence relations similar to those of [85], and [86], relating networks constructed from non-minimal cycles to networks constructed from minimal cycles. For example, similar to the linear-threshold (LT) networks [87,88], we may consider the Hopfield-type network (1.10) with delay in a different but closely related form,

$$\dot{\mathbf{u}} = -\mathbf{u} + \tanh\left(\beta\left(C_0\mathbf{J^0}\mathbf{u} + C_1\mathbf{J}\mathbf{u}_\tau\right)\right), \tag{6.1}$$

where $\beta = \beta_K\lambda$ and $\mathbf{u}_\tau = \mathbf{u}(t-\tau)$. While (1.10) is invariant under arbitrary permutations of the neurons, it can be shown that (6.1) is invariant under a larger class of linear transformations that allows to define broad equivalence relations among admissible cycles. In comparison to (1.10), the only disadvantage (6.1) may have is that it is less biologically plausible, because in biological neural networks neurons usually are coupled with each other through chemical synapses, which means that the firing rates instead of the membrane potentials of the presynaptic neurons change the membrane potential of the postsynaptic neuron.

In networks constructed from composite cycles, the complete isolation of the clusters of separable cycles means that each cluster has its own subcycle. The issue is that we cannot expect the different subcycles to synchronize, preventing the network to traverse the cycle states in the order prescribed

by the cycle matrix. In this case an additional synchronization mechanism must be introduced to enforce synchrony. Such a mechanism can be in the form of a small coupling among the clusters or through an external periodic input acting as pacemaker.

The generation of cyclic patterns in animal nervous systems is associated with CPG networks, and the storage and retrieval of cyclic patterns in such networks are fundamentally important. Recent experimental observations [8, 22, 23] suggested that CPGs may be highly flexible. As some animal movements, such as swallowing, gastrointestinal motility etc., often require the coordination of several functional groups of muscles, different CPGs controlling these muscles subsequently form during different phases of the movements. Such CPG networks consist of pools of neurons that can function in several CPGs involved in the organization of various motor behavior.

Recently, in order to account for the flexibility of memory representation observed in neurophysiological experiments, [88] studied the effect of saliency weights on the memory dynamics in LT neural networks. They showed that the saliency distribution determines the retrieval process of the stored patterns, and that a nonuniform saliency distribution can contribute to the disappearance of spurious states. Using our results on the relation between the structural features of a cycle and the network topology, a mechanism similar to the variable saliency factor introduced by [88] into LT networks may be used to combine different CPGs in one network, and to study how a sequence of several cycles determines a changing network structure.

6.2 Relaxation Dyanmics

Motivated by a simple observation of the asynchronous sign-changes during the network-state transitions for retrieving the cycles prescribed in the network, we developed a novel method, which we referred to as the Misalignment Length Analysis (MLA), for analyzing the relaxation oscillations corresponding to most admissible cycles. The method consists of two parts, a qualitative theory of binary patterns dynamics, and a quantitative method for misalignment length dynamics. The method was developed in the networks constructed from simple MC-cycles with intermediate patterns satisfying the transition conditions imposed by the cycles prescribed in the networks.

Directly starting from the cycle itself, we constructed a *backward-sequence matrix* (*MS-matrix*), and with the entries of the MS-matrix, we obtained a *backward sequence* $b_{i,n}$ for every neuron in

the network during the time interval for retrieving the n-th pattern, where the index i labels the neuron to which the sequence $b_{i,n}$ is associated, and defined the order between any two backward sequences. We showed that sign-changes of different neurons occur completely asynchronously during every network state transition, i.e., one at a time. Thus, if the Hamming distance between two consecutive patterns in the prescribed is greater than one, then the sign-changes occur in the order of the backward sequences $\{b_{i,n} : i = 1, \ldots, N,\ n \text{ is fixed}\}$. During each network state transition, we defined the sign (column) vector of the membrane potentials $\mathbf{u}(t)$ of the network between two sign-changes to be an *intermediate pattern*. We showed in examples in Chapter 3 that the long term behavior of the network constructed from admissible cycles is determined by these intermediate patterns and the cycles starting from them.

Based on the qualitative theory of binary patterns dynamics, we constructed a recurrence equation for every simple MC-cycle. By inductively solving the recurrence equation, a lower bound for the total number $\hat{n}$ of the prescribed patterns that can be successfully retrieved was obtained. Although the motivation for our quantitative MLA method is similar to that of the kinematical model for traveling waves in excitatory ring networks proposed by Horikawa and Kitajima [42], our method is fundamentally different from their model in two aspects. First, our method has a qualitative theory part, which uses the information from cycles prescribed in networks, and a complete qualitative description of the relaxation binary pattern dynamics can be obtained. Second, while Horikawa and Kitajima considered spatial blocks in their kinematical model, we consider temporal blocks in our MLA method. Using the qualitative description, we can construct a recurrence equation for every network constructed from a simple MC-cycle with intermediate patterns satisfying the transition conditions imposed by the prescribed cycle. By iteratively solving the recurrence equation, the exact number $\hat{n}$ of binary patterns from the prescribed cycle can be calculated. Moreover, based on our theory about the order relation of the backward sequences associated to binary row vectors, for any network constructed from an admissible cycle, we may find a lower bound for the number of the binary patterns from the prescribed cycle that can be successfully retrieved. Therefore our method is applicable to a much broader class of networks than the unidirectionally coupled ring networks to which the kinematical model is applicable. Also, as the time interval for retrieving a binary prescribed pattern is larger than but close to τ, the value

$\hat{n}\tau$ can be taken as a lower bound for the duration of the transient oscillations relaxing to either a stable equilibrium or a stable periodic solution.

6.3 Retrievability and Bifurcations

In Chapter 4, we studied retrieval of admissible cycles in Hopfield-type networks with and without delay. For networks with $C_0 = 0$, and $\lambda = \beta \to \infty$, we proved that for any given positive integer n, there exists a finite delay time $\tau > 0$, such that the quantitative MLA method provides a lower bound $\hat{n} > n$ for pattern retrieval. Hence more than n successive patterns from the prescribed cycle Σ can be retrieved, which implied that every simple MC-cycle with intermediate patterns satisfying the transition condition imposed by the prescribed cycle Σ is weakly retrievable. In terms of the linear stability analysis, we decomposed each of the characteristic equations (5.7) and (5.8) into a product of N factors, each corresponding to an n_i index in the characteristic equation, which turns out to be an integer between 0 and $p-1$. Based on this decomposition, we obtained a scenario of all possible local bifurcations of the trivial solution for every network constructed from an admissible cycle. Clearly, the scenario is determined by the prescribed admissible cycle in terms of its structural features by selecting the n_i indices appearing in the characteristic equations (5.7) and (5.8). In [26], we have explained how an admissible cycle determines which N integers among those from 0 to $p-1$ are chosen to be the n_i indices. Since these n_i indices determine the arrangement of the curves of characteristic roots with zero real part, which provides a scenario of all possible local bifurcations of the trivial solution, the prescribed cycle determines the structure of the local bifurcations of the trivial solution with its structural features by "selecting" the n_i indices. In the context of networks of coupled oscillators, a similar idea has been used for determining the stability of synchronized oscillations [89–92]. In [26], we have demonstrated a possible extension of our study to networks of coupled oscillators to a network of spiking neurons with bistable membrane behavior and postinhibitory rebound.

Using the MatLab packages, MatCont 3.1 and DDE-BIFTOOL 2.03, for numerical continuations and bifurcation analysis, we showed that addmissible cycles are stored and retrieved in the networks as different objects. Anti-symmetric simple MC-cycles with $N = p/2$ are stored and retrieved as attracting limit cycles bifurcating from the trivial solution via the "principal" Hopf

bifurcation. Anti-symmetric cycles of period two are stored and retrieved as unstable periodic solution bifurcating from the trivial solution via the "extra" Hopf bifurcation corresponding to the index $n_i = p/2$, and the unstable periodic solution stays in the one-dimensional subspace corresponding to the symmetric diagonal $\{\mathbf{u} \in \mathbb{R}^N \mid \mathbf{u} = (u, -u, u, \ldots, u)^T$, if N is odd; and $\mathbf{u} = (u, -u, u, \ldots, -u)^T$, if N is even, with $u \in \mathbb{R}$ $\}$ in the phase space of the network. The other admissible cycles for the same network are stored and retrieved as long lasting transient oscillations. For τ sufficiently large, the transient oscillation practically lasts forever.

While theoretical investigations [37,41,44] suggest that solution trajectories of excitatory unidirectional ring networks should in general eventually converge to stable equilibria, numerical simulations usually show long lasting oscillatory patterns [37]. Pakdaman et al and many others [37,42,84] have studied such long lasting transient oscillations and their properties in details. It has been shown that such long lasting transient oscillations do not exist in networks without delay, and can not be explained by the asymptotic dynamics of the networks with delay. In this dissertation, we illustrated that many admissible cycles are stored and retrieved in networks with delay as transient oscillations, and based on the observations from the bifurcation analysis and numerical continuation computations of both the stable/unstable equilibrium solutions and periodic solutions, we conjecture that the transient oscillations are a consequence of the interactions among the attracting limit cycle, unstable periodic solutions and equilibrium solutions. To clarify how the interactions among these dynamical objects shape the long lasting transient oscillations would be a very interesting future direction to extend our study on the storage and retrieval of the cyclic patterns representing phase-locked oscillations.

Cyclic patterns of neuronal activity in animal nervous systems are partially responsible for generating and controlling rhythmic movements from locomotion to gastrointestinal musculature activities. Neural networks of relatively small sizes that can produce cyclic patterned outputs without rhythmic sensory or central input are called central pattern generators (CPGs). So far, different models have been proposed to account for the mechanisms underlying the generation of rhythmic activities [22,25,93,94]. Among them, the "half-center oscillator" is one of the most widely used models for studying CPGs [94–97], and the ring network model is another one [81,82,94]. It has been shown that the classical half-center oscillator can be viewed as a limit cycle oscillator [98], and

so are the ring networks. During the past few decades, limit-cycle oscillators have played key roles in understanding the rhythmogenesis in animal CPG networks [24, 25, 99–101]. Recently, transient dynamics has been suggested to take important roles in generating cyclic patterns [102], and *stable heteroclinic channels* [103, 104], or *stable heteroclinic sequences* [105]. In this dissertation, we have illustrated that cyclic patterns except for those with special symmetric structures are stored and retrieved as transient oscillations, and those long lasting transient oscillations may be shaped by the interactions among the attracting limit cycle, unstable periodic solutions, saddles and nodes. Since heteroclinic connections may be constructed between a saddle or hyperbolic periodic orbit and another saddle or hyperbolic periodic orbit by identifying the stable submanifold of the previous one with the unstable submanifold of the latter one, some of the long lasting transient oscillations may correspond to such heteroclinic channels.

6.4 Storing Cycles in Networks of Spiking Neurons

The results presented in this dissertation were developed in the framework of Hopfield-type networks. However, these results may also be extended to the storage and retrieval of cyclic patterns in other neural networks. In this section, we introduce a network model of identical spiking neurons with bistable membrane behavior and postinhibitory rebound, and show an example of a successfully retrieved cycle in a network constructed using the pseudoinverse method.

We consider the simplest single-compartment neuron model, the passive integrate-and-fire (PIF) model [73, 106]. The model is described by the following first-order nonlinear ordinary differential equation,

$$c_m \frac{dV_i}{dt} = -I_L^{(i)}(t) - I_{nl}^{(i)}(t) + I_{synE}^{(i)}(t) + I_{synI}^{(i)}(t), \tag{6.2}$$

where $V_i(t)$ is the membrane potential of the i-th neuron in the network, and if $V_i(t) \geq \theta$ where $\theta = -45\text{mV}$ is the threshold for the firing action potentials, then $V_i(t+dt) = 0$, and $V_i(t+2dt) = V_{reset}$ with $dt = 0.005\text{ms}$ and $V_{reset} = -55\text{mV}$. After each action potential, an absolute refractory period $t_{Refr} = 1\text{ms}$ is imposed, and during the refractory period the membrane potential $V_i(t)$ is fixed at V_{reset}. The parameter c_m, chosen as $c_m = 20\text{nF/mm}^2$, is the specific membrane capacitance. The membrane and synaptic currents of the i-th neuron are respectively given as follows.

Leakage membrane current:

$$I_L^{(i)}(t) = g_L(V_i(t) - E_L), \tag{6.3}$$

where $g_L = 1\mu\text{S/mm}^2$ and $E_L = -68\text{mV}$.

Nonlinear membrane current:

$$I_{nl}^{(i)}(t) = g_{nl}(V_i(t) - E_1)(V_i(t) - E_2)(V_i(t) - E_3) - \delta, \tag{6.4}$$

where $g_{nl} = 0.03\text{mV}^{-2}$, $E_1 = -72\text{mV}$, $E_2 = -58\text{mV}$, $E_3 = -44\text{mV}$ and δ is a parameter for shifting the nonlinear membrane current to control the stability of the up state. In the simulation shown in this section, we chose $\delta = -31.685$.

Excitatory synaptic current:

$$I_{_{synE}}^{(i)}(t) = \bar{g}_{_{synE}} s_i(t)(V_i(t) - E_{_{synE}}), \tag{6.5}$$

where $\bar{g}_{_{synE}} = 68\mu\text{S/mm}^2$, $E_{_{synE}} = -120\text{mV}$, and the activation variable $s_i(t)$ satisfies the following first order differential equation,

$$\frac{ds_i}{dt} = \alpha_E\Big(s_i - 10\sum_{j=1}^{N}\Theta(J_{ij})J_{ij}\Theta(V_j(t-\tau) - V_{thr})\Big), \tag{6.6}$$

where $\alpha_E = 1$, $V_{thr} = -45\text{mV}$, $\tau = 10\text{ms}$, $\Theta(x)$ is the Heaviside step function, and the J_{ij} are the components of the connectivity matrix $\mathbf{J}$.

Inhibitory synaptic current:

$$I_{_{synI}}^{(i)}(t) = \bar{g}_{_{synI}} z_i(t)(V_i(t) - E_{_{synI}}), \tag{6.7}$$

where $\bar{g}_{_{synI}} = 118\mu\text{S/mm}^2$, $E_{_{synI}} = -120\text{mV}$, and the activation variable is given by $z_i(t) = (x_i(t) + y_i(t))/2$, with $x_i(t)$ and $y_i(t)$ satisfying the following first order differential equations,

$$\begin{aligned}
\frac{dx_i}{dt} &= \alpha_I\Big(x_i - 10\sum_{j=1}^{N}\Theta(-J_{ij})J_{ij}\Theta(V_j(t-\tau) - V_{thr})\Big), \\
\frac{dy_i}{dt} &= \beta_I\Big(y_i + 10\sum_{j=1}^{N}\Theta(-J_{ij})J_{ij}\Theta(V_j(t-\tau) - V_{thr})\Big),
\end{aligned} \tag{6.8}$$

with $\alpha_I = 2$, $\beta_I = 0.08$, and $\tau = 10\text{ms}$.

With the parameters of a single neuron fixed as above, the dynamics of a network of N PIF-neurons is fully determined by the connectivity matrix $\mathbf{J}$. We constructed $\mathbf{J}$ from prescribed cycles

using the pseudoinverse learning rule $\mathbf{J} = \Sigma\mathbf{P}\Sigma^{+}$, i.e. without invoking a fixed point condition. Figure 6.1 illustrates a successfully retrieved 6×8 cycle Σ. The first four rows of Σ are $\sigma_1\mathbf{P}^{j-1}$, $j = 1, 2, 3, 4$, and the last two rows are σ_2 and $\sigma_2\mathbf{P}$, where $\sigma_1 = (+, +, +, +, -, -, -, -)$ and $\sigma_2 = (+, +, -, -, +, +, -, -)$.

Figure 6.1**A** shows the retrieved traces of the membrane potentials $V_i(t)$ of the six neurons in the network. Since the firing rates are not included as variables in the model, they have to be extracted from the time series. Following [73], we counted for given t the number of times t' within the time window $t - \Delta t/2 \leq t' \leq t + \Delta t/2$ at which neuron i fired, and divided this number by Δt. The resulting function, $R_i(t)$, is considered as an approximation of the firing rate of the i-th neuron. For Δt we chose $\Delta t = 5$ms. We also introduce the normalized firing rates, $v_i(t) = 2R_i(t)/\max R_i(t) - 1$ (so that $-1 \leq v_i(t) \leq 1$, analogous to the firing rates used in continuous-time Hopfield-type networks), and define the overlaps $m^{(\nu)}(t)$ as in equation (1.11).

To compare the membrane potentials with the prescribed cycle, we extracted the time spans between the first spike and the last spike in each up-state, and identified their average divided by 4 as the time span for each binary state. The resulting time span is 11.3ms and is slightly larger than the time-delay $\tau = 10$ms in the synaptic couplings. In Figure 6.1**A**, the gray strips in the background indicate these time spans, and the dark gray $+$'s and $-$'s label the corresponding binary states in the prescribed cycle. The firing rates $R_i(t)$ and the overlaps $m^{(\nu)}(t)$ are displayed in Figure 6.1**B** and **C**, respectively. The black arrows in **A**, **B**, and **C** indicate the time span when the first binary pattern, $\xi^{(1)} = (+, +, +, +, +, +)^T$, in the prescribed cycle is retrieved for the first time in the displayed time range. The plots in Figure 6.1 clearly demonstrate that the cycle is retrieved successfully.

Other cycles were retrieved successfully as well, but in contrast to continuous time Hopfield-type networks, especially with delayed couplings, we observed in simulations that some prescribed cycles are difficult to be retrieved in networks of the spiking neurons introduced in this subsection. This is likely because of the complicated dynamics of the individual neurons, which makes the appropriate choice of parameter values more difficult. In general, especially in physiologically based neural network models, the neuronal dynamics may take key roles in shaping the dynamics of the networks, and reinforce or weaken the contribution of the network structure in reproducing

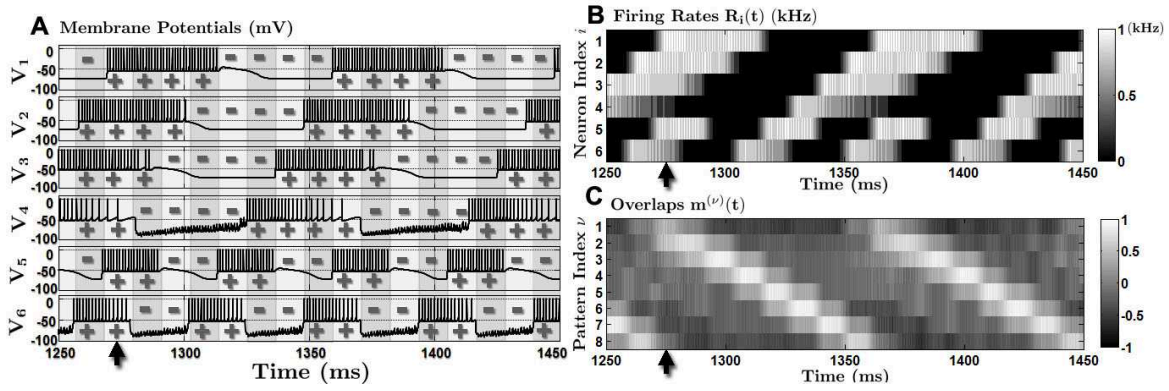

Figure 6.1: Successful retrieval of a cycle Σ with eight states prescribed in a network of six spiking neurons with the pseudoinverse learning rule. **A**: membrane potential, **B**: Firing rates, and **C**: Overlaps (see text for details).

prescribed cycles. In this case, it is important to find out whether a cyclic patterned output in a system arises from a network-based mechanism or not, and if it does, then to which extent and how the cyclic patterned output is determined by the network architecture.

6.5 Future Work

The work presented in this dissertation can be extended in the following three directions.

Storing and Retrieving Cycles in Other Neural Networks Although our main methods and results were developed and obtained in continuous-time Hopfield-type neural networks, our results about admissibility of cyclic patterns are applicable to discrete-time Hopfield-type neural networks, and in the preceding section, we have seen that using the pseudoinverse learning rule, cyclic patterns can be stored and retrieved in the biologically more realistic spiking neuronal network (6.2). As cyclic patterns are special complex sequences [1–3], and storage and retrieval of complex sequences in discrete-time neural networks can be related to sequential memory in animal neural systems [107], it would be both important and interesting to extend our results about admissibility and retrievability of cyclic patterns to neural networks with more complicated and biologically plausible neuronal dynamics, such as Hodgkin-Huxley neurons, multiple compartment neurons, and so on. As in the network (6.2), we introduced a virtual ion current (6.4) to account for the bistability of the CPG/cortical neurons with up and down states. Therefore, to find the real ion current, or a combination of ion currents, which can be approximated by the virtual current (6.4)

would be a good starting point. After the realistic ion current or a combination of ion currents are identified, we would continue to find an appropriate representation of the admissibility and retrievability of cycles in networks of such neurons, and study the corresponding delay induced dynamics.

It was recently suggested that heteroclinic cycles may take key roles in memory formation and other advanced neural functions [102, 108]. As we have seen in Chapters 3 and 5, many cyclic patterns we studied are stored and retrieved in Hopfield-type networks as long-lasting transient oscillations, and some of them may even correspond to heteroclinic cycles. Therefore another extension of our research presented in this dissertation is to seek a proper form for the biologically more plausible spiking neuron networks such that robust heteroclinic cycles can be constructed in them and our results for Hopfield-type networks can be extended. To this end, summarizing the identified CPG networks in invertebrate animals and seeking the conditions under which robust heteroclinic cycles may exist would be a good starting point. The main goal of this extension would be to explore the underlying mechanisms for generating multiple cyclic/sequential patterns in CPG networks with robust heteroclinic cycles, and study transitions among these cyclic/sequential patterns.

Delay-Induced Bifurcations in Hopfield-type Networks The (codimension two) Bogdanov-Takens bifurcation [79] has been recently observed and extensively investigated in Hopfield-type networks with ring topology and single or multiple discrete delays [58, 59, 109]. In Chapter 5, we have seen that the Bogdanov-Takens bifurcation occurs not only in networks with ring topology but also in other networks with more complicated topology. To fully understand the dynamics of the networks constructed from simple MC-cycles, or even more general admissible cycles, it is necessary to elucidate the general mechanism of the Bogdanov-Takens bifurcation, and clarify its role in creating and shaping both persistent and transient oscillations in the networks.

Other aspects of the extension of our results include bifurcations in Hopfield-type networks with multiple discrete delays, state-dependent delay(s), and distributed delay(s). Although these aspects have attracted much attentions during the past few years [110–113], a systematical study of networks constructed from admissible cycles with multiple discrete delays, state-dependent delays(s), and distributed delay(s) is still lacking. Therefore, it would be both theoretically and

practically important to extend our admissibility and retrievability studies to these networks, and study bifurcations in these networks.

MLA Method for Networks with Multiple Discrete Delays In Chapter 3, we developed a novel method for analyzing the relaxation dynamics of networks with single delay and constructed from simple MC-cycles. However, in both analog electronic circuits modeling neural networks or real animal neural networks, delays coming from both finite switching time and inter-unit transmission delays are not uniform, they may be even distributed or state-dependent [114,115]. Therefore, as a first step of the extension of our MLA method, we would consider networks with multiple discrete delays first, and then distributed and state-dependent delays.

In this dissertation, the MLA method was developed under the condition $\lambda \to \infty$, the gain scaling parameter λ, which can be related to the membrane constant of the neurons in the network, is usually finite. Therefore, another extension of our results is to study the case of finite but still large λ. Recently, Glyzin et al [76] studied a single Hopfield neuron and a Hopfield-type neural network of three unidirectionally coupled neurons. They investigated the network under the condition $\varepsilon \to 0$, where $\varepsilon = 1/\lambda$, and then extended the results from $\varepsilon \to 0$ to finite but small ε using a perturbation analysis. In this second extension of our MLA method, we will use a perturbation method which is similar to that of Glyzin et al [76], but for more general and complicated networks constructed from simple MC-cycles.

REFERENCES

[1] I. Guyon, L. Personnaz, J. Nadal, and G. Dreyfus, "Storage and retrieval of complex sequences in neural networks," *Phys. Rev. A*, vol. 38, pp. 6365–6372, Dec. 1988.

[2] D. Wang and M. Arbib, "Complex temporal sequence learning based on short-term memory," *Proc. IEEE*, vol. 78, pp. 1536–1543, Sep. 1990.

[3] D. Wang, "Temporal pattern processing," in *The Handbook of Brain Theory and Neural Networks, 2nd Ed., Arbib M.A. (ed.)*, (MIT Press, Cambridge MA), pp. 1163–1167, 2003.

[4] C. Gray, "Synchronous oscillations in neuronal systems: mechanisms and functions," *J. Computat. Neurosci.*, vol. 1, pp. 11–38, Jun. 1994.

[5] G. Laurent and M. Naraghi, "Odorant-induced oscillations in the mushroom bodies of the locust," *J. Neurosci.*, vol. 14, pp. 2993–3004, May. 1994.

[6] J. Lisman and M. Idiart, "Storage of 7 $\pm$ 2 short-term memories in oscillatory subcycles," *Science*, vol. 267, pp. 1512–1515, Mar. 1995.

[7] E. Marder and R. Calabrese, "Principles of rhythmic motor pattern generation," *Physiol. Rev.*, vol. 76, pp. 687–717, Jul. 1996.

[8] A. Jean, "Brain stem control of swallowing neuronal network and cellular mechanisms," *Physiol. Rev.*, vol. 81, pp. 929–969, Apr. 2001.

[9] S. Hooper, "Central pattern generators," in *Encyclopedia of life sciences*, (John Wiley & Sons., New York, NY), pp. 1–9, Apr. 2001.

[10] M. MacKay-Lyons, "Central pattern generation of locomotion: a review of the evidence," *Phys. Ther.*, vol. 82, pp. 69–83, Jan. 2002.

[11] E. Marder, D. Bucher, D. Schulz, and A. Taylor, "Invertebrate central pattern generation moves along," *Curr. Biol.*, vol. 15, pp. R685–R699, Sep. 2005.

[12] R. Yuste, "Circuit neuroscience: the road ahead," *Front. Neurosci.*, vol. 2, pp. 6–9, Aug. 2008.

[13] P. Guertin, "Central pattern generator for locomotion: anatomical, physiological, and pathophysiological considerations," *Front. Neurol.*, vol. 3, pp. 1–15, Feb. 2013.

[14] T. Gencic, M. Lappe, G. Dangelmayr, and W. Guettinger, "Storing cycles in analog neural networks," in *Parallel Processing in Neural Systems and Computers, Eckmiller, R., Hartmann, G. and Hauske, G. (eds.)*, (North Holland), pp. 445–450, 1990.

[15] Y. Horikawa and H. Kitajima, "Experiments on transient oscillations in a circuit of diffusively coupled inverting amplifiers," in *AIP Conf. Proc., vol. 922*, (Tokyo, JP), pp. 569–572, Sep. 2007.

[16] M. Forti, B. Garay, M. Koller, and L. Pancioni, "An experimental study on long transient oscillations in cooperative cnn rings," in *Cellular Nanoscale Networks and Their Applications*, (Turin, IT), pp. 1–6, Aug. 2012.

[17] D. Wilson, "The central nervous control of locust flight," *J. Exp. Biol.*, vol. 38, pp. 471–490, Jan. 1961.

[18] N. Syed, A. Bulloch, and K. Lukowiak, "In vitro reconstruction of the respiratory central pattern generator of the muollusk lymnaea," *Science*, vol. 250, pp. 282–285, Oct. 1990.

[19] N. Syed, D. Harrison, and W. Winlow, "Respiratory behavior in the pond snail *Lymnaea stagnalis* i. behavioral analysis and the identification of motor neurons," *J. Comp. Physiol. A*, vol. 169, pp. 541–555, Nov. 1991.

[20] N. Syed, I. Roger, R. Ridgway, L. Bauce, K. Lukowiak, and A. Bulloch, "Identification, characterisation and in vitro reconstruction of an interneuronal network of the snail helisoma trivolvis," *J. Exp. Biol.*, vol. 174, pp. 19–44, Jan. 1993.

[21] A. Selverston, "Invertebrate central pattern generator circuits," *Phil. Trans. R. Soc. B*, vol. 365, pp. 2329–2345, Aug. 2010.

[22] P. Dickinson and M. Moulins, "Interactions and combinations between different networks in the stomatogastric nervous system," in *Dynamic biological networks: the stomatogastric nervous system, Harris-Warrick, R.M., Marder, E., Selverston, A.I., and Moulins, M. (eds)*, (Cambridge, MA: MIT), pp. 139–160, Oct. 1992.

[23] P. Meyrand, J. Simmers, and M. Moulins, "Dynamic construction of a neural network from multiple pattern generators in the lobster stomatogastric nervous system," *J. Neurosci.*, vol. 14, pp. 630–644, Feb. 1994.

[24] M. Golubitsky, I. Stewart, P.-L. Buono, and J. Collins, "Symmetry in locomotor central pattern generators and animal gaits," *Nature*, vol. 401, pp. 693–695, Oct. 1999.

[25] P.-L. Buono and M. Golubitsky, "Models of central pattern generators for quadruped locomotion," *J. Math. Biol.*, vol. 42, pp. 291–326, Apr. 2001.

[26] C. Zhang, G. Dangelmayr, and I. Oprea, "Storing cycles in hopfield-type networks with pseudoinverse learning rule - admissibility and network topology," *Neural Networks*, vol. 46, pp. 283–298, Oct. 2013.

[27] C. Zhang, G. Dangelmayr, and I. Oprea, "Storing cycles in hopfield-type networks with pseudoinverse learning rule - retrievability and bifurcation analysis." In preparation, 2014.

[28] C. Zhang, G. Dangelmayr, and I. Oprea, "Delay-induced long-lasting transient oscillations in hopfield-type neural networks." In preparation, 2014.

[29] J. Hopfield, "Neural networks and physical systems with emergent collective computational abilities," *Proc. Natl. Acad. Sci. USA*, vol. 79, pp. 2554–2558, Apr. 1982.

[30] J. Hopfield, "Neurons with graded response have collective computational properties like those of two-state neurons," *Proc. Natl. Acad. Sci. USA*, vol. 81, pp. 3088–3092, May. 1984.

[31] W. Little, "The existence of persistent states in the brain," *Math. Biosci.*, vol. 19, pp. 101–120, Feb. 1974.

[32] R. McEliece, E. Posner, Rodemich, E.R., and S. Venkatesh, "The capacity of the hopfield associative memory," *IEEE Transactions on Information Theory IT*, vol. 33, pp. 461–482, Jul. 1987.

[33] J. Šíma and P. Orponen, "Continuous-time symmetric hopfield nets are computationally universal," *Neural Computation*, vol. 15, pp. 693–733, Mar. 2003.

[34] D. López-Rodríguez, E. Mérida-Casermeiro, and J. Ortiz-de Lazcano-Lobato, "Hopfield network as associative memory with multiple reference points," in *proceeding of: International Enformatika Conference*, (Prague, Czech Republic), pp. 62–67, Aug. 2005.

[35] H. Bersini, M. Saerens, and L. Sotelino, "Hopfield net generation, encoding and classification of temporal trajectories," *IEEE Trans. Neural Netw.*, vol. 5, pp. 945–953, Nov. 1994.

[36] U.-P. Wen, K.-M. Lan, and H.-S. Shih, "A review of hopfield neural networks for solving mathematical programming problems," *Eur. J. Oper. Res.*, vol. 198, pp. 675–687, Nov. 2009.

[37] K. Pakdaman, C. Malta, C. Grotta-Ragazzo, O. Arino, and J. Vibert, "Transient oscillations in continuous-time excitatory ring neural networks with delay," *Phys. Rev. E*, vol. 55, pp. 3234–3248, Mar. 1997.

[38] S. Campbell, S. Ruan, and J. Wei, "Qualitative analysis of a neural network model with multiple time delays," *Internat. J. Bifur. Chaos Appl. Sci. Engrg.*, vol. 9, pp. 1585–1595, Aug. 1999.

[39] S. Campbell, Y. Yuan, and S. Bungay, "Equivariant hopf bifurcation in a ring of identical cells with delayed coupling," *Nonlinearity*, vol. 18, pp. 2827–2846, Oct. 2005.

[40] S. Campbell, I. Ncube, and J. Wu, "Multistability and stable asynchronous periodic oscillations in a multiple-delayed neural system," *Physica D*, vol. 214, pp. 101–119, Feb. 2006.

[41] S. Guo and L. Huang, "Pattern formation and continuation in a trineuron ring with delays," *Acta Math. Sin. (Engl. Ser.)*, vol. 23, pp. 799–818, Sep. 2007.

[42] Y. Horikawa and H. Kitajima, "Duration of transient oscillations in ring networks of unidirectionally coupled neurons," *Physica D*, vol. 238, pp. 216–225, Jan. 2009.

[43] F. Pasemann, "Characterization of periodic attractors in neural ring networks," *Neural Networks*, vol. 8, pp. 421–429, Mar. 1995.

[44] H. Smith, "Monotone dynamical systems an introduction to the theory of competitive and cooperative systems," in *Mathematical Surveys and Monographs, vol. 41*, (American Mathematical Society, Providence), 1995.

[45] Y. Chen and J. Wu, "Existence and attraction of a phase-locked oscillation in a delayed network of two neurons," *Differ. Integral Equ.*, vol. 14, pp. 1181–1236, Oct. 2001.

[46] C. Cheng, K. Lin, and C. Shih, "Multistability in recurrent neural networks," *SIAM J. Appl. Math.*, vol. 66, pp. 1301–1320, Mar. 2006.

[47] C. Cheng, K. Lin, and C. Shih, "Multistability and convergence in delayed neural networks," *Physica D*, vol. 225, pp. 61–74, Jan. 2007.

[48] Y. Yuan and S. Campbell, "Stability and synchronization of a ring of identical cells with delayed coupling," *J. Dyn. Diff. Equ.*, vol. 16, pp. 709–744, Jul. 2004.

[49] D. Perkel and B. Mulloney, "Motor pattern production in reciprocally inhibitory neurons exihibiting postinhibitory rebound," *Science*, vol. 185, pp. 181–183, Jul. 1974.

[50] K. Matsuoka, "Sustained oscillations generated by mutually inhibiting neurons with adaptation," *Biol. Cybern.*, vol. 52, pp. 367–376, Oct. 1985.

[51] H. Sompolinsky and I. Kanter, "Temporal association in asymmetric neural networks," *Phys. Rev. Lett.*, vol. 57, pp. 2861–2864, Dec. 1986.

[52] D. Kleinfeld, "Sequential state generation by model neural networks," *Proc. Natl. Acad. Sci. USA*, vol. 83, pp. 9469–9473, Dec. 1986.

[53] D. Kleinfeld and H. Sompolinsky, "Associative neural network model for the generation of temporal patterns, theory and application to central pattern generators," *Biophys. J.*, vol. 54, pp. 1039–1051, Dec. 1988.

[54] S. Srinivasan, R. Gander, and H. Wood, "A movement pattern generator model using artificial neural networks," *IEEE Trans. Biomed. Eng.*, vol. 39, pp. 716–722, Jul. 1992.

[55] R. Ghigliazza and P. Holmes, "A minimal model of a central pattern generator and motoneurons for insect locomotion," *SIAM J. Appl. Dyn. Syst.*, vol. 3, pp. 671–700, Dec. 2004.

[56] L. Personnaz, I. Guyon, and G. Dreyfus, "Collective computational properties of neural networks: new learning mechanisms," *Physical Review A*, vol. 34, pp. 4217–4228, Nov. 1986.

[57] J. Wu, "Symmetric functional differential equations and neural networks with memory," *Trans. Amer. Math. Soc.*, vol. 350, pp. 4799–4838, Dec. 1998.

[58] S. Campbell and Y. Yuan, "Zero singularities of codimension two and three in delay differential equations," *Nonlinearity*, vol. 21, pp. 2671–2691, Oct. 2008.

[59] G. Fan, S. Campbell, G. Wolkowicz, and H. Zhu, "The bifurcation study of 1:2 resonance in a delayed system of two coupled neurons," *J. Dynamics Differential Equations*, vol. 25, pp. 193–216, Jan. 2013.

[60] S. Guo and J. Wu, *Bifurcation theory of functional differential equations.* New York, NY: Springer, 2013.

[61] J. Hale and S. Lunel, *Introduction To Functional Differential Equations.* New York, NY: Springer-Verlag, 1993.

[62] O. Diekmann, S. Gils, S. Lunel, and H. Walther, *Delay Equations - Functional-, Complex-, And Nonlinear Analysis.* New York, NY: Springer-Verlag, 1995.

[63] J. Tapson and A. Schaik, "Learning the pseudoinverse solution to network weights," *Neural Networks*, vol. 45, pp. 94–100, Sep. 2013.

[64] D. Plenz and S. Kitai, "Up and down states in striatal medium spiny neurons simultaneously recorded with spontaneous activity in fast-spiking interneurons studied in cortex-striatum-substantia nigra organotypic cultures," *J. Neurosci.*, vol. 18, pp. 266–283, Jan. 1998.

[65] W. McCulloch and W. Pitts, "A logical calculus of the ideas immanent in nervous activity," *Bull. Math. Biophys.*, vol. 5, pp. 115–133, Dec. 1943.

[66] V. Straub, K. Staras, G. Kemenes, and P. Benjamin, "Endogenous and network properties of lymnaea feeding central pattern generator interneurons," *J. Neurophysiol.*, vol. 88, pp. 1569–1583, Oct. 2002.

[67] S. Grillner, "The motor infrastructure: from ion channels to neuronal networks," *Nature Rev. Neurosci.*, vol. 4, pp. 573–586, Jul. 2003.

[68] M. Sanchez-Vives and D. McCormick, "Cellular and network mechanisms of rhythmic recurrent activity in neocortex," *Nature Neurosci.*, vol. 3, pp. 1027–1034, Oct. 2000.

[69] R. Cossart, D. Aronov, and R. Yuste, "Attractor dynamics of network up states in neocortex," *Nature*, vol. 423, pp. 283–289, May. 2003.

[70] P. Lancaster and M. Tismenetsky, *The theory of matrices (2nd ed.)*. San Diego, CA: Academic Press, 1985.

[71] W. J. Miller, *Symmetry groups and their applications*. New York, NY: Academic Press, 1972.

[72] D. Dummit and R. Foote, *Abstract Algebra (3rd ed.)*. Hoboken, NJ: John Willey & Sons, Inc., 2004.

[73] P. Dayan and L. Abbott, *Theoretical neuroscience - computational and mathematical modeling of neural systems*. Cambridge, Massachusetts: The MIT Press, 2001.

[74] C. Petersen, T. Hahn, M. Mehta, A. Grinvald, and B. Sakmann, "Interaction of sensory responses with spontaneous depolarization in layer 2/3 barrel cortex," *Proc. Natl. Acad. Sci. USA*, vol. 100, pp. 13638–13643, Sep. 2003.

[75] R. Driver, *Ordinary And Delay Differential Equations*. New York, NY: Springer-Verlag, 1977.

[76] S. Glyzin, A. Kolesov, and N. Rozov, "Relaxation self-oscillations in hopfield networks with delay," *Izvestiya: Mathematics*, vol. 77, pp. 271–312, Feb. 2013.

[77] F. Hoppensteadt and E. Izhikevich, *Weakly Connected Neural Networks*. New York, NY: Springer-Verlag, 1997.

[78] R. Horn and C. Johnson, *Matrix Analysis*. New York, NY: Cambridge University Press, 1985.

[79] G. Dangelmayr and J. Guckenheimer, "On a four parameter family of planar vector fields," *Arch. Rat. Mech. Anal.*, vol. 97, pp. 321–352, Dec. 1987.

[80] G. Gutierrez, "Variable-frequency oscillators," in *Wiley Encyclopedia of Electrical and Electronics Engineering, J.G. Webster, ed.*, (John Wiley: New York, NY), pp. 75–84, December 1999.

[81] J. Collins and I. Stewart, "A group-theoretic approach to rings of coupled biological oscillators," *Biol. Cybern.*, vol. 71, pp. 95–103, Jan. 1994.

[82] R. Dror, C. Canavier, R. Butera, J. Clark, and J. Byrne, "A mathematical criterion based on phase response curves for stability in a ring of coupled oscillators," *Biol. Cybern.*, vol. 80, pp. 11–23, Jan. 1999.

[83] A. Dhooge, W. Govaerts, and Y. Kuznetsov, "Matcont: A matlab package for numerical bifurcation analysis of odes," *ACM TOMS*, vol. 29, pp. 141–164, Jun. 2003.

[84] Y. Horikawa and H. Kitajima, "Effects of noise and variations on the duration of transient oscillations in unidirectionally coupled bistable ring networks," *Phys. Rev. E*, vol. 80, p. 021934(R), Aug. 2009.

[85] M. Golubitsky, I. Stewart, and A. Torok, "Patterns of synchrony in coupled cell networks with multiple arrows," *SIAM J. Appl. Dynam. Sys.*, vol. 4, pp. 78–100, Feb. 2005.

[86] M. Golubitsky and I. Stewart, "Nonlinear dynamics of networks: the groupoid formalism," *Bull. Amer. Math. Soc.*, vol. 43, pp. 305–364, May. 2005.

[87] H. Tang, K. Tan, and E. Teoh, "Dynamics analysis and analog associative memory of networks with lt neurons," *IEEE Trans. Neural Networks*, vol. 17, pp. 409–418, Mar. 2006.

[88] H. Tang, H. Li, and R. Yan, "Memory dynamics in attractor networks with saliency weights," *Neural Computation*, vol. 22, pp. 1899–1926, Jul. 2010.

[89] L. Pecora and T. Carroll, "Master stability functions for synchronized coupled systems," *Phys. Rev. Lett.*, vol. 80, pp. 2109–2112, Mar. 1998.

[90] P. Ashwin and G. Dangelmayr, "Reduced dynamics and symmetric solutions for globally coupled weakly dissipative oscillators," *Dynamical Systems*, vol. 20, pp. 333–367, Sep. 2005.

[91] G. Orosz, "Decomposing the dynamics of delayed networks: equilibria and rhythmic patterns in neural systems," *Time Delay Systems*, vol. 10, no. 1, pp. 173–178, 2012.

[92] R. Szalai and G. Orosz, "Decomposing the dynamics of heterogeneous delayed networks with applications to connected vehicle systems," *Phys. Rev. E*, vol. 88, p. 040902(R), Oct. 2013.

[93] S. Grillner and P. Wallén, "Central pattern generators for locomotion, with special reference to vertebrates," *Ann. Rev. Neurosci.*, vol. 8, pp. 233–261, Mar. 1985.

[94] P. Guertin, "The mammalian central pattern generator for locomotion," *Brain Res. Rev.*, vol. 62, pp. 45–56, Dec. 2009.

[95] D. McCrea and I. Rybak, "Organization of mammalian locomotor rhythm and pattern generation," *Brain Res. Rev.*, vol. 57, pp. 134–146, Jan. 2008.

[96] T. Ko and G. Ermentrout, "Phase-response curves of coupled oscillators," *Phys. Rev. E*, vol. 79, p. 016211, Jan. 2009.

[97] C. Zhang and T. Lewis, "Phase response properties of half-center oscillators," *J. Comput. Neurosci.*, vol. 35, pp. 55–74, Aug. 2013.

[98] A. Cohen, P. Holmes, and R. Rand, "The nature of the coupling between segmental oscillators of the lamprey spinal generator for locomotion," *J. Math. Biol.*, vol. 13, pp. 345–369, Jan. 1982.

[99] A. Cohen, G. Ermentrout, T. Kiemel, N. Kopell, K. Sigvardt, and T. Williams, "Modelling of intersegmental coordination in the lamprey central pattern generator for locomotion," *Trends. Neurosci.*, vol. 15, pp. 434–438, Nov. 1992.

[100] E. Izhikevich, *Dynamical Systems in Neuroscience: The Geometry of Excitability and Bursting*. Cambridge, Massachusetts: MIT Press, 2007.

[101] J. Rubin, N. Shevtsova, G. Ermentrout, J. Smith, and I. Rybak, "Multiple rhythmic states in a model of the respiratory central pattern generator," *J. Neurophysiol.*, vol. 101, pp. 2146–2165, Apr. 2009.

[102] M. Rabinovich, R. Huerta, and G. Laurent, "Transient dynamics for neural processing," *Science*, vol. 321, pp. 48–50, Jul. 2008.

[103] M. Rabinorich, A. Volkovskii, P. Lecanda, R. Huerta, H. Abarbanel, and G. Laurent, "Dynamical encoding by networks of competing neuron groups: winnerless competition," *Phys. Rev. Lett.*, vol. 87, p. 068102, Aug. 2001.

[104] R. Huerta and M. Rabinovich, "Reproducible sequence generation in random neural ensembles," *Phys. Rev. Lett.*, vol. 93, p. 238104, Dec. 2004.

[105] V. Afraimovich, V. Zhigulin, and M. Rabinovich, "On the origin of reproducible sequential activity in neural circuits," *Chaos*, vol. 14, pp. 1123–1129, Dec. 2004.

[106] N. Parga and L. Abbott, "Network model of spontaneous activity exhibiting synchronous transitions between up and down states," *Front. Neurosci.*, vol. 1, pp. 57–66, Oct. 2007.

[107] G. Deco and E. Rolls, "Sequential memory: a putative neural and synaptic dynamical mechanism," *J. Cognitive Neurosci.*, vol. 17, pp. 294–307, Feb. 2005.

[108] M. Rabinorich, I. Tristan, and P. Varona, "Neural dynamics of attentional cross-modality control," *PLoS ONE*, vol. 8, p. e64406, May. 2013.

[109] T. Dong and X. Liao, "Bogdanov-takens bifurcation in a tri-neuron bam neural network model with multiple delays," *Nonlinear Dyn.*, vol. 71, pp. 583–595, Feb. 2013.

[110] J. Belair, S. Campbell, and P. Driessche, "Frustration, stability, and delay-induced oscillations in a neural network model," *SIAM J. Appl. Math.*, vol. 56, pp. 245–255, Feb. 1996.

[111] H. Huang, G. Feng, and J. Cao, "State estimation for static neural networks with time-varying delay," *Neur. Net.*, vol. 23, pp. 1202–1207, Dec. 2010.

[112] R. Jessop and S. Campbell, "Approximating the stability region of a neural network with a general distribution of delays," *Neur. Net.*, vol. 23, pp. 1187–1201, Dec. 2010.

[113] C. Feng and R. Plamondon, "An oscillatory criterion for a time delayed neural ring network model," *Neur. Net.*, vol. 29-30, pp. 70–79, May. 2012.

[114] C. Eurich, K. Pawelzik, U. Ernst, J. Cowan, and J. Milton, "Dynamics of self-organized delay adaptation," *Phys. Rev. Lett.*, vol. 82, pp. 1594–1597, Feb. 1999.

[115] Y. Buskila, J. Morley, J. Tapson, and A. Schaik, "The adaptation of spike backpropagation delays in cortical neurons," *Front. Cell. Neurosci.*, vol. 7, pp. 1–9, Oct. 2013.

APPENDIX A

CYCLOTOMIC POLYNOMIALS

We summarize here the basic properties of the cyclotomic polynomials used in Chapter 2, for details see [72].

The cyclotomic polynomial of order p is defined by $\Phi_p(x) = \prod_r (x - x_r)$, $x \in \mathbb{C}$, where the x_r encompass all primitive p-th roots of unity, that is, $x_r^p = 1$ and $x_r^n \neq 1$ if $1 \leq n < p$. The total number of such primitive roots is given by *Euler's totient function*, $\varphi(p)$. If $p = \prod_j p_j^{m_j}$ with distinct primes p_j is the prime factorization of p, then $\varphi(p) = \prod_j p_j^{m_j - 1}(p_j - 1)$. The important property of the cyclotomic polynomial is that they have integer coefficients and are irreducible over the rationals. Moreover, $\Phi_p(x)$ is the minimal polynomial for each root x_r, and the product of all $\Phi_d(x)$ for which d is a factor of p and $1 \leq d \leq p$ is $x^p - 1$. The only cyclotomic polynomials of odd degree are $\Phi_1(x) = 1 - x$ and $\Phi_2(x) = 1 + x$, all $\Phi_p(x)$ for $p > 2$ have even degrees as their primitive roots are all complex. Some basic properties of $\Phi_p(x)$ are:

1. $\Phi_p(x) = \sum_{i=1}^{p} x^{i-1}$, if p is prime;
2. $\Phi_{2p}(x) = \Phi_p(-x)$, if p is odd;
3. $\Phi_p(x) = \Phi_q(x^{p/q})$, where q is the radical of p, i.e. the product of all distinct prime numbers occurring in the prime factorization of p.

The last property implies in particular $\Phi_p(x) = 1 + x^n$ if $p = 2n = 2^k$, $k \geq 1$. The third cyclotomic polynomial is $\Phi_3(x) = 1 + x + x^2$ and has the roots $e^{\pm 2\pi \mathbf{i}/3}$.